Immediate Deflection Calculations of Transition and Cracked Prestressed Concrete Sections

A THESIS
SUBMITTED TO THE FACULTY OF THE
UNIVERSITY OF MINNESOTA
BY

Rachel M. Wagner

IN PARTIAL FULFILLMENT OF THE REQUIREMENTS
FOR THE DEGREE OF MASTER OF SCIENCE

DR. ANDREA J. SCHOKKER

March 2024

Acknowledgements

My research would not have been possible without the PCI Daniel P. Jenny Fellowship that provided funding for my work as well as facilitating funds for the testing of two full-size double tees. Additionally, I am grateful for the Metromont team that assisted in the coordination, fabrication, and testing of the full-size test specimens.

I am extremely grateful for the patience and mentorship I have received from my advisor, Dr. Andrea Schokker. Your guidance and support throughout my undergraduate and graduate career have motivated me to be a better engineer and better person. I would like to also extend my thanks to my committee members, Dr. Ben Dymond and Dr. Alison Hoxie. I appreciate the perspective each one brings to this research and am thankful for your time and experience you have put into reviewing my work.

I would like to also thank my parents, sister and brother-in-law, nephew, and friends for your unwavering support.

Abstract

Prestressed concrete is commonly used in floor, roof, and bridge members. In prestressed concrete, the steel strands are tensioned/pulled and then concrete is cast around the strands in the form. Once the concrete has set, the strands are cut, and the member is put into compression from the pre-tensioned strands. Concrete is classified as uncracked, transition, and cracked based on the stress in a critical section (ACI, 2019). In practice, the member is designed to remain uncracked during its service life. When this is not possible, the code requires additional calculations that can increase the complexity of the design, one of these being deflection calculations. Transition and cracked section deflection calculations utilize an effective or cracked moment of inertia that adjusts the stiffness according to the relationship between the applied moment and cracking moment ratio. Though these methods are commonly used, current equations and models are unable to estimate the immediate deflections of transition and cracked prestressed concrete sections in flexure reliably and accurately. The goal of this research is to determine if a solution with current methods exists for transition and cracked sections used in practice, particularly double-tee members.

A sample of rectangular and double tees (n = 26) with prestressed reinforcement ratios varying from 0.06% to 0.45% was selected. Each specimen was modeled with five different equations to predict the deflection and loaded incrementally, to provide a plot of applied moment to deflection, and loads at specific stress limits and service moments. As the section progressively cracks under increasing loads, the neutral axis gets smaller as the cracks propagate towards the compressive face. This reduces the available area in the section to provide stiffness and resist the loads. Without calculating the cracked section properties, the reinforcement ratio is used to predict the cracked moment of inertia. The methods consider different ways to account for the changes in the member as it cracked, when to begin softening of the member, and alternative moments to shift the behavior closer to the experimental data. Some limitations to this study include a lack of full-scale double tee deflection specimens and specimens with low reinforcement ratios tested to failure.

The methods considered in this study did not provide any greater performance than those already in use. As expected, there was general agreement between the

estimated and tested data during the uncracked phase. But as the specimens were further stressed with loading past the cracking moment, the results became less consistent between methods. The equations that had the best results were the PCI and Auburn methods. These methods trended conservatively in their predictions and were computationally straightforward. The other alternative methods diverged from the experimental results as the stress in the member increased, making them a poorer choice for deflection prediction in cracked sections. Due to the overall lack of confidence in the deflection methods for transition and cracked sections, the recommended method continues to be the PCI for its simplicity in computation and performance in this group of test specimens. The Auburn method shows promise and can be revisited with the inclusion of additional data from deflections in full sized specimens.

Table of Contents

List of Tables

List of Figures

Notation

a	=	Distance from center of support to nearest concentrated load
A_g	=	Gross concrete of concrete
A_s	=	Area of nonprestressed longitudinal tension reinforcement
A_{ps}	=	Area of prestressed longitudinal tension reinforcement
b	=	Section width
b_w	=	Width of web
b_f	=	Flange width
c	=	Neutral axis depth
c_{cr}	=	Neutral axis depth of cracked section
c_c	=	Clear cover
d	=	Distance from extreme compression fiber to centroid of nonprestressed longitudinal tension reinforcement
d_p	=	Distance from extreme compression fiber to centroid of prestressing reinforcement (ACI)
e	=	Distance between centroid of prestressed strands and centroid of cross-section
E_c	=	Modulus of elasticity of concrete
e_{cr}	=	Distance between centroid of prestressed strands and centroid of cracked cross-section
E_{ps}	=	Modulus of elasticity of prestressed steel
E_s	=	Modulus of elasticity of steel
e_{tr}	=	Eccentricity of reinforcement relative to centroid of uncracked transformed concrete cross section
f_b	=	Stress in bottom fiber of cross section
f'_c	=	Compressive strength of concrete
f_{dc}	=	Decompression stress
f_l	=	Stress due to service live load
f_{tot}	=	Final calculated total stress in the component under service loads

f_{pe} = Compressive stress in concrete due only to effective prestress forces, after allowance for all prestress losses, at extreme fiber of section if tensile stress is caused by externally applied loads

f_{ps} = Stress in prestressed reinforcement at nominal flexural strength

f_{pu} = Specified tensile strength of prestressing steel

f_r = Modulus of rupture of concrete

f_{se} = Stress in prestressed reinforcement after losses

f_t = Stress in top fiber of cross section

f_y = Specified yield strength for nonprestressed reinforcement

h = Section depth

h_f = Flange depth

I = Moment of inertia about centroidal axis

I_{cr} = Moment of inertia of cracked section transformed into concrete

I_{cr} = Transformed moment of inertia for cracked section, fully cracked section in prestressed members (Bischoff et. al., 2018)

I'_{cr} = Actual cracked section moment of inertia for aprtialy cracked section of prestressed member (Bischoff et. al., 2018)

I''_{cr} = Intermediate moment of inertia for trilinear response approach

I_e = Effective moment of inertia

I_e* = Effective moment of inertia of partially cracked section relative to shifted moment (Bischoff et. al. , 2018)

I_g = Moment of inertia of gross concrete section about centroidal axis, neglecting reinforcement

I_{tr} = Uncracked transformed moment of inertia

L = Clear span

l_n = Clear span of member from inside face to face of supports

M'' = Moment intercept at second change in slope

M_1 = Moment intercept of shifted cracked moment of inertia, I_{cr}

M'_1 = Moment intercept of shifted cracked moment of inertia, I'_{cr}

M_a = Applied service load moment

M_{cr}	=	Cracking moment
M_D	=	Dead load moment
M_{dec}	=	Moment that induces zero stress at the tension face
$M_{service}$, M_s	=	Total service moment
M_{sw}	=	Moment due to self-weight
M_{zc}	=	Zero curvature moment corresponding to product of P_o and e_{tr}
n	=	Modulus of elasticity ratio, E_c/E_s
P_e	=	Effective prestress force on section
P_o	=	Fictious decompression force
S_b	=	Section modulus for tension face
S_t	=	Section modulus for compression face
q	=	Shear flow, applied load
y_s	=	Distance from centroidal axis of prestressed reinforcement to bottom fiber
y_t	=	Distance from centroidal axis of gross section, neglecting reinforcement, to face
y_{tps}	=	Distance from tension face to center of gravity of transformed prestressing steel
ρ	=	Mild reinforcement ratio of A_s to A_g
ρ_p	=	Prestressed reinforcement ratio of A_{ps} to bd (or bd_p)

1 Introduction

1.1 Background of Prestressed Concrete

Concrete is a material that has been used for centuries in buildings, roads, and other structures. It is a cost-effective solution for new and renovation construction projects. Concrete is comprised of three main components, cement, aggregate, and water. Traditionally, reinforced concrete consists of a ribbed, deformed steel bar placed in the concrete. The concrete is given time to set, cure, and then begin its service life. Prestressed, pre-tensioned, concrete differs from reinforced concrete in both fabrication and behavior. Prestressed concrete members are typically fabricated in a precast concrete plant. Seven-wire steel strand is placed in the casting bed where the concrete is cast or extruded around it. Secondary reinforcement such as mild steel, deformed steel bar mentioned previously in reinforced concrete, or welded wire reinforcement, may also be included in the prestressed member (PCI, 2017). The steel strands are pulled by jacks on the end of the casting bed, tensioning the steel and creating a prestressing force. Once tensioned and the concrete has set and gained the required initial strength, the strands are cut. The member continues to develop strength and is shipped to the project site once it has reached its required strength. Early in the development of prestressed concrete, steel strand was susceptible to a significant loss of stress in the strand due to relaxation. The loss due to relaxation reduces the stress in the strand, therefore reducing the capacity of the member. With the novel invention of low relaxation strand, lo-lax, losses were greatly reduced. Today, manufacturers use lo-lax strand and concrete to make many varieties of prestressed products.

A major benefit to concrete is its excellent performance in compression; steel reinforcement is added to provide the tensile capacity that the concrete lacks. Prestressed concrete has a higher capacity than traditionally reinforced concrete due to the prestressing force from the steel strands. The prestressing force places the concrete into a state of compression as the strands try to retract to their original position which can cause upward deflection called camber. As the beam is introduced to service loads, the member will return to zero deflection or deflect downwards. Due to concrete's excellent

performance in compression and the prestressing force inducing camber, these members are able to be more efficient than traditionally reinforced concrete sections.

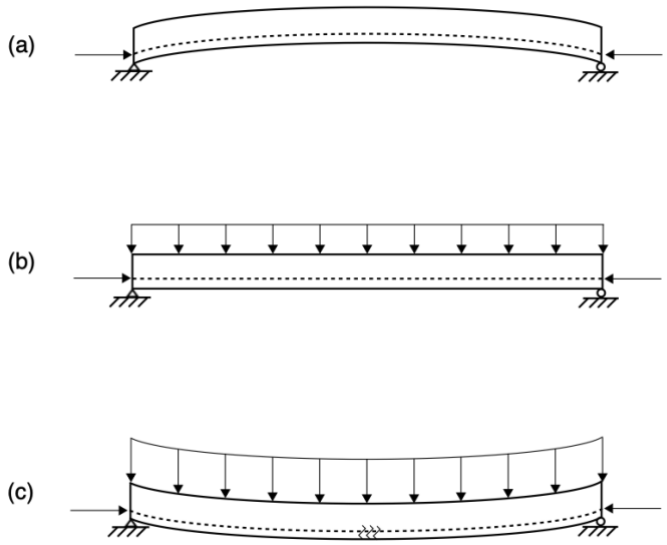

Figure 1.1. (a) Prestressed member with camber, (b) prestressed member under service loading, (c) prestressed member with loads causing downward deflection

1.1.1 Code Development

The American Concrete Institute (ACI) and Precast Concrete Institute (PCI) are a few of the governing and reference documents for concrete design, which have provisions for both strength and serviceability. Strength design of members is a safety requirement that entails shear, flexure, and torsion design. Serviceability requirements refer to the member's behavior in service and include stress checks, deflections, crack widths, and vibrations. Serviceability requirements ensure that the member can function the way it was intended to perform.

Prestressed concrete is covered in the ACI 318 Building Code (ACI 318, 2019) but development of design guidelines specifically made for prestressed concrete began in 1954, with the first edition of the PCI Handbook. Continued investment in prestressed concrete research has generated higher strength concrete mixes, strands with low relaxation, and novel shapes to improve efficiency in the material. Prestressed concrete has increased in demand and continues to be an economic choice for structural systems.

1.2 Deflections

Deflections are an important limit state for structural integrity, durability and performance. Deflections can be categorized into two cases, short and long term. Long term deflections refer to the deflections that occur over long periods of time including creep, shrinkage, and relaxation of prestressed strands. Short term deflections are characterized by service loads and superimposed dead loads. The primary focus of this research will be on short term, instantaneous deflections.

As deflections increase in the member, it may crack. Excessive cracking allows for the introduction of corrosive agents. These agents may cause degradation of the strands which reduces the prestressing force in the member and weakens the whole section. Other impacts that deflections may have on nonstructural elements as the deflection may introduce stress in locations that are greater than the nonstructural component can carry, for example a topping slab reinforced with fibers, cracking due to deflections. Additionally, excessive deflections of main structural members can damage other framing members interacting with it.

Concrete has three defined sections, uncracked (U), transition (T), and cracked (C); historically, T and C sections have been referred to as partially prestressed members. Sections that remain U under loading behave elastically, with tensile stress $f_t < 7.5\sqrt{f'_c}$. These members will deform but return to their original shape if the load is removed, representative of elastic materials. Transition sections can be characterized by having a tensile stress at service between $7.5\sqrt{f'_c} < f_t \leq 12\sqrt{f'_c}$. The behavior of transition sections is between uncracked and cracked, as the name suggests. Under load, the member may display some cracking, but under no load, the cracks will close. Cracked sections are characterized as having stresses greater than $f_t < 12\sqrt{f'_c}$. Under these conditions, the cracks will not fully close if the load is removed; this is now plastic deformation. Prior to defining sections as transition or cracked, it was common to refer to these sections as partially prestressed. Generally, reinforced concrete members are designed to be U sections. Prestressed concrete is commonly designed as U sections but may require T or C sections if the design for U is unfeasible. When sections are designed as T or C, the engineer must specify additional mild reinforcement as required to control

cracking and further investigate deflections as the section properties become more complex. It is common practice to design prestressed sections as U to take advantage of the benefits of a fully prestressed section and to avoid any requirements that T or C sections may have, but this may not be an option for some situations.

1.3 Motivation

Current methods of calculating deflections for transition and cracked prestressed concrete, specifically double tee specimens, fail to yield accurate results without introducing complexity. Some models yield better results but introduce complexity for the user. The governing documents for structural concrete do not have an optimized equation that is both computationally simple and generate accurate results.

1.4 Research Objectives

The primary research objective in this report is to model existing and alternative methods used to predict the deflections of transition and cracked prestressed concrete sections to determine whether a change to the ACI 318 Building Code is warranted at this time.

1.5 Thesis Organization

Chapter 2 presents the methods currently and previously used to predict the instantaneous deflections of transition and cracked members. A literature review of previous research in both reinforced and prestressed concrete deflections is also defined in this chapter. Chapter 3 covers the database selection and equation compatibility. Chapter 4 analyzes the results generated from each prediction method. Chapter 5 includes the conclusions and recommendations for deflections in cracked and transition prestressed concrete members.

2 Literature Review

2.1 Methods to Predict Deflection

2.1.1 ACI 318

ACI 318 is a building code for structural concrete, both reinforced and prestressed, that provides guidance on design and construction of structural concrete (2019). Since its development in early 1900's, ACI 318 has undergone numerous iterations to update the standards to reflect research that has been conducted (Kerekes and Reid, 1954).

ACI characterizes concrete sections based on the extreme fiber stress in tension. The code provides a prescriptive method for each section of concrete. As stated in section 1.2, the stresses for the member at transition and service must be checked and categorized according to their limits. It is permissible for unbonded and bonded prestressed flexural members to be designed in class U, T, or C sections, but two-way slab systems are only permitted to be designed in uncracked, class U, sections.

When calculating deflections, Class U and T sections are permitted to utilize the gross section; class C must perform the calculation using a cracked transformed section. Under Class T and C behavior, the deflection must be calculated using a bilinear method as opposed to uncracked elastic analysis. This accounts for the change in elastic and inelastic behavior shown during cracking. Additionally, Table R24.5.2 states that crack control for Class C sections must provide reinforcement according to section 24.3. Mild steel is added to help in durability and appearance of the member. Table 2.1 shows the spacing of crack control bars. As stated in R24.4.1 it is preferable to have many fine cracks rather than few wide cracks; therefore, more smaller diameter bars are preferred to fewer larger diameter bars.

Table 2.1. Classification of prestressed flexural members based on f_t (ACI Table 24.5.2.1)

Assumed behavior	Class	Limits of f_t
Uncracked	U	$f_t \leq 7.5\sqrt{f'_c}$
Transition between uncracked and cracked	T	$7.5\sqrt{f'_c} \leq f_t \leq 12\sqrt{f'_c}$
Cracked	C	$f_t > 12\sqrt{f'_c}$

Table 2.2. Maximum spacing of bonded reinforcement in nonprestressed and Class C prestressed one-way slabs and beams (ACI 318, 2014)

Reinforcement Type	Maximum Spacing, s	
Deformed bars or wires	Lesser of:	$15\left(\frac{40{,}000}{f_s}\right) - 2.5c_c$
		$12\left(\frac{40{,}000}{f_s}\right)$
Bonded prestressed reinforcement	Lesser of:	$(\frac{2}{3})\left[15\left(\frac{40{,}000}{\Delta f_{ps}}\right) - 2.5c_c\right]$
		$(\frac{2}{3})\left[12\left(\frac{40{,}000}{f_s}\right)\right]$
Combined deformed bars or bonded prestressed reinforcement	Lesser of:	$(\frac{5}{6})\left[15\left(\frac{40{,}000}{\Delta f_{ps}}\right) - 2.5c_c\right]$
		$(\frac{5}{6})\left[12\left(\frac{40{,}000}{f_s}\right)\right]$

Deflections are calculated using the loads on the member, span length, moment of inertia, and material properties. Uncracked sections are permitted to use gross section properties, giving them the greatest stiffness to resist loads. As the section is loaded and the stresses reach transition or cracked states, the allowable section properties are reduced; this decreases the stiffness of the member. To estimate the stiffness as a function of the cracking in the section, the effective moment of inertia is used.

$$I_e = (\frac{M_{cr}}{M_a})^3 I_g + [1 - \left(\frac{M_{cr}}{M_a}\right)^3] I_{cr} \quad 2.1$$

Calculating cracking moment, as shown below, is a function of the modulus of rupture, compressive strength in the concrete due to prestress, the gross moment of inertia, and the distance from the centroidal axis to the tension face.

$$M_{cr} = \frac{(f_r + f_{pe}) I_g}{y_t} \quad 2.2$$

Table 2.4 specifies the maximum allowable deflection based on the type of member, loading condition, and its length. Immediate deflection of a uniformly distributed load simply supported can be calculated using the equation below. When utilizing a member that is uncracked, the gross moment of inertia may be used. The highest deflections are typically at midspan. Table 2.3 is used to predict the deflections with the correct moment of inertia for the section according to its loading; see Figure 2.1, Figure 2.2, and Figure 2.3 for each load case used.

Table 2.3. Deflection calculations of simply supported beams (PCI, 2017)

Load Case	Δ at $\frac{L}{2}$
Uniformly distributed load, *w*	$\frac{5wL^4}{384EI}$
Point load at midspan, *P*	$\frac{PL^3}{48EI}$
Two-point loads, *P*, spaced *a* away from each support	$\frac{Pa}{6EI}(3L^2 - 4a^2)$

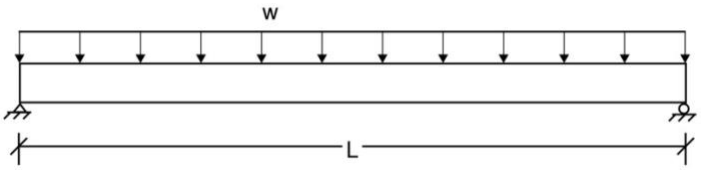

Figure 2.1. Uniformly distributed load on simply supported beam

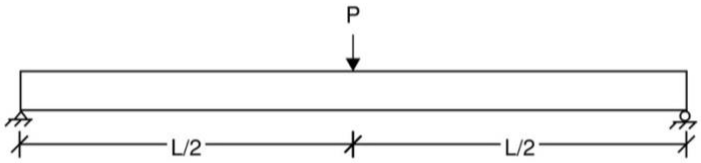

Figure 2.2. Point load at midspan on a simply supported beam

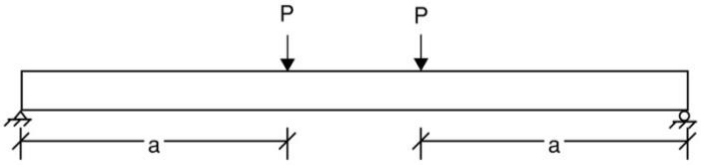

Figure 2.3. Two-point loads 'a' away from support on simply supported beam

Table 2.4. Maximum permissible calculated deflections (ACI, 2019)

Member	Condition		Deflection to be considered	Deflection limitation
Flat roof	Not supporting or attached to nonstructural elements likely to be damaged by large deflections		Immediate deflection due to maximum $\boldsymbol{L_r}$, $\boldsymbol{S}$, and $\boldsymbol{R}$	*l/180*
Floors			Immediate deflection due to $\boldsymbol{L}$	*l/360*
Roof or floors	Supporting or attached to nonstructural elements	Likely to be damaged by large deflections	That part of the total deflection occurring after attachment of nonstructural elements,	*l/480*

Member	Condition		Deflection to be considered	Deflection limitation
Roof or floors	Supporting or attached to nonstructural elements	Not likely to be damaged by large deflections	which is the sum of time-dependent deflection due to all sustained loads and the immediate deflection due to any additional live load	*l/240*

2.1.2 PCI

The Precast and Prestressed Concrete Institute (PCI) promotes the design and use of precast and prestressed concrete members. The PCI Handbook offers generous information about precast prestressed concrete design, including design aids and worked-out examples to assist in the design of prestressed concrete.

As deflections cause sections to move from uncracked to transition and cracked stress limits, the analysis for deflections is permitted to be computed through two different methods. Bilinear analysis involves using the gross moment of inertia and cracked moment of inertia. The gross moment of inertia is to be used until the applied moment is equal to the cracking moment. Then the cracked moment of inertia is used to calculate the deflections. An alternative method uses an effective moment of inertia. The effective moment of inertia is a weighted average of the gross moment of inertia compared to the cracked moment of inertia. Figure 2.4 shows the different methods in comparison. Though the effective moment of inertia is computationally simple, this method may not provide enough specificity to satisfy class C or component design (PCI, 2017).

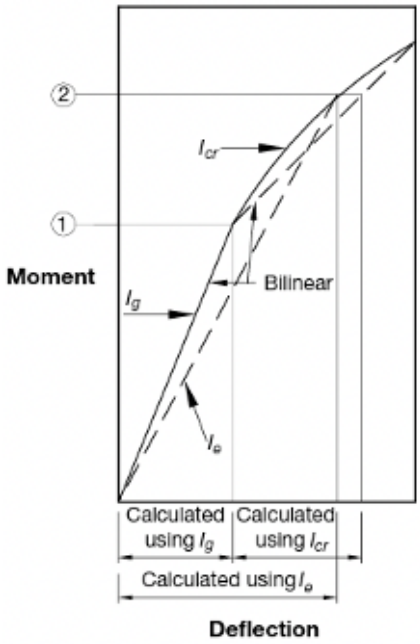

Figure 2.4. Bilinear moment-deflection (PCI, 2017)

The PCI Handbook follows the stress limits set by ACI 318-19 for uncracked, transition, and cracked sections. As the section moves from uncracked to transition and cracked, the PCI Handbook provides guidance on the procedure. Determining the modulus of rupture, f_r, and max tensile stress at service, typically the bottom tension stress at midspan, will specify if the member is in U, T, or C behavior.

$$f_r = 7.5\lambda\sqrt{f'_c} \qquad 2.3$$

Transition and cracked members are required to use the cracked moment of inertia for deflection calculations. The area of steel is transformed into equivalent areas of concrete based on the modulus of elasticity of both steel and concrete, otherwise known as the modular ratio, *n*. The reinforcement ratio, equation 2.5, is the ratio of the area of prestressing to the width of the section multiplied by the depth of the concrete to prestressing strands. When calculating maximum deflections, the depth to prestressing may be permitted to use the depth to prestressing strand at midspan (PCI, 2017). These

factors contribute to the calculation of the cracked moment of inertia and ultimately the effective moment of inertia.

$$n = \frac{E_s}{E_c} \quad 2.4$$

$$\rho_p = \frac{A_{ps}}{bd_p} \quad 2.5$$

$$I_{cr} = nA_{ps}{d_p}^2\left(1 - 1.6\sqrt{n\rho_p}\right) \quad 2.6$$

The PCI Handbook allows for a different calculation of the M_{cr}/M_a ratio. Instead of the ratio between cracking and applied moment, the difference between the final stress, f_{tot}, and modulus of rupture, f_r, are divided by the stress introduced by the live load, f_l. Using the difference in stresses, the effective moment of inertia calculation controls over the gross moment of inertia when the applied moment is greater than the cracking moment. Upon completion of the effective moment of inertia calculation, the deflections may be calculated using Table 2.1 for simply supported members.

$$\frac{M_{cr}}{M_a} = 1 - \left(\frac{f_{tot} - f_r}{f_l}\right) \quad 2.7$$

2.2 Decompression Moment

To define deflections for transition and cracked prestressed concrete sections, the concept of the decompression moment is introduced in this section.

Prestressing strands introduce an axial force into the member due to force in the strands, typically resulting in a stress in tension at the top of the section and compressive stress at the bottom of the section. This is commonly referred to as the precompression force of the member. As load is added to the member, the section overcomes the force induced by prestressing, and experiences tension in the bottom and compression in the top of the section. The force at which the bottom of the section experiences zero stress is the decompression force, see Figure 2.5. In simply supported sections that are fully loaded, the member has tension on the bottom and compression in the top of the section.

After surpassing the decompression stress, the member moves towards transition and cracked stages where the neutral axis will shift towards the compressive face.

Decompression was initially introduced to understand the behavior of transition and cracked prestressed members (Nilson, 1976). Before the expression of decompression stress and moment, designers were restricted to designing fully prestressed members where the bottom tension could not exceed $6\sqrt{f'_c}$. If the bottom tension was greater than that stress limit, service deflection was required to be calculated and further analysis of the member to ensure adequate performance. In practical uses, the decompression moment is used in calculating the neutral axis as the prestressed member is progressively cracking due to loads. The decompression moment is equal to the stress in a prestressed member after losses multiplied by the section modulus for the bottom of the section. Using the stress in the member after losses equates to the initial amount of prestress in the section.

$$M_{dec} = S_b \left(\frac{P_e}{A} + \frac{P_e e}{S_b} \right) \qquad 2.8$$

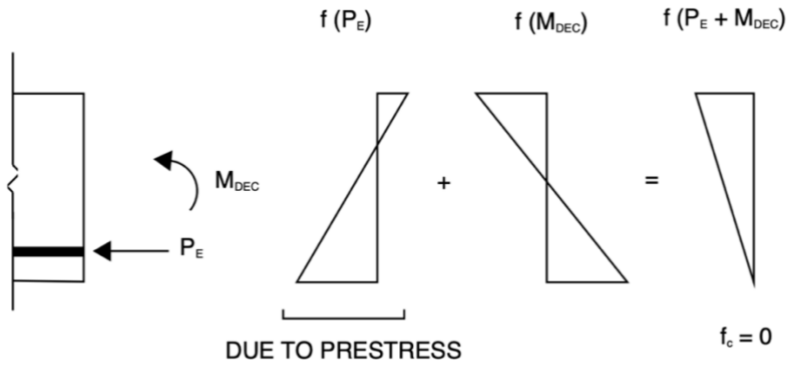

Figure 2.5 Superposition of decompression moment on prestressed concrete (Bachmann, 1984)

2.3 Development of Effective Moment of Inertia Equations

2.3.1 Branson

It was common practice for designers to use the average of the gross and cracked moment of inertias in deflection calculations (Branson, 1963). Advances in concrete performance in design and materials created a gap in knowledge of a deflections. The

previous methods used would not represent the behavior that occurred in the members. Branson identified that the serviceability of concrete members is important, as they can be seen and felt by the end user of the product. More accurate deflections became critical to the design and are needed to be considered when designing members. Branson states that variables affecting the short-time deflections of a prestressed concrete beam are the magnitude and distribution of the load, length of the span, the size and configuration of the cross section, and the quality of the concrete (Branson, 1963). Short-time deflections are synonymous to instantaneous deflections, mentioned previously. In addition to the importance of quality concrete which affects the modulus of elasticity of concrete, relaxation loss of the steel strands can impact the deflection of the member. Relaxation loss occurs from the stressed strand losing some of its initial stress after the strands have been cut and the concrete is curing around the strands.

Early in prestressed concrete analysis, a method to calculate deflections for cracked sections was to use the cracked transformed moment of inertia. This typically generated results that were too great and needed to be reduced. The factors placed in front of the deflections were dependent on the end span conditions; these correspond to simple beams, one end continuous, and both ends continuous for 2.9, 2.10, and 2.11 respectively (Branson, 1963).

$$\Delta = 0.9\Delta_{cr}^{t} \quad (2.9)$$

$$\Delta = 0.8\Delta_{cr}^{t} \quad (2.10)$$

$$\Delta = 0.7\Delta_{cr}^{t} \quad (2.11)$$

Previous methods smeared the average moment of inertia, between gross and cracked moment of inertia, across the length of the beam and did not represent behavior found in members between uncracked and cracked stress states. A downfall to this method and previous methods, is that they neglect to include the tension stiffening action in the concrete between the cracks. As members move into cracked behavior, tension stiffening occurs in the concrete. Tension stiffening is the contribution of tensile strength of concrete between cracks. Branson's new method of calculating a moment of inertia

between uncracked and cracked behavior would account for behaviors found in concrete members.

The effective moment of inertia was introduced in 1963, where an equation relating the cracking moment and applied moment, generated results between the two known cases, uncracked and cracked behavior. The effective moment of inertia includes the concrete in the tension zone that remains uncracked; as the cracks propagate along the section, the effective moment reduces until it is controlled by the cracked moment of inertial. This weighted average produced results that utilizes the tensile strength from the concrete between cracks, known as tension stiffening. Setting *m* to 4 includes the tension stiffening at the point of analysis; setting *m* to 3 approximates the effective moment of inertia over the entire section (Bischoff, 2005). Additionally, *M* is the total service moment. Codes began using the effective moment of inertia to calculate deflections in the 1970s for reinforced and prestressed concrete members (Branson and Trost, 1982).

$$I_{eff} = I_{ucr}^{t} - [I_{ucr}^{t} - I_{cr}^{t}]\left[1 - \left(\frac{M_{cr}}{M}\right)^{m}\right] \qquad 2.12$$

$$I_{eff} = \left[\left(\frac{M_{cr}}{M}\right)^{m}\right] I_g + [1 - \left(\frac{M_{cr}}{M}\right)^{m}] I_{cr}^{t} \qquad 2.13$$

Branson introduced another instantaneous deflection calculation for prestressed members. This method included the effects of prestressing and slightly shifted the cracking moment calculation. The new cracking moment included the prestressing force, shifting the cracking moment up. Branson's new method accounts for the upward deflection induced by camber of the member, seen in equation 2.15. The next portion of the calculation is the dead load deflection of the member. The moment dead, self-weight, and the sustained dead loads, is multiplied by the length squared and divided by the stiffness of the member, the modulus of elasticity of concrete multiplied by the gross moment of inertia. The next step in calculating the deflection is calculating the portion of the live load to produce zero deflection, M_{L1}, see equation 2.17. The total live load at the section, M_{L2}, is calculated by subtracting the applied live load moment by the live load causing zero deflection. M_{L2} is then used to calculate the deflection associated with the

total live load. This method does not explicitly use the effective moment of inertia, but parts of this procedure can be used to calculate a new effective moment of inertia, equation 2.22. Figure 2.6 shows the relationship of each deflection calculated in the procedure described above. Branson defined the prestressing deflection coefficient, K_p, equal to 0.0997 and defined both live and dead deflection coefficients, K_L and K_D, equal to 0.1042 or *5/48*. The dead and live load deflection coefficient were given values that were associated with uniformly distributed loads.

$$M'_{cr} = \frac{f_r I_g}{c_2} + \frac{P_e I_g}{A_g c_2} \quad 2.14$$

$$\Delta'_p = K_p P_e e_p L^2 / E_c I_g \quad 2.15$$

$$\Delta'_D = K_D M_D L^2 / E_c I_g \quad 2.16$$

$$M_{L1} = \left({K_p}/{K_l}\right) P_e e_p - \left({K_D}/{K_l}\right) M_D \quad 2.17$$

$$\Delta_{L1} = K_L M_{L1} L^2 / E_c I_g \quad 2.18$$

$$M_{L2} = M_L - M_{L1} \quad 2.19$$

$$\Delta_{L2} = K_L M_{L2} L^2 / E_c I_g \quad 2.20$$

$$\Delta = -\Delta'_p + \Delta'_D + \Delta_{L1} + \Delta_{L2} = \Delta_{L2} \quad 2.21$$

$$(I_e)_{L2} = \left(\frac{M'_{cr}}{M_{L2}}\right)^3 I_g + \left[1 + \left(\frac{M'_{cr}}{M_{L2}}\right)^3\right] I_{cr} \quad 2.22$$

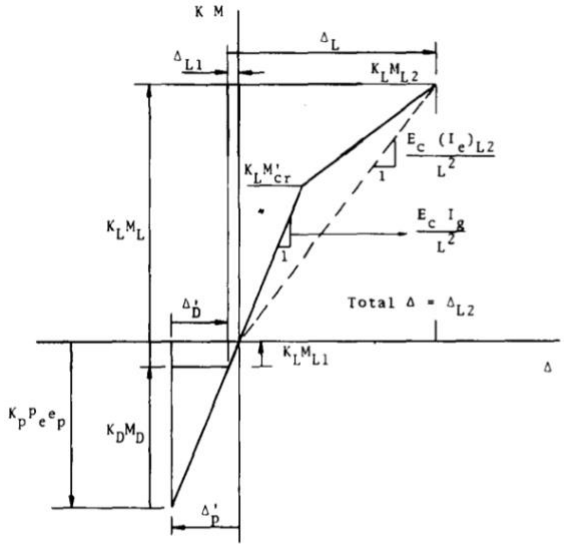

Figure 2.6. Idealized moment deflection graph (Branson and Trost, 1982)

The focus of Branson's work in the later portion of his career was on long-term deflections, more specifically timestep approaches for these deflections which is beyond the scope of this research.

2.3.2 Bischoff

Bischoff has worked and continues to work on generating more accurate deflection models for reinforced and prestressed concrete. In 2005, Bischoff introduced a new method of calculating the effective moment of inertia based off Branson's original equation for reinforced concrete.

Defining a member as cracked or transition does not mean that the entire length of the member is cracked, rather there is different behavior along the length of the member to account for the variation in stiffness. Typically cracking occurs at the critical section, midspan for uniformly distributed loads or where the concentrated load is placed, leaving the remainder of the member to be uncracked or transition sections. Branson's equation smears the effective moment of inertia across the length of the beam, which is not representative of the true behavior of the member.

To model stiffness along the length of the member, a simple spring system was analyzed for similar behavior. Simple springs are measured by their stiffness; when force is placed on the system the springs deform and return to their original state. Springs can be placed in either series or parallel and can be rotational or linear. Springs in series have displacements that are representative of their stiffness and the total displacement is a summation of all the displacements. Springs in parallel have total displacement that is equivalent to the other.

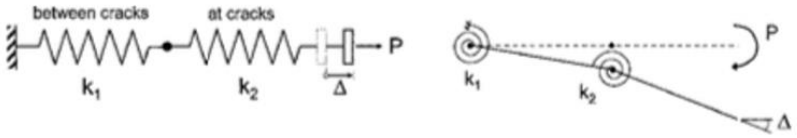

Figure 2.7. Springs in series (Bischoff and Scanlon, 2007)

Figure 2.8. Springs in parallel (Bischoff and Scanlon, 2007)

$$\frac{1}{k_e} = \frac{1}{k_1} + \frac{1}{k_2} \qquad 2.23$$

$$k_e = k_1 + k_2 \qquad 2.24$$

Branson's method of adding weighted averages together resembles the equation for springs in parallel. The behavior of cracked and transition concrete sections is like springs in series, as they have displacement representative of their stiffness and added together. Springs in parallel have displacement that is equivalent between the springs.

Bischoff and Scanlon related the different stiffnesses of springs to the uncracked and cracked stiffness of concrete (Bischoff and Scanlon, 2007). The simple spring analysis resulted in equating the uncracked and cracked members to be similar to springs in series. Bringing Branson's equation into the analysis, this method looked at the

stiffness as springs in parallel since the sum of the stiffnesses was equivalent to the total stiffness. Bischoff's inverse moment of inertia method has been adopted for traditionally reinforced concrete members in ACI 318-19 code. This equation has is being adapted for use in prestressed members but has been investigated for its viability through further analysis.

$$\frac{1}{I_e} = \left(\frac{M_{cr}}{M_a}\right)^m \frac{1}{I_g} + \left[1 - \left(\frac{M_{cr}}{M_a}\right)^m\right] \frac{1}{I_{cr}} \geq \frac{1}{I_g} \quad 2.25$$

$$I_e = \frac{I_{cr}}{1 - \left(\frac{M_{cr}}{M_a}\right)^m \left[1 - \frac{I_{cr}}{I_g}\right]} \leq I_g \quad 2.26$$

Bischoff introduced a rational model that would provide a more accurate method of predicting the effective moment of inertia by adjusting some factors in the inverted effective moment of inertia. Bischoff's rational method calculates the cracked section properties, using a new cracked moment of inertia equation that accounts for the total stress of the section. After the cracked neutral axis is calculated, the eccentricity from the cracked centroid to the reinforcement is found by the difference between the depth to the prestressing reinforcement and the cracked centroid.

$$f_{total} = \frac{P_e}{A_g} + \frac{P_e e_g y_t}{I_g} + f_r \quad 2.27$$

$$M_{cr} = \left(\frac{P_e}{A_g} + \frac{P_e e_g y_t}{I_g} + f_r\right) \frac{I_g}{y_t} = f_{total} * S_b \quad 2.28$$

$$c_{cr} = d_p \left[\sqrt{\left(d_p\right)^2 + 2n_p\rho_p} - n_p\rho_p\right] \quad 2.29$$

$$e_{cr} = d_p - c_{cr} \quad 2.30$$

The neutral axis is solved for by calculating a cubic root in 2.34 for the k'_{cr} term to determine the partially cracked neutral axis by equation 2.36. Alternatively, an iterative solution may be used to determine the neutral axis depth based on gross and

transition section properties (Mast, 1998). If the section is a tee or double tee beam and with the depth of the neutral axis greater than the thickness of the flange, equation 2.35 must be used with the appropriate factors shown below. Alternative means to calculating the neutral axis are shown in Example 5.2.2.5 and 5.2.2.6in the PCI Design Handbook.

$$A_{tps} = A_{ps} n_p \tag{2.31}$$

$$f_{dc} = f_{se} + n_p \left(\frac{P_e}{A_g} + \frac{P_e {e_g}^2}{I_g} \right) = E_p \Delta \varepsilon_p \tag{2.32}$$

$$P_o = f_{dc} A_{ps} \tag{2.33}$$

$$\frac{P_o d_p}{M_s} (k'_{cr})^3 + 3 \left[1 - \frac{P_o d_p}{M_s} \right] (k'_{cr})^2 - 6 n_p \rho_p [1 - k'_{cr}] = 0 \tag{2.34}$$

$$\begin{aligned} \frac{P_o d_p}{M_s} (k'_{cr})^3 + 3 \left[1 - \frac{P_o d_p}{M_s} \right] (k'_{cr})^2 \\ - 6 n_p \rho_p [1 - k'_{cr}] \\ - \alpha_b \left(k'_{cr} - \alpha_f \right)^2 \left[3 \right. \\ \left. - \frac{P_o d_p}{M_s} \left(3 - k'_{cr} - 2\alpha_f \right) \right] = 0 \end{aligned} \tag{2.35}$$

$$c'_{cr} = k'_{cr} d_p \tag{2.36}$$

$$\alpha_b = 1 - \frac{b_w}{b_f} \tag{2.37}$$

$$\alpha_f = \frac{h_f}{d_p} \tag{2.38}$$

$$A'_{cr} = A_{tps} + bc \tag{2.39}$$

$$\bar{y}'_{cr} = \frac{bc\left({}^{c}/_{2}\right) + A_{tps} d_p}{A'_{cr}} \tag{2.40}$$

$$I'_{cr} = \frac{bc^3}{12} + bc \left(\bar{y}'_{cr} - \frac{c}{2} \right)^2 + A_{tps} \left(d_p - \bar{y}'_{cr} \right)^2 \tag{2.41}$$

The next steps in Bischoff's rational method are calculating moment intercepts according to the decompression force. These moments are used to calculate the offset or shifted moment, M_1, where this shifts the deflection prediction according to prestressing and the tension stress state of the member.

$$M_{zc} = P_o e_g \quad (2.42)$$

$$M_o = P_o e_{cr} \quad (2.43)$$

$$M'_o = P_o e'_{cr} \quad (2.44)$$

When the applied moment is greater than the cracking moment and when the shifted moment, M_1, is less than the cracking moment, the shifted moment is calculated using 2.45. With the shifted moment, the effective moment of inertia is calculated by 2.46. If M_1 is larger than the cracking moment, equation 2.45 is no longer valid and another shift moment is calculated, M'_1. Under the new shifted moment, the partially cracked moment of inertia is calculated, see equation 2.41, and the new effective moment of inertia is calculated with equation 2.48. Once the load produces an M'_1 value greater than the cracking moment, the effective moment of inertia is to be taken as the partially cracked moment of inertia. As load continues to be applied, I'_{cr} converges to I_{cr} (Bischoff, 2022).

$$M_1 = \frac{\left[M_o - M_{zc}\left(\frac{I_{cr}}{I_g}\right)\right]}{1 - \frac{I_{cr}}{I_g}} \quad (2.45)$$

$$I_e{}^* = \frac{I_{cr}}{1 - \left(\frac{M_{cr} - M_1}{M_a - M_1}\right)^2 \left(1 - {I_{cr}}/{I_g}\right)} \quad (2.46)$$

$$M'_1 = \frac{\left[M'_o - M_{zc}\left(\frac{I'_{cr}}{I_g}\right)\right]}{1 - \frac{I'_{cr}}{I_g}} \quad (2.47)$$

$$I_e{}^* = \frac{I'_{cr}}{1 - \left(\frac{M_{cr} - M'_1}{M_a - M'_1}\right)^2 \left(1 - {I'_{cr}}/{I_g}\right)} \quad (2.48)$$

The final adjustment in this procedure is to adjust the load to reflect the shifted live load moment, M_1.

$$w'_1 = \frac{8M'_1}{L^2} \tag{2.49}$$

$$\Delta_L = (w'_1 - w_D)\frac{5L^4}{384E_cI_g} + (w_D + w_L - w'_1)\frac{5L^4}{384E_cI'_e} \tag{2.50}$$

With the understanding that the rational method is complex, Bischoff introduced a simplified trilinear method attempting to maintain accuracy in predicting the stiffness of members yet remain straightforward in calculation. The trilinear method uses the same cracked section properties, decompression stresses, and some of the same moment intercepts as shown previously. The trilinear method introduces a moment at the second change in slope, *M''* taken as 1.5 times the decompression moment. Using the trilinear method avoids calculating the neutral axis of the section to calculate the cracked moment of inertia. This intermediate cracked moment of inertia, equation 2.52, models the behavior between gross and cracked moment of inertias. Similar to the rational method introduced previously, the cracking load can be shifted to fit the deflection using equations 2.53 and 2.54.

$$M'' = 1.5M_o \tag{2.51}$$

$$I''_{cr} = \left[\frac{(M'' - M_{cr})}{(M'' - M_o) - (M_{cr} - M_{zc})\left(I_{cr}/I_g\right)}\right] I_{cr} \tag{2.52}$$

$$w_{cr} = \frac{8M_{cr}}{L^2} \tag{2.53}$$

$$\Delta_L = (w_{cr} - w_D)\frac{5L^4}{384E_cI_g} + (w_D + w_L - w_{cr})\frac{5L^4}{384E_cI''_{cr}} \tag{2.54}$$

2.3.3 Auburn University

Research conducted recently by Yendle Hughes at Auburn University introduced a new method calculating immediate deflections for class T and C prestressed beams (2023). This work focused on the decompression moment and its relationship within Branson's effective moment of inertia equation. The addition of the decompression moment into the effective moment of inertia equation helps quantify the tension stiffening that occurs in prestressed members as the section becomes more cracked. The new method, equation 2.55 is applied similarly to the application of the current effective moment of inertia. Uncracked section properties are used to calculate deflection until the applied moment equals the decompression moment. After the load exceeds the decompression moment, the new I_e equation is used to calculate deflection. A comparison of the performance between the new method and other methods was conducted to validate the latest iteration of the effective moment of inertia equation.

$$I_e = \left(\frac{M_{cr} - M_{dec}}{M_a - M_{dec}}\right)^3 I_g + \left[1 - \left(\frac{M_{cr} - M_{dec}}{M_a - M_{dec}}\right)^3\right] I_{cr} \qquad 2.55$$

3 Database

3.1 Database Selection

Deflection-specific testing with typical sections found in practice is rare and much of the database is from other types of testing, i.e., shear or flexure papers that include applied moment and deflection curves. The following will describe the section properties and testing conditions for the members in this database.

3.1.1 Aswad et. al. 2004

Aswad et. al. tested three full sized double tee specimens. The primary goal of this research was to test full size double tee members without web reinforcement. Each specimen was 12 ft wide, 30 in. deep, and 62 ft span. The specimens used straight, low relaxation strands with 270 ksi yield stress and 6,000 psi design compressive strength. Three different manufacturers produced the different specimens which correspond to

differing areas of prestressed strand or mild steel reinforcement. The testing sequence for each member was patterned to simulate a simply supported uniformly loaded member at different stress levels until failure. The first loading stage was when the anticipated first flexural cracking occurred, at the modulus of rupture. The second stage was full live load. Third loading stage corresponded to an intermediate load intensity equal to $w_1 = 0.85(1.4D + 1.7L)$ (ACI-318, 2002). The fourth stage was equal to the ultimate load as predicted by $w_2 = w_u = 1.2D + 1.6L$. The final loading, stage five, was equivalent to the anticipated failure load given by $w_3 = (1.2D + 1.6L)/0.9$. Overall, the loading schedule set by Aswad et. al. generated results that a typical double tee would encounter in service and then increase the loading to the expected failure load.

Specimen one used twenty 1/2 in. special strands, area of prestress of the strand is 0.167 square in. and this specimen did not have mild steel. The strands were stressed to approximately 69%. Additionally, four of these strands were debonded for 10 ft from each end. The testing pattern for this specimen used 3 kip blocks arranged as shown in Figure 3.1. At ultimate failure, the measured deflection was 39 in.

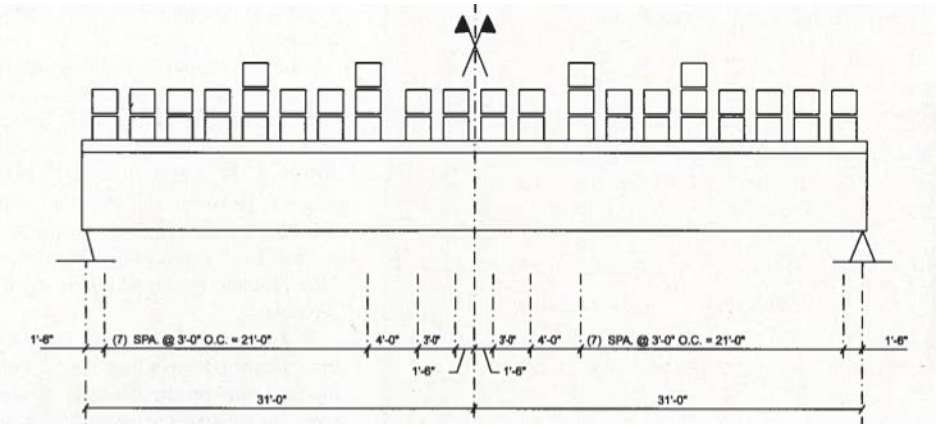

Figure 3.1. Failure loading pattern for specimen one (Aswad, et. al., 2004)

Specimen two used fourteen 9/16 in. strand, with the steel stressed to 75% of yield. Mild steel of specimen two was a single 20 ft. number 6 bar placed 5 in. above the bottom of each stem, centered at midspan. For testing of specimen two, 5.7 kip blocks

were loaded across the length and additional 2.75 kip blocks placed at 16 ft from each end, see Figure 3.2. The final deflection at failure was 39 in. for specimen two.

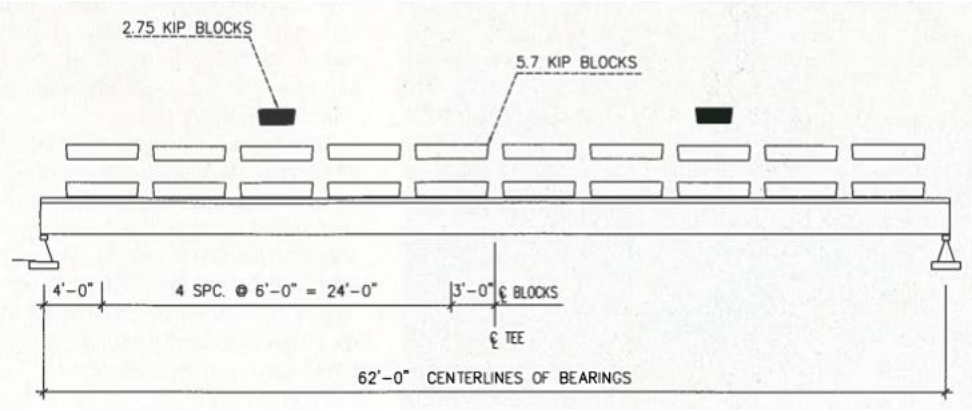

Figure 3.2. Failure loading pattern for specimen two (Aswad, et. al., 2004)

Specimen three had twelve 9/16 in. strand with the strands stressed to 75% yield. One number 7 bar was placed 7 in. above the bottom for 20 ft. centered at midspan in each stem. To achieve the desired loading, a mixture of 2.531 kip, 1.114 kip, and 1.138 kip blocks were placed, see Figure 3.3 for reference. Failure loading resulted in deflection of 16 in. for specimen three.

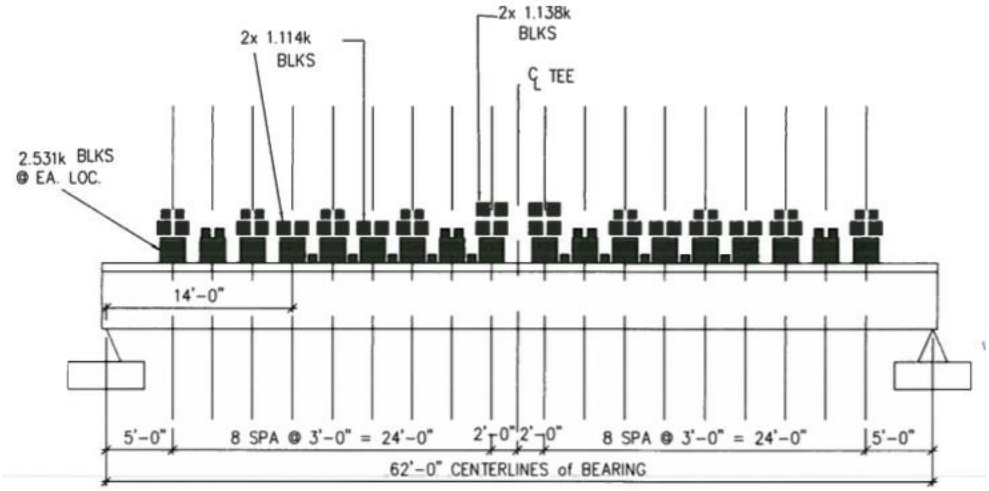

Figure 3.3. Failure loading pattern for specimen three (Aswad, et. al., 2004)

3.1.2 Frosch and Saqan 2009

Frosch and Saqan tested nine 14 in. by 28 in. nominal beams for shear strength while considering the flexural reinforcement. There were three series of differing prestressing strand amounts and within those three series consisted of three beams with different levels of mild steel in the section. The first series had four presetressing strands and varying amounts of mild steel. The first had no additional mild steel, the second had three number 5 bars placed, and the third section had three number 8 bars. The second series consisted of sections with 7 strands and varying amounts of mild steel. Similar to the previous series, the first specimen had no additional mild steel, the second specimen had four number 5 bars and one number 7 bar added, and the third had three number 8 bars placed in the section. The final series of members used 10 prestressing strands with varied mild steel additions. The first specimen had no additional mild steel, second had one number 5 bar and two number 7 bars, and the third specimen had three number 8 bars in the section. The design compressive strength was 6000 psi with actual compressive strength values as high as 7900 psi. The members were tested under simply supported conditions with a concentrated point load at midspan; specimens were tested until failure.

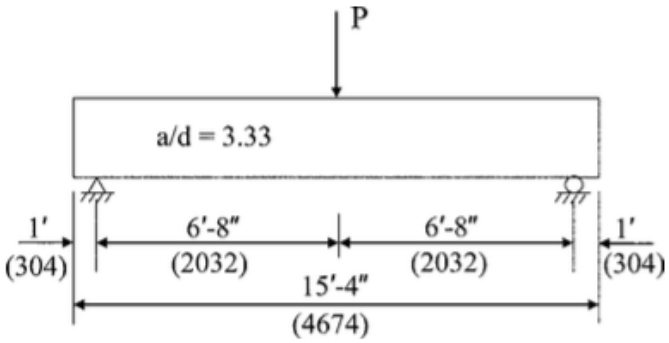

Figure 3.4. Load diagram for Frosch and Saqan test specimens (Frosch and Saqan, 2009)

3.1.3 Kulzer 2022

A total of twelve specimens were tested by Kulzer comprising of three beams with four variations. Each cross sections were 12 in. by 18 in. deep with a design compressive strength of 10,000 psi. Each specimen spanned 18 ft 6 in. and was simply

supported on pin and roller supports. The strands used in this project were 270 ksi 1/2 in. low relaxation strands stressed to 70% yield. The first series of beams used five prestressed strands with no additional tension mild steel reinforcement. The second series of beams used 5 prestressed strands and a second layer of tension reinforcement consisting of two number 6 rebar lengths. This series also debonded one of the prestressed strands over the full length of the strand so it was not part of the prestressing force (it was an artifact of the fabrication setup). The third set of test specimens consisted of one layer of tension reinforcement containing three prestressed strands with two number 8 bars. The final set of specimens used two layers of tension reinforcement with the lowest level containing three prestressed strands and two number 8 bars and the second layer of reinforcement containing two number 5 bars. Additionally, one prestressed strand was debonded for the length of the strand. The load was applied to each specimen using a spreader beam and actuator until failure, see Figure 2.3. The goal of this project was to gather more data for deflection in transition and cracked prestressed concrete members.

3.1.4 Metromont 2022

Two full size double tee specimens were provided and tested by Metromont Corporation under the Jenny Research PCI fellowship grant. Kulzer (2022) conducted the testing setup and compressive strength testing for the specimens. The specimens were 10 ft 8 5/8 in. wide, 2 ft 6 in. deep, and spanned 60 ft 1/2 in. in length. Bearing pads beneath the double tee stems at each end consisted of a 5 1/2 in. by 5 1/2 in. rubber pads atop steel plates. Each specimen used sixteen 1/2 in. special strands stressed to 70% yield and had four strands debonded for 5 ft at each end. There was no additional mild steel or welded wire reinforcement added to these specimens. Testing the specimens consisted of placing 5 kip blocks using the spacing provided in Figure 3.5. The arrangement and concentration of the blocks was to create a loading pattern similar to service loading, uniformly distributed loads.

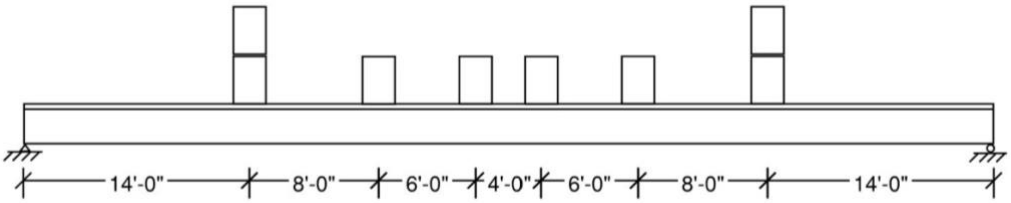

Figure 3.5. Loading diagram for Metromont specimens

3.2 Equation Selection

Sections 1 and 2 outlined the research that went into developing the current methods used in predicting deflections. The equations used in this study include Branson's effective moment of inertia, PCI's bilinear, Rational method, Trilinear, and Auburn's method. The methods were selected on their use in practice and/or ability to effectively calculate the deflections according to literature. Using the specimens discussed in section 3.1, the methods were used to predict the deflections.

3.3 Database Information

The tables in this section summarize the key variables of the members in the database used in the analysis for this research.

Table 3.1 Specimen label, section shape, span, loading data

Label as noted in original testing	Member Label	Section Shape	Span	Loading
V-4-0	FS_4.0	R	13'-4"	1P
V-4-0.93	FS_4.1	R	13'-4"	1P
V-4-2.37	FS_4.2	R	13'-4"	1P
V-7-0	FS_7.0	R	13'-4"	1P
V-7-1.84	FS_7.1	R	13'-4"	1P
V-7-2.37	FS_7.2	R	13'-4"	1P
V-10-0	FS_10.0	R	13'-4"	1P
V-10-1.51	FS_10.1	R	13'-4"	1P
V-10-2.37	FS_10.2	R	13'-4"	1P
U-1	K_U1	R	18'-6"	2P
U-2	K_U2	R	18'-6"	2P
U-3	K_U3	R	18'-6"	2P

Label as noted in original testing	Member Label	Section Shape	Span	Loading
T-1	K_T1	R	18'-6"	2P
T-2	K_T2	R	18'-6"	2P
T-3	K_T3	R	18'-6"	2P
CA-1	K_CA1	R	18'-6"	2P
CA-2	K_CA2	R	18'-6"	2P
CA-3	K_CA3	R	18'-6"	2P
CB-1	K_CB1	R	18'-6"	2P
CB-2	K_CB2	R	18'-6"	2P
CB-3	K_CB3	R	18'-6"	2P
DT for T Design	M_T	DT	60'-0"	UDL
DT for C Design	M_C	DT	60'-0"	UDL
DT1	A_1	DT	62'-0"	UDL
DT2	A_2	DT	62'-6"	UDL
DT3	A_3	DT	62'-8"	UDL

Table 3.2 Geometric section properties

Member Label	b (in.)	b_f (in.)	h (in.)	h_f (in.)	A (in.)	I_g ($in.^4$)	y_s (in.)	y_{top} (in.)	y_{bot} (in.)	S_{top} ($in.^3$)	S_{bot} ($in.^3$)
FS_4.0	14.25		28	0	399	26068	4	14	14	1862	1862
FS_4.1	14.5		28	0	406	26525	4	14	14	1895	1895
FS_4.2	14.68		28	0	411	26855	4	14	14	1918	1918
FS_7.0	14.12		28	0	395	25830	4	14	14	1845	1845
FS_7.1	14.25		28	0	399	26068	4	14	14	1862	1862
FS_7.2	14		28	0	392	25611	4	14	14	1829	1829
FS_10.0	14.25		28	0	399	26068	4	14	14	1862	1862
FS_10.1	14.25		28	0	399	26068	4	14	14	1862	1862
FS_10.2	14.25		28	0	399	26068	4	14	14	1862	1862
K_U1	12		18	0	216	5832	2	9	9	648	648
K_U2	12		18	0	216	5832	2	9	9	648	648
K_U3	12		18	0	216	5832	2	9	9	648	648
K_T1	12		18	0	216	5832	2	9	9	648	648
K_T2	12		18	0	216	5832	2	9	9	648	648
K_T3	12		18	0	216	5832	2	9	9	648	648

Member Label	b (in.)	b_f (in.)	h (in.)	h_f (in.)	A (in.)	I_g (in.^{4})	y_s (in.)	y_{top} (in.)	y_{bot} (in.)	S_{top} (in.^{3})	S_{bot} (in.^{3})
K_CA1	12		18	0	216	5832	2	9	9	648	648
K_CA2	12		18	0	216	5832	2	9	9	648	648
K_CA3	12		18	0	216	5832	2	9	9	648	648
K_CB1	12		18	0	216	5832	2	9	9	648	648
K_CB2	12		18	0	216	5832	2	9	9	648	648
K_CB3	12		18	0	216	5832	2	9	9	648	648
M_T*	10.25	128	30	4	798	50169	9.625	6.43	23.57	7802	2129
M_C*	10.25	143.5	30	4	858	51500	9.63	6.43	23.57	8009	2185
A_1*	12.9	144	30	4	911	61708	9.63	7.2	22.8	8571	2706
A_2*	10.76	144	30	4	856	54827	8	6.67	23.33	8220	2350
A_3*	14	144	30	4	940	68322	5.82	7.63	22.37	8954	3054

*b_w was taken as the average stem width multiplied by the number of stems in the section

Table 3.3 Mild reinforcement

Member Label	a_s (in.^{2})	d (in.)
FS_4.0		
FS_4.1	0.93	26
FS_4.2	2.37	26
FS_7.0		
FS_7.1	1.84	26
FS_7.2	2.37	26
FS_10.0		
FS_10.1	1.51	26
FS_10.2	2.37	26
K_U1		
K_U2		
K_U3		
K_T1	0.88	14
K_T2	0.88	14
K_T3	0.88	14
K_CA1	1.58	16
K_CA2	1.58	16
K_CA3	1.58	16
K_CB1	2.2	15.37
K_CB2	2.2	15.37

Member Label	a_s (in.^{2})	d (in.)
K_CB3	2.2	15.37
M_T		
M_C		
A_1		
A_2	0.88	25
A_3	1.2	23

Table 3.4 Prestressed reinforcement and properties

Member Label	No. Strands	Strand Type	a_{ps} (in.2)	d_{ps} (in.)	e (in.)	ρ_p	f_{se} (ksi)	P_e (kip)
FS_4.0	4	1/2"	0.612	24	10	0.18%	176.5	108.0
FS_4.1	4	1/2"	0.612	24	10	0.18%	176.5	108.0
FS_4.2	4	1/2"	0.612	24	10	0.17%	176.5	108.0
FS_7.0	7	1/2"	1.071	24	10	0.32%	103.0	110.3
FS_7.1	7	1/2"	1.071	24	10	0.31%	103.0	110.3
FS_7.2	7	1/2"	1.071	24	10	0.32%	103.0	110.3
FS_10.0	10	1/2"	1.53	24	10	0.45%	72.6	111.1
FS_10.1	10	1/2"	1.53	24	10	0.45%	72.6	111.1
FS_10.2	10	1/2"	1.53	24	10	0.45%	72.6	111.1
K_U1	5	1/2"	0.765	16	7	0.40%	158.5	121.3
K_U2	5	1/2"	0.765	16	7	0.40%	158.5	121.3
K_U3	5	1/2"	0.765	16	7	0.40%	158.5	121.3
K_T1	5	1/2"	0.765	16	7	0.40%	163.6	125.2
K_T2	5	1/2"	0.765	16	7	0.40%	163.6	125.2
K_T3	5	1/2"	0.765	16	7	0.40%	163.6	125.2
K_CA1	3	1/2"	0.459	16	7	0.24%	169.0	77.6
K_CA2	3	1/2"	0.459	16	7	0.24%	169.0	77.6
K_CA3	3	1/2"	0.459	16	7	0.24%	169.0	77.6
K_CB1	3	1/2"	0.459	16	7	0.24%	169.1	77.6
K_CB2	3	1/2"	0.459	16	7	0.24%	169.1	77.6
K_CB3	3	1/2"	0.459	16	7	0.24%	169.1	77.6
M_T	16	1/2" Spc.	2.672	20.375	13.94	0.10%	166.9	445.9
M_C	16	1/2" Spc.	2.672	20.375	13.94	0.09%	170.5	455.5
A_1	20	1/2" Spc.	3.34	24.375	13.17	0.10%	159.2	531.8
A_2	14	9/16"	2.688	26	15.33	0.07%	174.3	468.5
A_3	12	9/16"	2.304	28.18	16.55	0.06%	174.7	402.5

4 Deflection Prediction Results

4.1 Section Analysis Methods

A total of 26 specimens described in section 3 were analyzed. Spreadsheets were developed to calculate the deflections according to each method. The predictions accounts for the prestressed and mild reinforcement in gross section properties. In specimens with material data, the experimental compressive strength was used. Each section was analyzed along length of the member at one tenth of the total length increments. The critical section for the predictions was the midspan deflection; the deflections from testing were measured at the midspan. The specimens were analytically loaded in increments until the moment applied was greater than the applied load in testing. The goal of the incremental loading was to generate a moment deflection plot to compare to the measured results. The midspan deflection was calculated using the Branson, PCI, Auburn, Rational, and Trilinear methods.

The deflections were predicted using Excel to enter each step of the method. Each method included the calculation of stresses to determine the classification of the beam. Branson and PCI methods did not require any additional checks beyond if the beam was in transition or cracked level stresses to utilize the effective moment of inertia. Their simplicity reduced potential for errors and was computationally efficient. Auburn, Rational, and Trilinear methods required calculating shifted moments and determining the neutral axis. To calculate the neutral axis, Mast's iterative method was implemented by using the Goal Seek function in excel that was used to fast track the iterations (Mast, 1999). The simplicity of the Branson and PCI methods allowed for minimal hassle in setup. These methods did not require the calculation of cracked transformed sections in determining the effective moment of inertia.

4.2 Moment Deflection Curves

The moment deflection curves plotted the behavior of the specimen during loading. Positive deflection plotted on the graph corresponds to the downward deflection and negative deflection reflects the upward camber because of the initial prestressing. Key stress limits, which include the modulus of rupture, $12\sqrt{f'_c}$, compression limit, decompression, and service moments, were plotted to identify the critical load points in

the member. The following graphs, Figure 4.1 through Figure 4.26, will show the predicted and measured behavior compared to the key stress limits.

The camber due to prestressing was only measured for one of the test groups, Aswad double tees. Due to insufficient data on initial camber for the other testing groups, the plotted moments begin at the self-weight moment and plotted the change in deflection from that point. The behavior plotted for the specimens is in agreement with the mechanics of prestressed concrete members, where the slope initially displays elastic behavior and softens as the neutral axis of the section reduces due to cracking. The plots with stress and moment limits identifies where there are discrepancies between experimental behavior and predicted. See Appendix A: Moment Deflection Curves the full moment deflection of each specimen.

Specimens with larger quantities of mild reinforcement tended to retain more stiffness as the member continued to crack. In the moment deflection plots, elastic behavior was shown until initial cracking for all of the specimens. The moment cracking was accurately estimated for the sections without the addition of mild reinforcement. For the sections that had the additional mild reinforcement, softening of the member after the elastic section was extended and provided more stiffness than anticipated by the prediction methods. Frosch and Saqan figures showed the performance of Branson, PCI, and Auburn methods having greater accuracy to estimate the deflection as the loads increased. The performance of all deflection methods greatly decreased as the moment exceeded the stress limit of $12\sqrt{f'_c}$. For Kulzer specimens predicted with the PCI method and most of the other methods, it diverged. In the moment deflection curves, the measured data is noticeably less stiff during the uncracked stress phase of testing. The data measured from the Kulzer specimens diverged from the anticipated behavior from all of the prediction methods. The behavior of the Metromont specimens displayed elastic properties as predicted for the transition section, M_T, but had a slightly softer elastic section for the cracked specimen, M_C. Under service loads, the Branson equation appears to estimate the deflection accurately for M_T where the PCI and Auburn methods appear to have better performance in M_C. After service loads, the methods PCI and Auburn methods performed well compared to the measured deflections until the

specimens had completed the test. For the Aswad et. al. (2004) sections, the service load deflections were best estimated using the Branson equation. But as the member continued to deflect, the PCI and Auburn methods predicted the deflections with more accuracy.

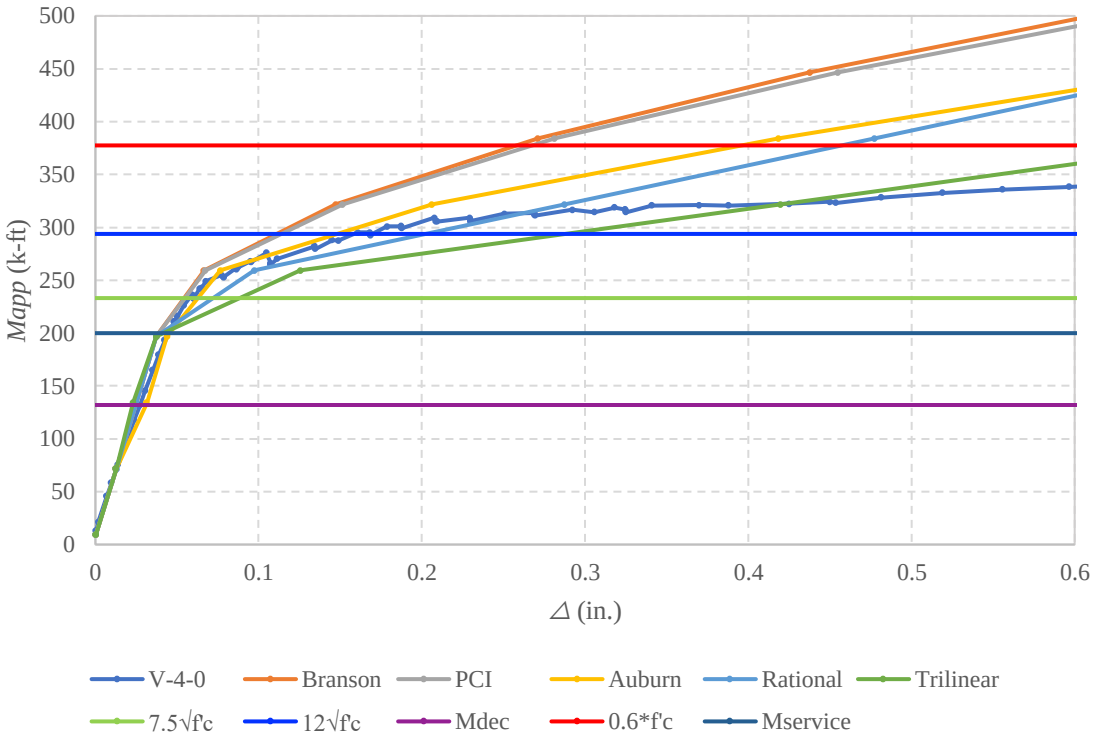

Figure 4.1 FS_4.0 moment deflection curve plotted with transition and cracked stress limits, compression limit, decompression moment, and service moments

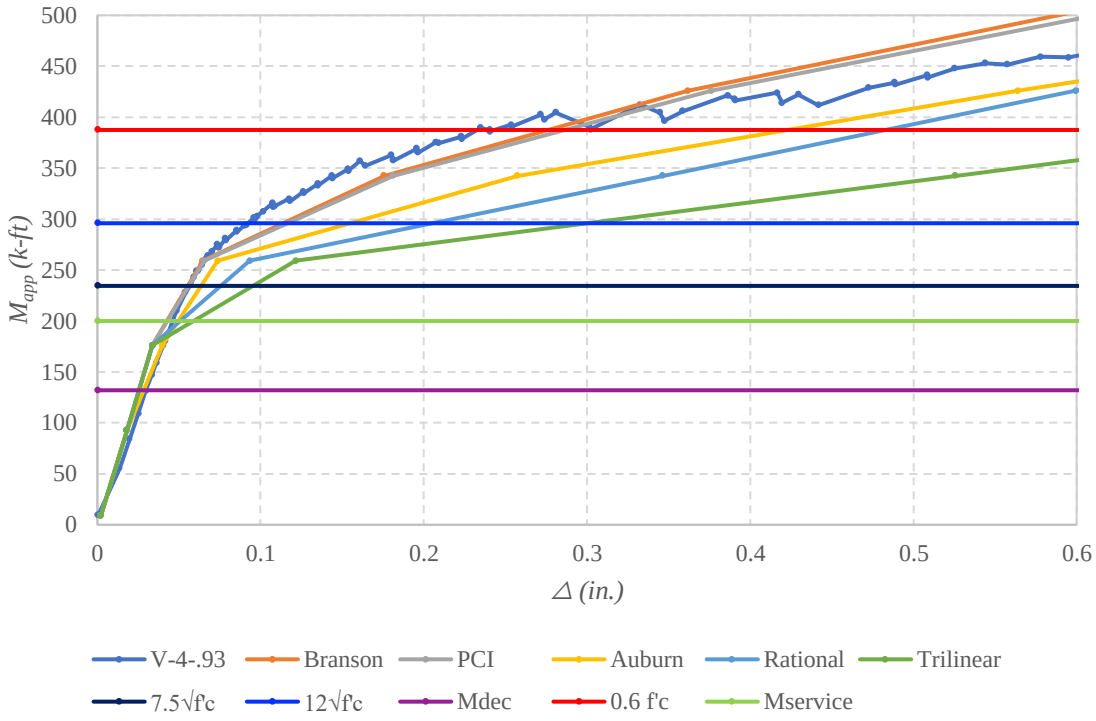

Figure 4.2 FS_4.1 moment deflection curve plotted with transition and cracked stress limits, compression limit, decompression moment, and service moments

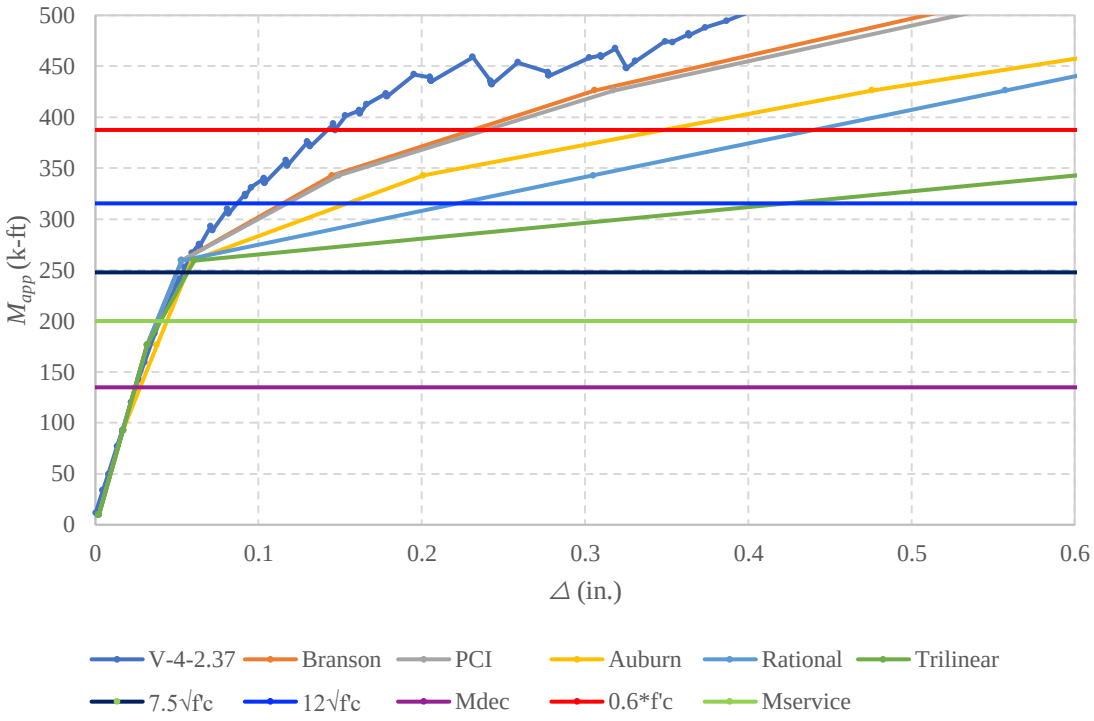

Figure 4.3 FS_4.2 moment deflection curve plotted with transition and cracked stress limits, compression limit, decompression moment, and service moments

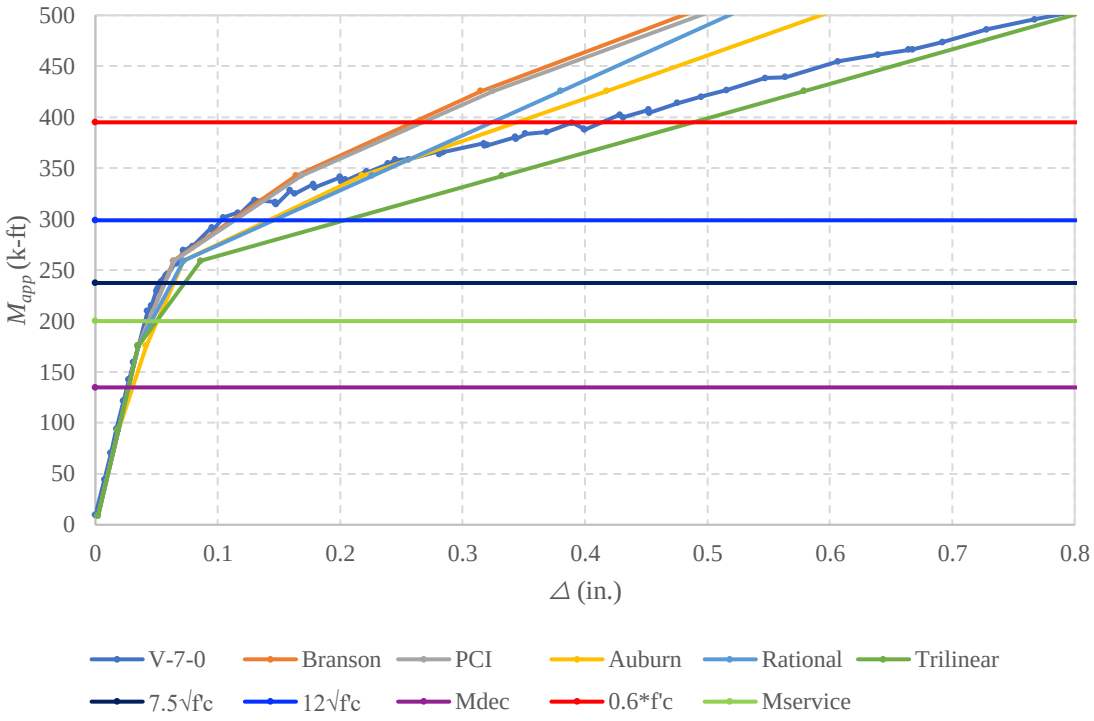

Figure 4.4 FS_7.0 moment deflection curve plotted with transition and cracked stress limits, compression limit, decompression moment, and service moments

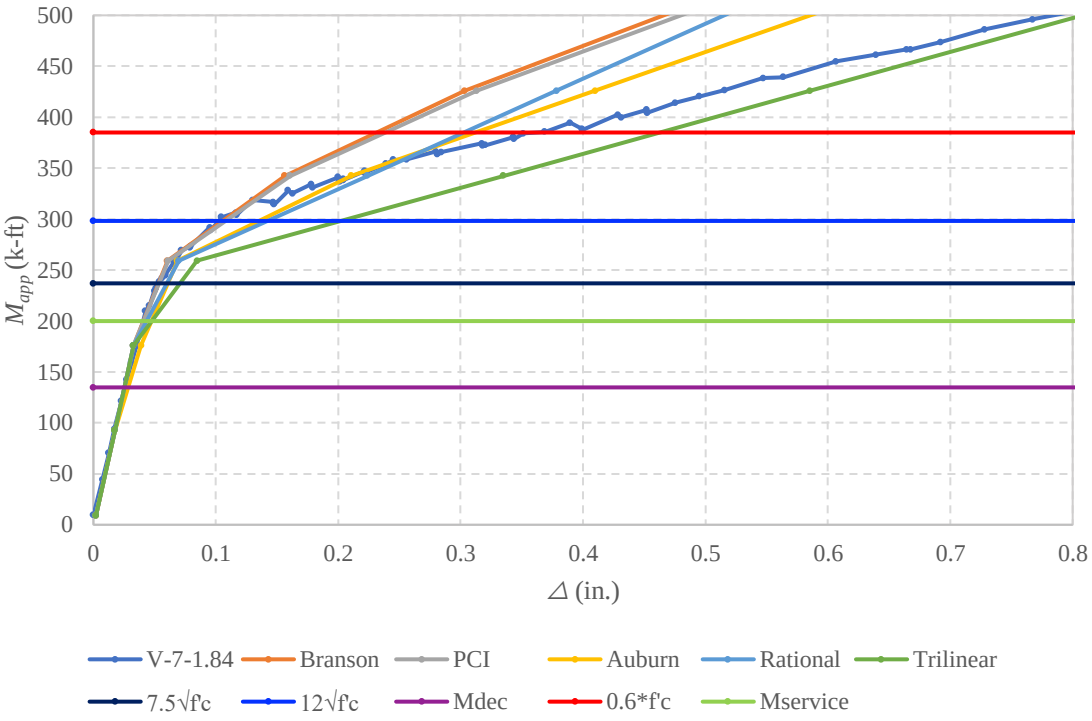

Figure 4.5 FS_7.1 moment deflection curve plotted with transition and cracked stress limits, compression limit, decompression moment, and service moments

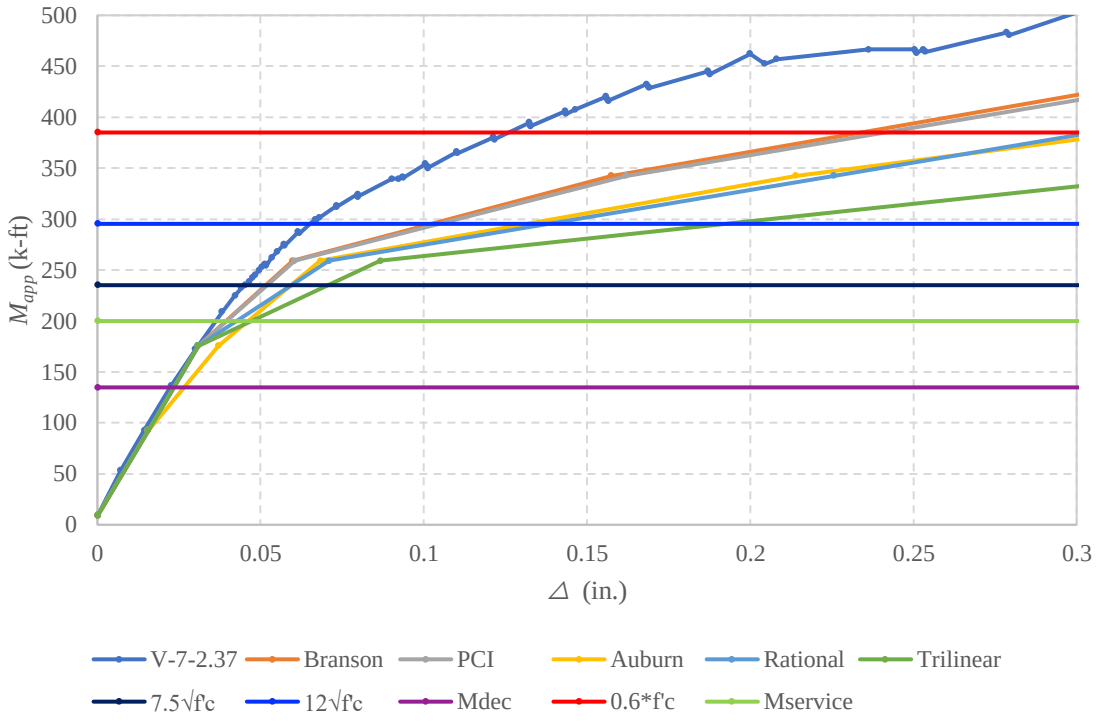

Figure 4.6 FS_7.2 moment deflection curve plotted with transition and cracked stress limits, compression limit, decompression moment, and service moments

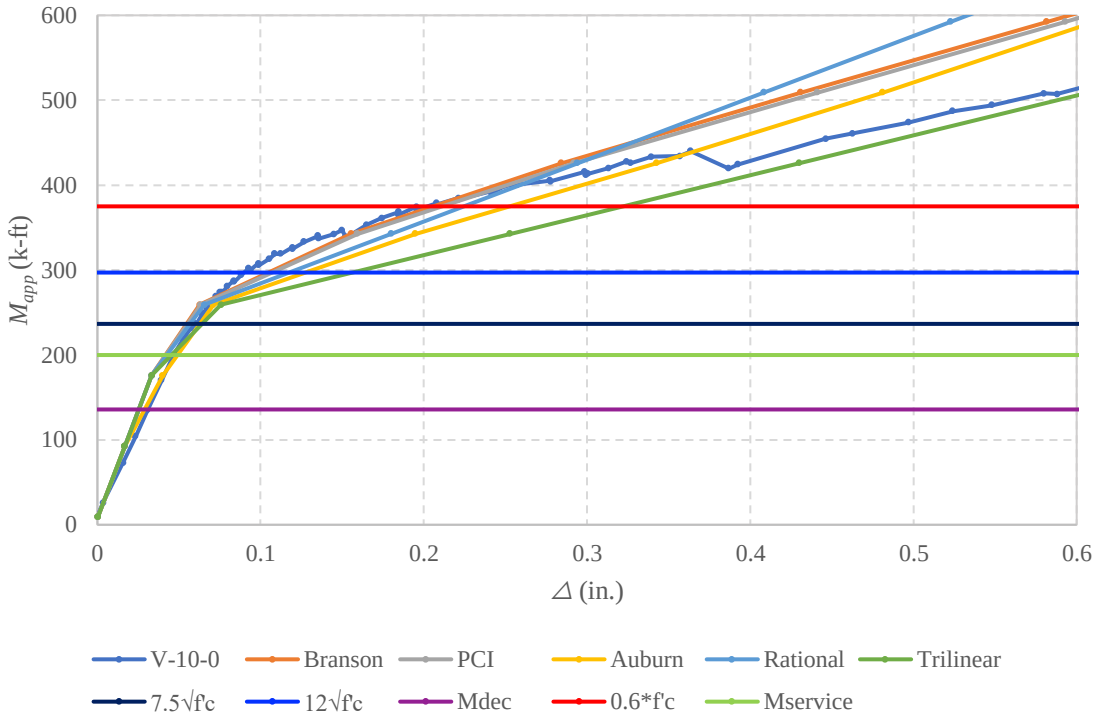

Figure 4.7 FS_10.0 moment deflection curve plotted with transition and cracked stress limits, compression limit, decompression moment, and service moments

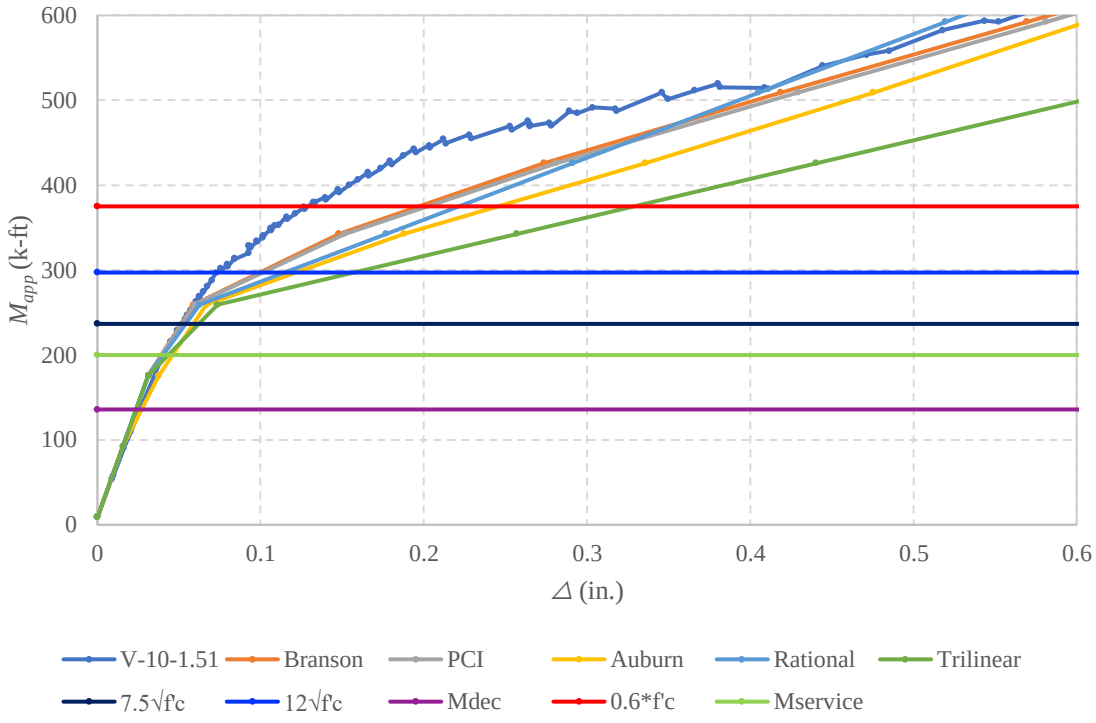

Figure 4.8 FS_10.1 moment deflection curve plotted with transition and cracked stress limits, compression limit, decompression moment, and service moments

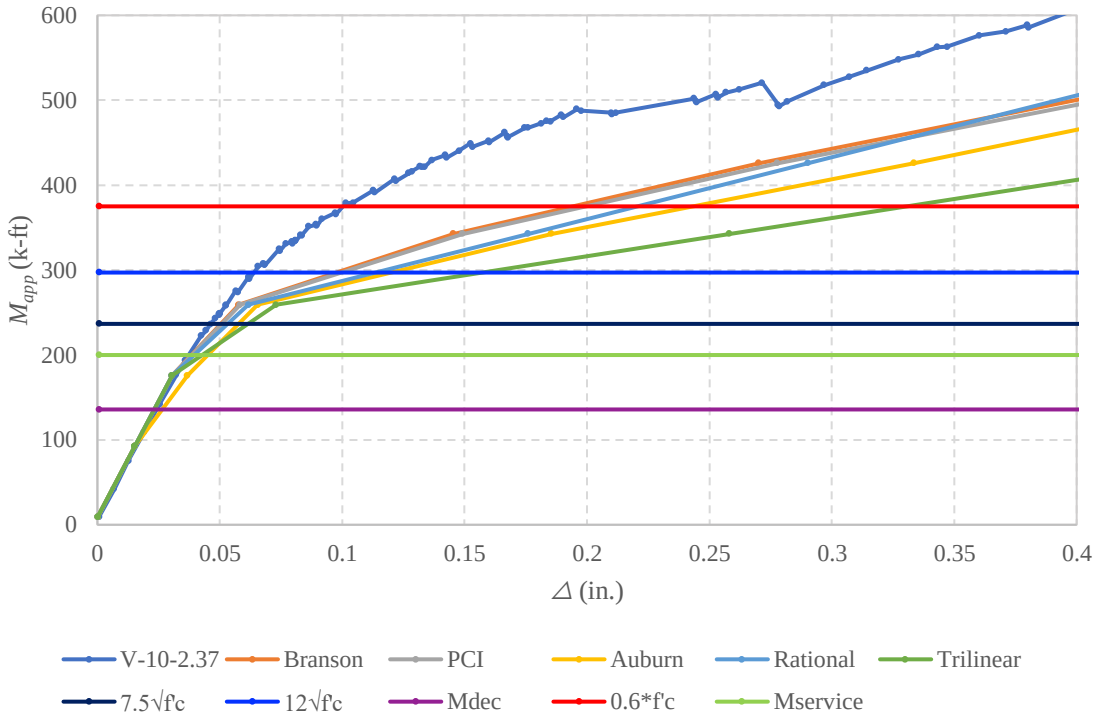

Figure 4.9 FS_10.2 moment deflection curve plotted with transition and cracked stress limits, compression limit, decompression moment, and service moments

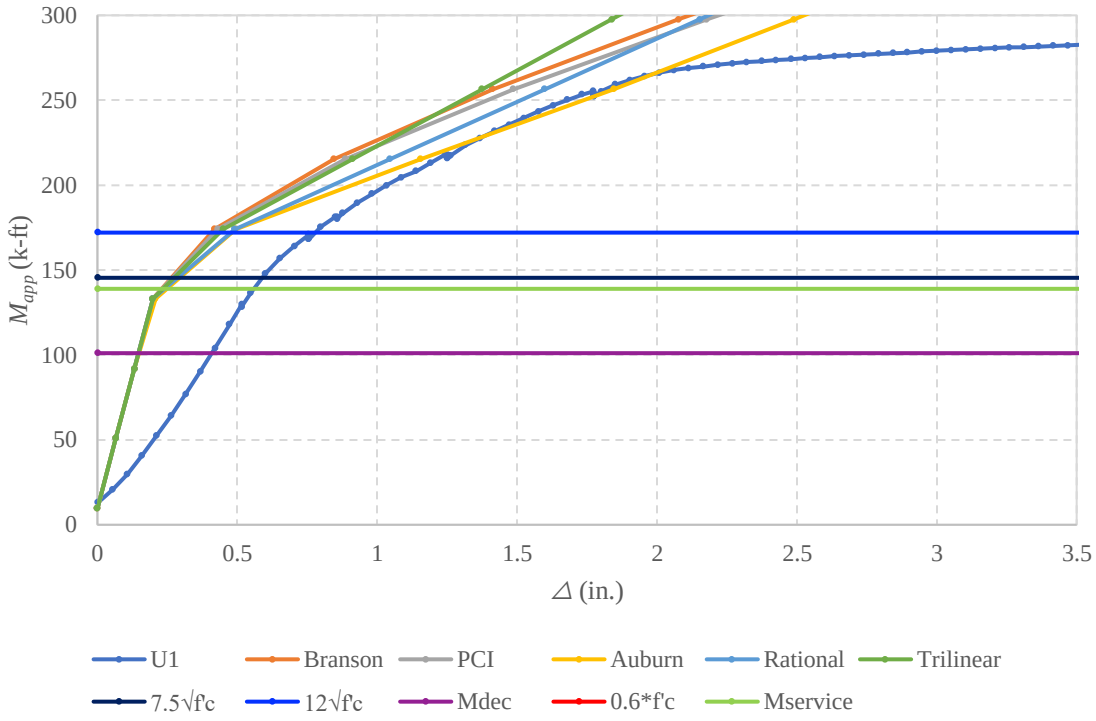

Figure 4.10 K_U1 moment deflection curve plotted with transition and cracked stress limits, compression limit, decompression moment, and service moments

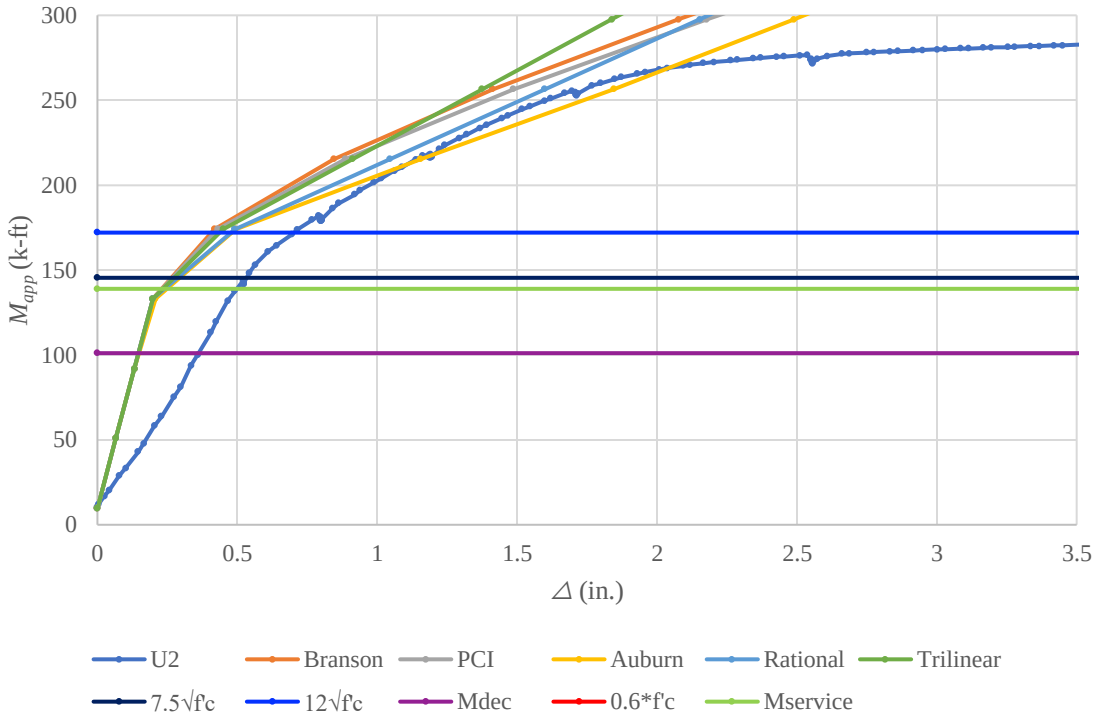

Figure 4.11 K_U2 moment deflection curve plotted with transition and cracked stress limits, compression limit, decompression moment, and service moments

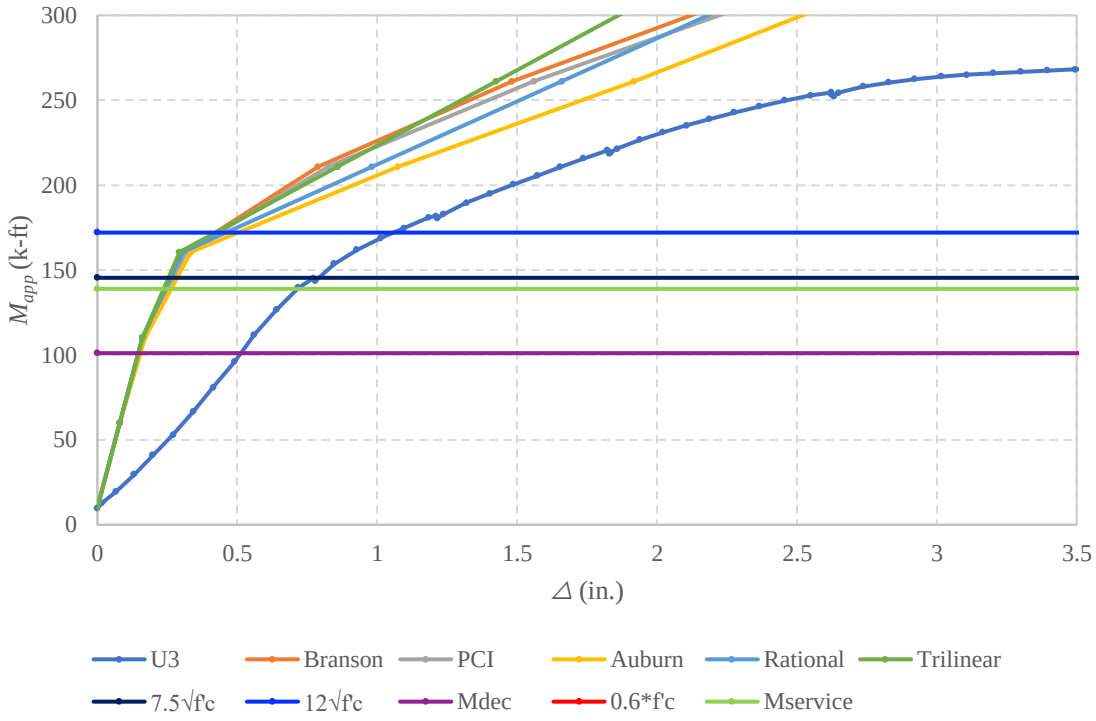

Figure 4.12 K_U3 moment deflection curve plotted with transition and cracked stress limits, compression limit, decompression moment, and service moments

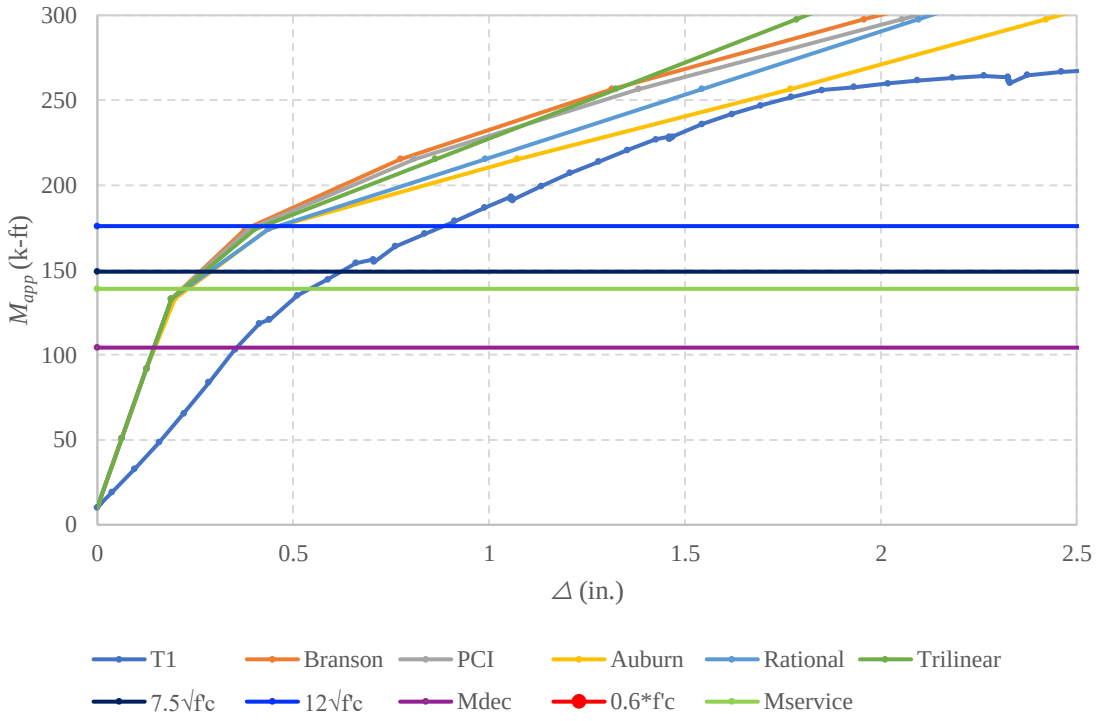

Figure 4.13 K_T1 moment deflection curve plotted with transition and cracked stress limits, compression limit, decompression moment, and service moments

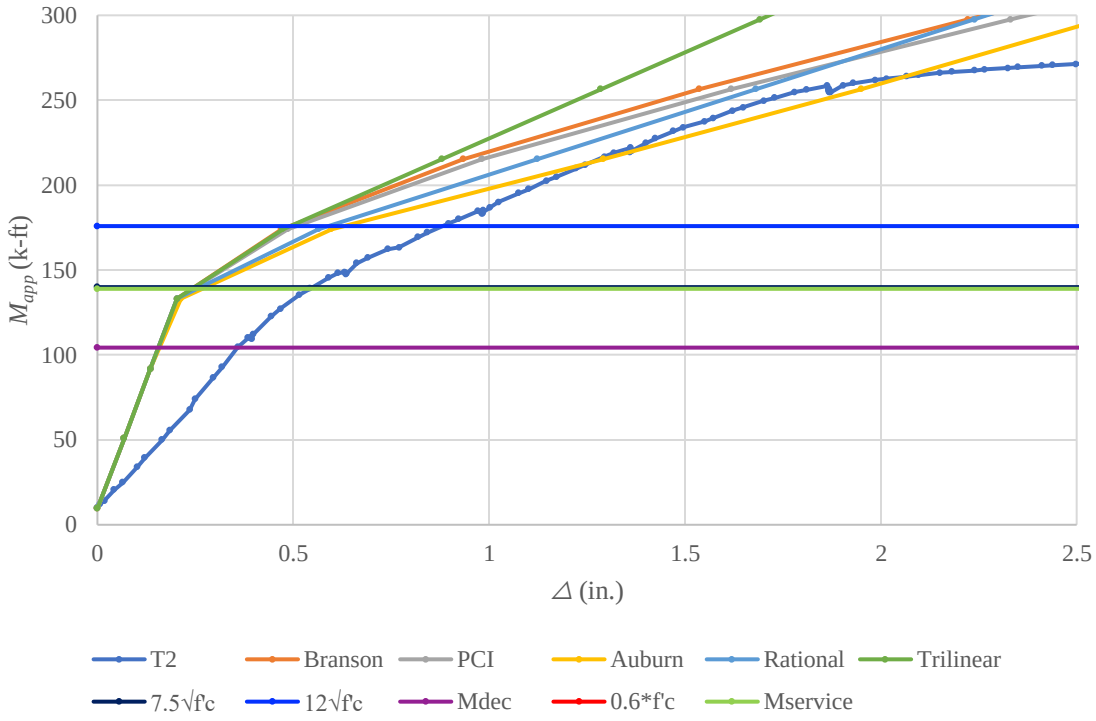

Figure 4.14 K_T2 moment deflection curve plotted with transition and cracked stress limits, compression limit, decompression moment, and service moments

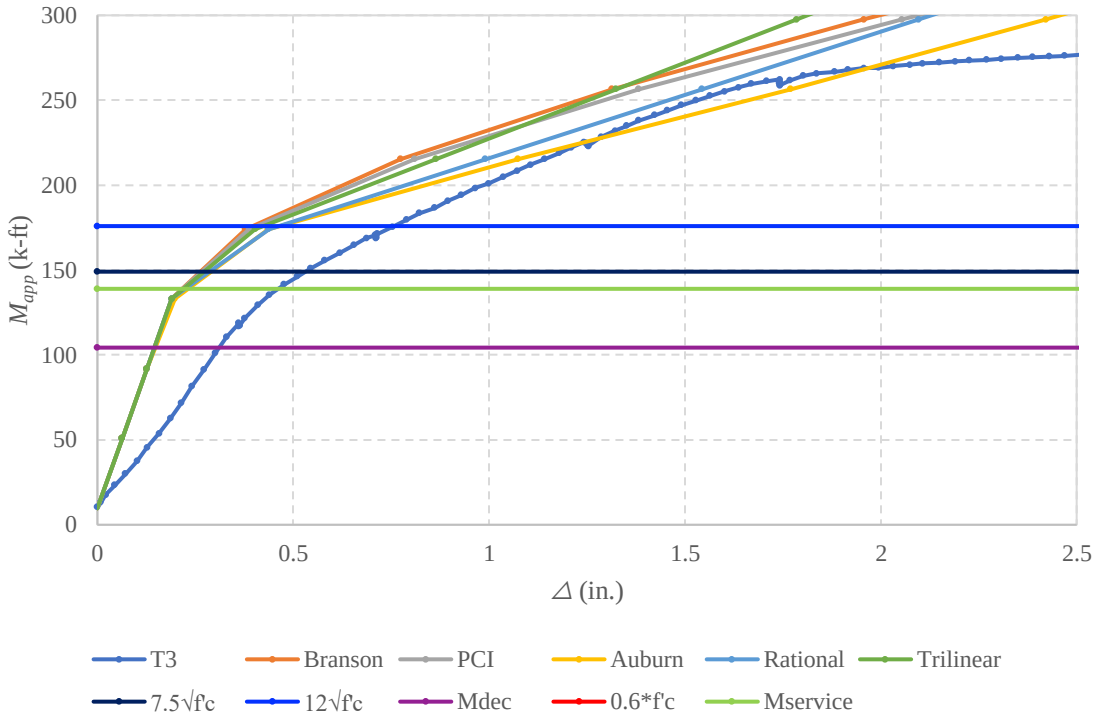

Figure 4.15 K_T3 moment deflection curve plotted with transition and cracked stress limits, compression limit, decompression moment, and service moments

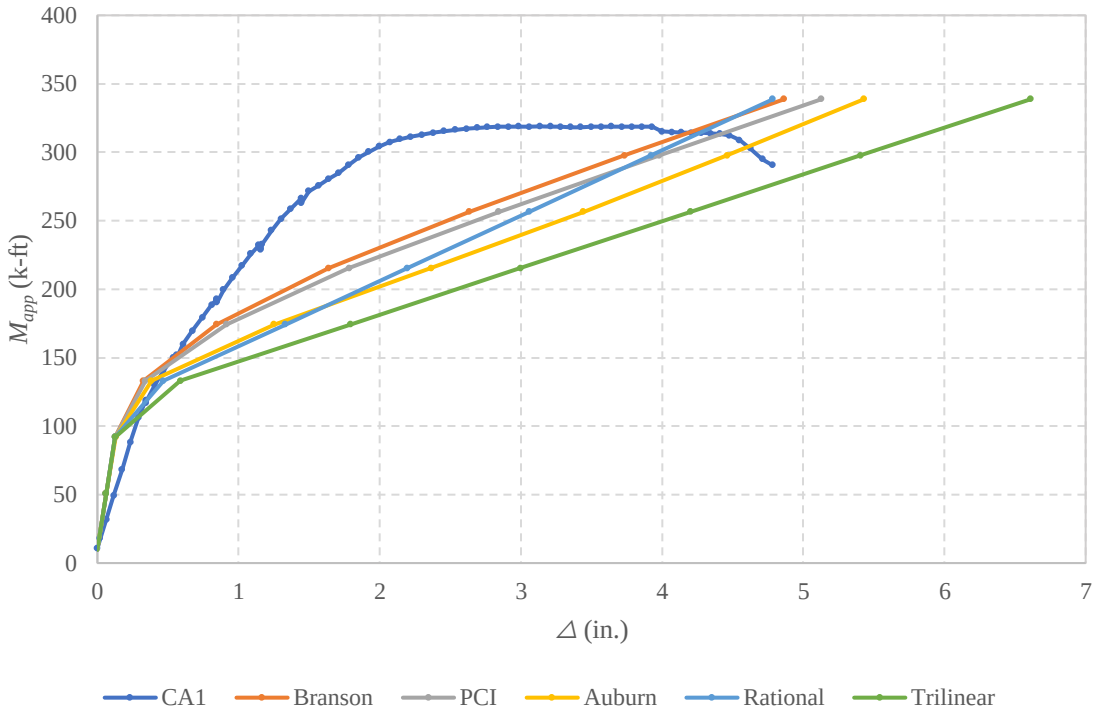

Figure 4.16 K_CA1 moment deflection curve plotted with transition and cracked stress limits, compression limit, decompression moment, and service moments

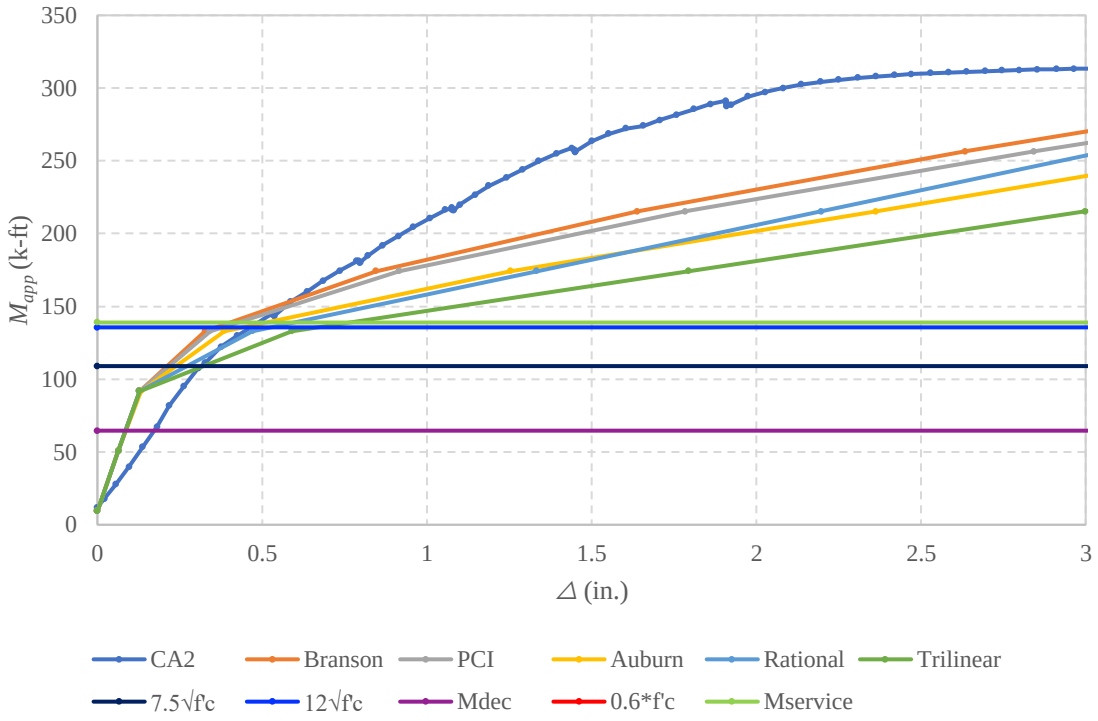

Figure 4.17 K_CA2 moment deflection curve plotted with transition and cracked stress limits, compression limit, decompression moment, and service moments

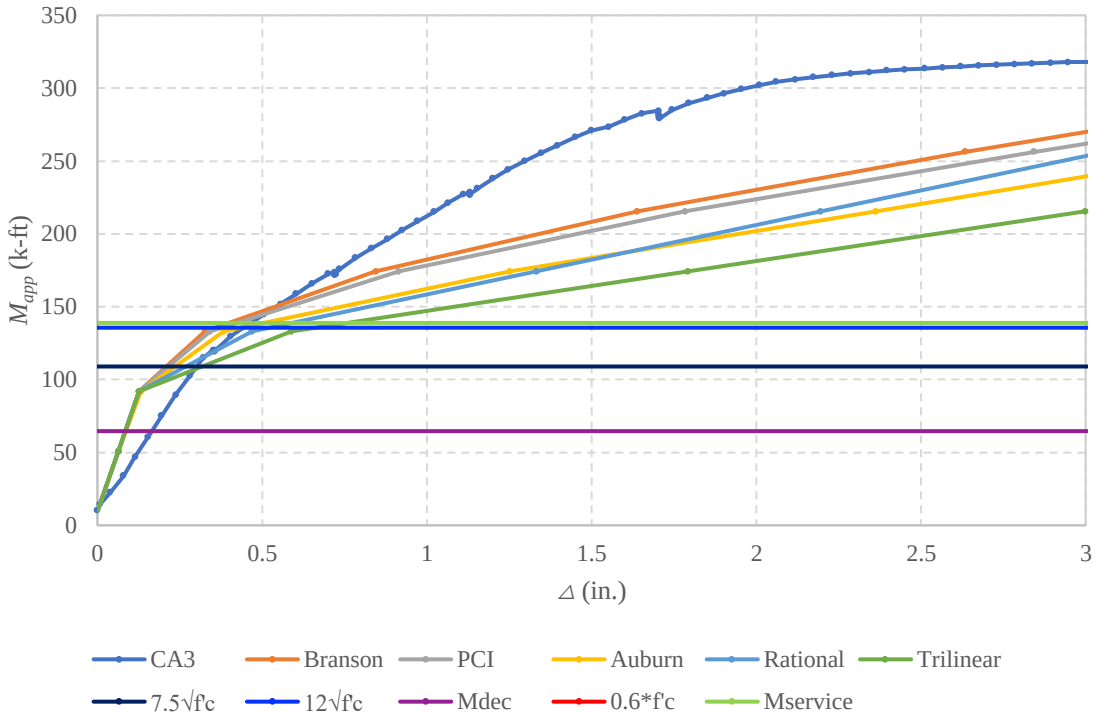

Figure 4.18 K_CA3moment deflection curve plotted with transition and cracked stress limits, compression limit, decompression moment, and service moments

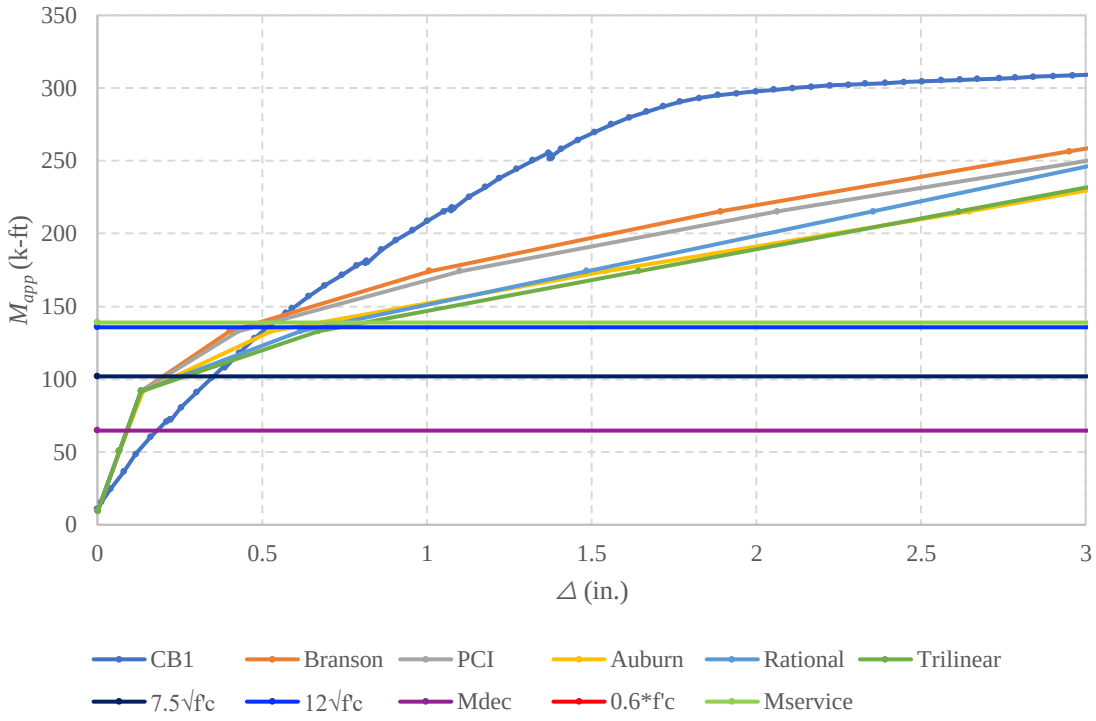

Figure 4.19 K_CB1 moment deflection curve plotted with transition and cracked stress limits, compression limit, decompression moment, and service moments

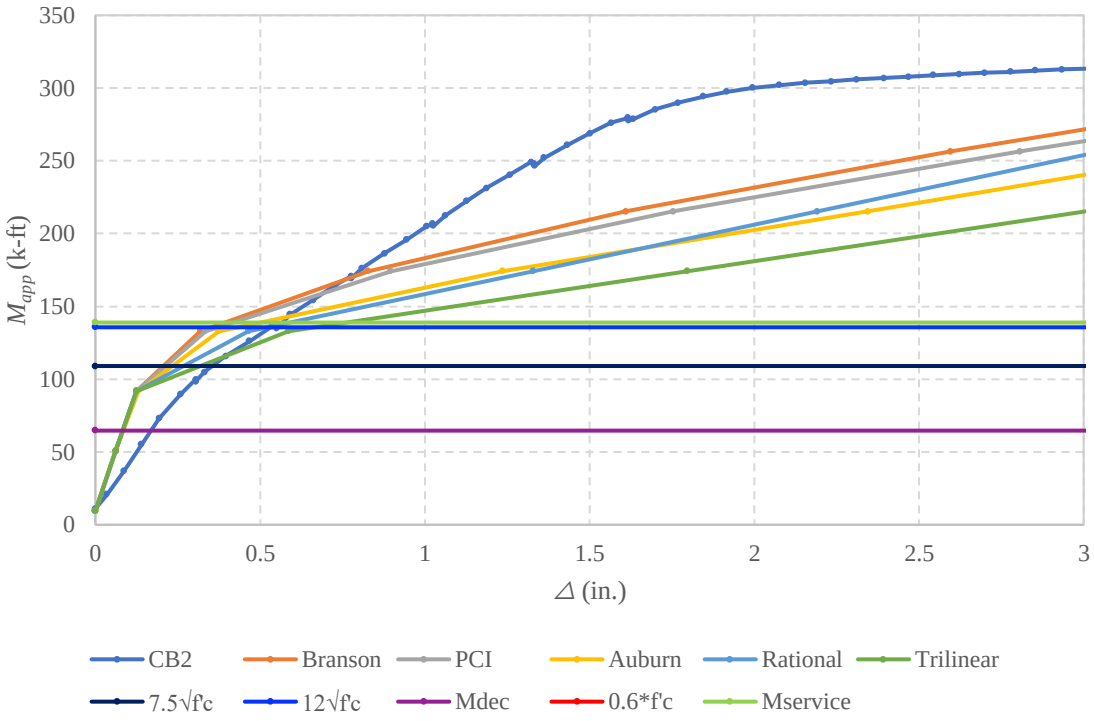

Figure 4.20 K_CB2 moment deflection curve plotted with transition and cracked stress limits, compression limit, decompression moment, and service moments

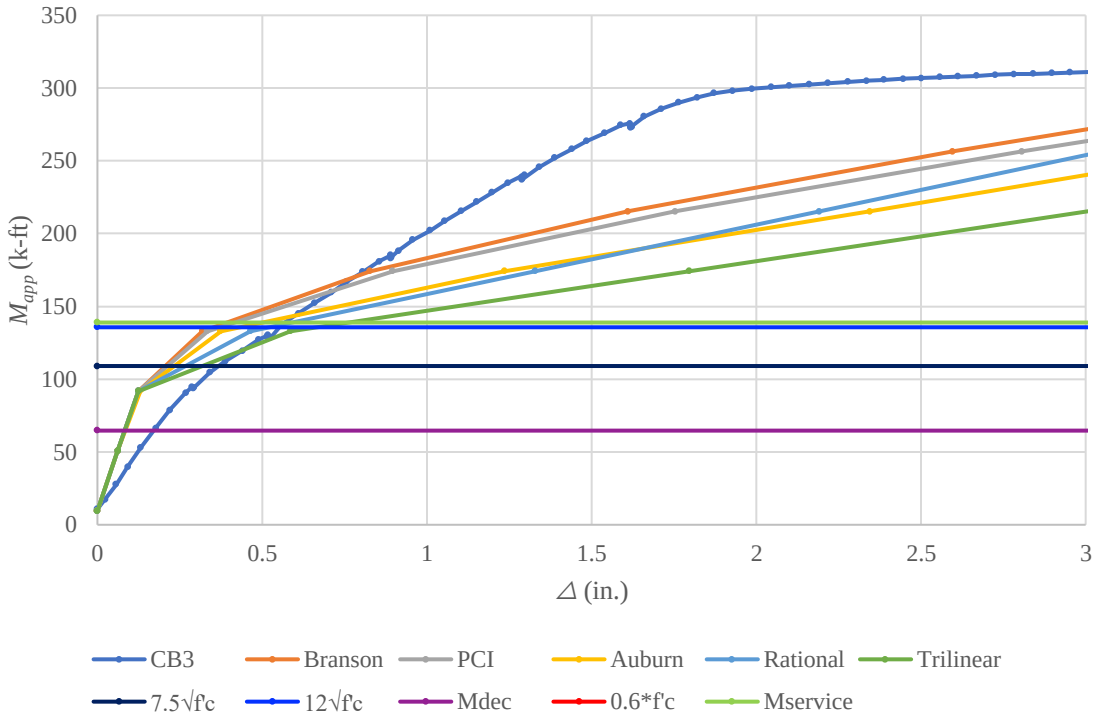

Figure 4.21 K_CB3 moment deflection curve plotted with transition and cracked stress limits, compression limit, decompression moment, and service moment

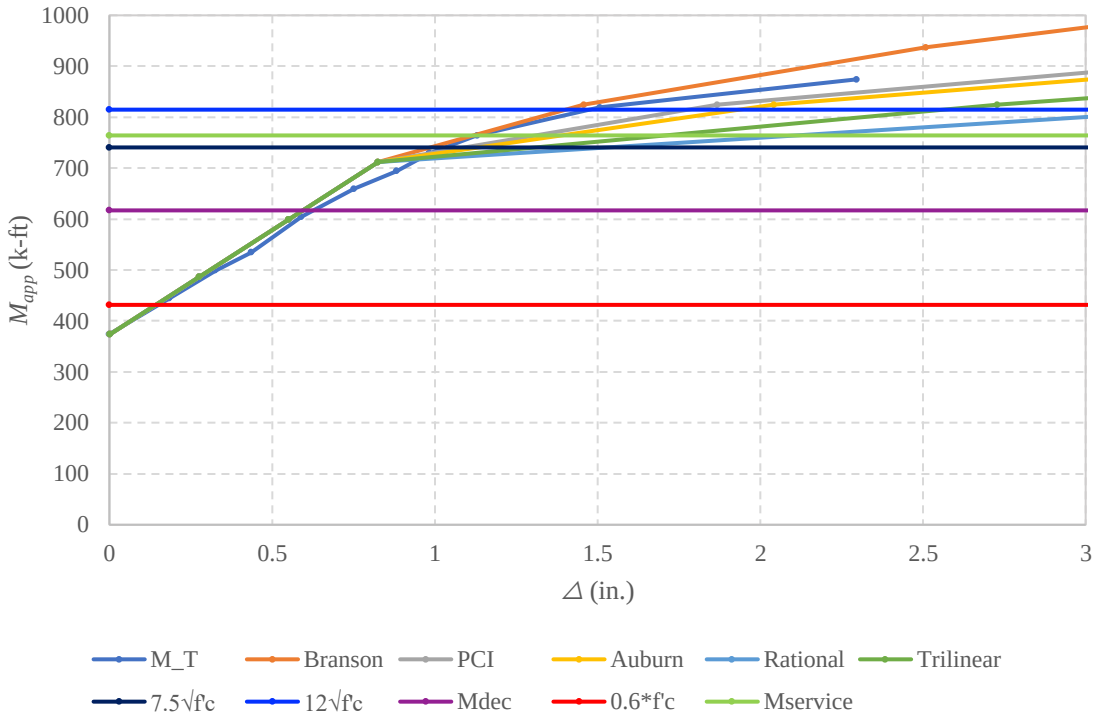

Figure 4.22 M_T moment deflection curve plotted with transition and cracked stress limits, compression limit, decompression moment, and service moments

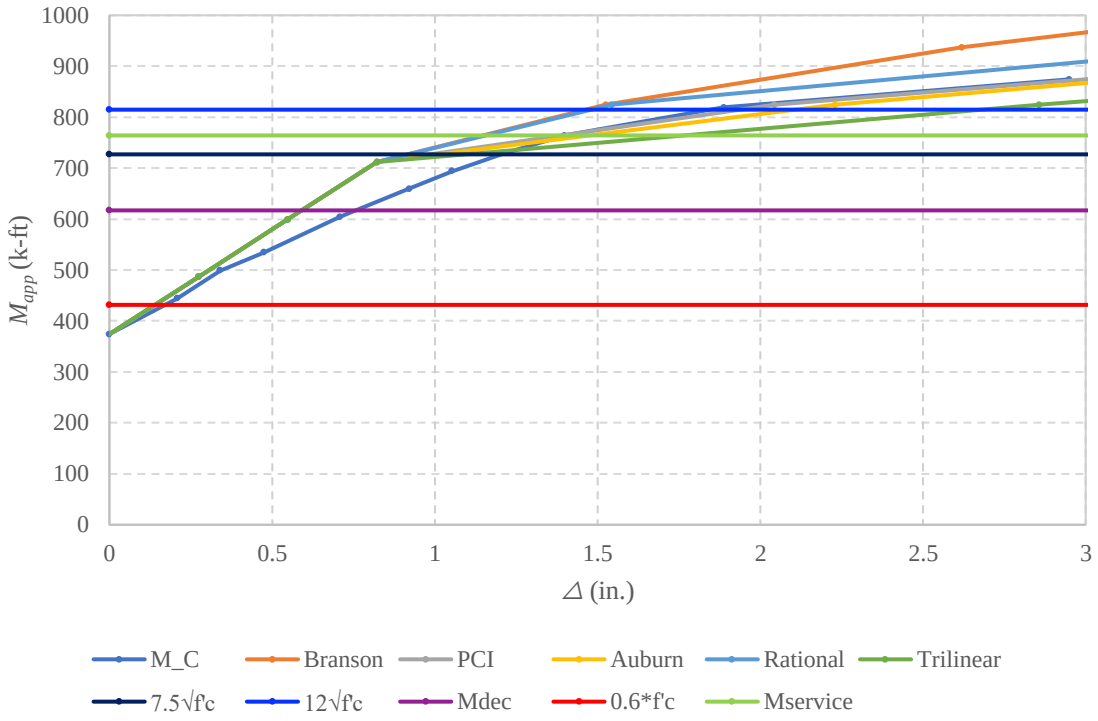

Figure 4.23 M_C moment deflection curve plotted with transition and cracked stress limits, compression limit, decompression moment, and service moments

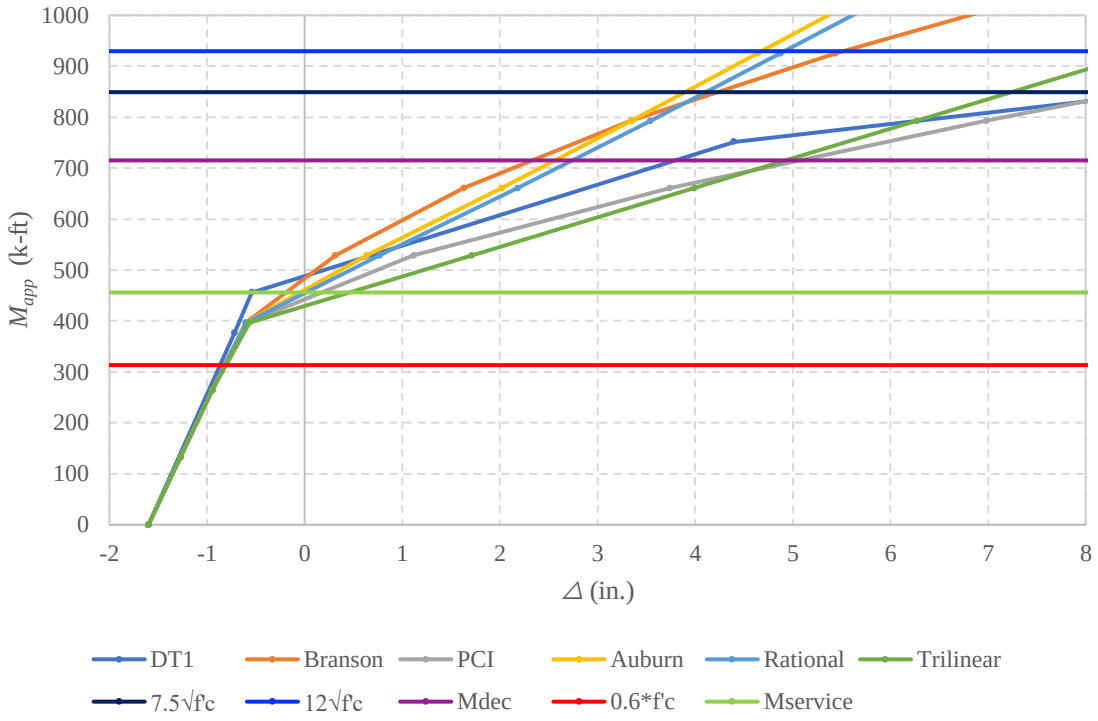

Figure 4.24A_1 moment deflection curves plotted with transition and cracked stress limits, compression limit, decompression moment, and service moments

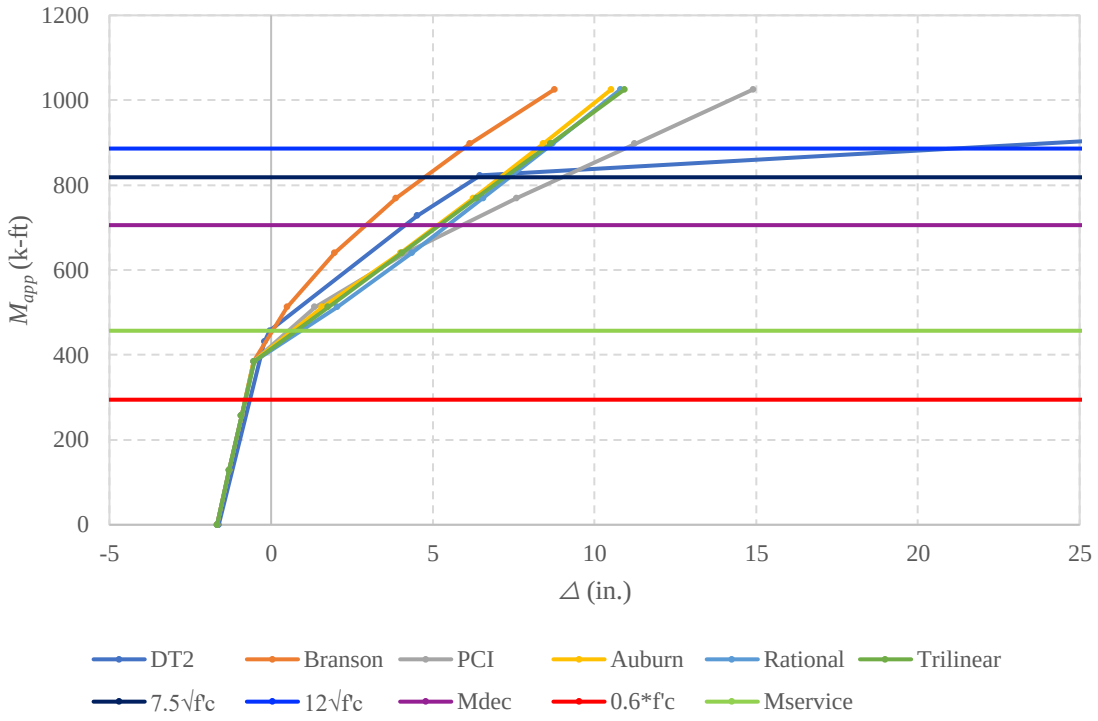

Figure 4.25 A_2 moment deflection curves plotted with transition and cracked stress limits, compression limit, decompression moment, and service moments

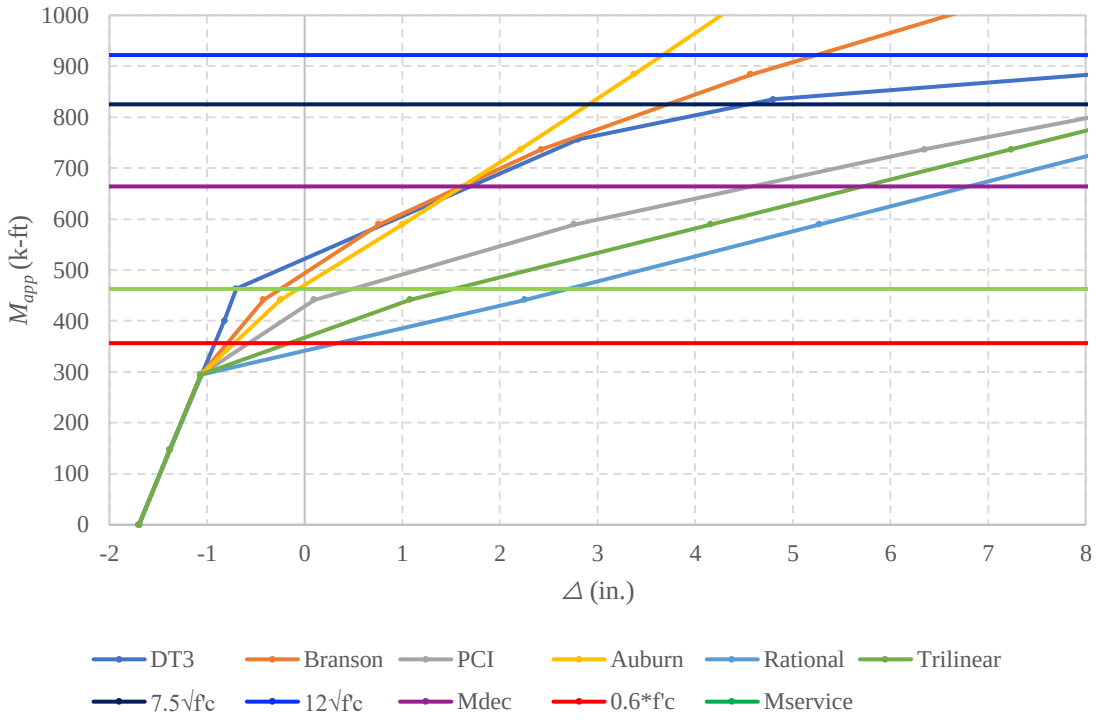

Figure 4.26 A_3 moment deflection curve plotted with transition and cracked stress limits, compression limit, decompression moment, and service moment

4.3 Prediction Analysis Results

The moment deflection curves help identify the trend of the estimated deflections, but an additional approach is needed to further investigate each method. In **Error! R eference source not found.** through **Error! Reference source not found.**, the measured deflection was plotted with the estimated data. The dashed line indicates the trend of an exact match between the measured and predicted deflections. With the predicted deflections on the y-axis and measured deflections on the x-axis, deflections that are to the left of the dashed line are conservative. The experimental data did not contain all the exact values to match the applied load from the predicted methods. The test specimens did not record exact data points for the applied moment values used by the predicted methods; interpolation between points allowed the measured data to be compared directly to the predicted data points.

The overall trend of the predicted methods does not install a high degree of confidence in any method, but looking into the dispersion can identify if a method is

more likely to diverge from the measured data. Branson's method underestimates the deflections and diverges as members progressed into higher stress states. PCI predicted both over and underestimated values. Auburn shows scattering of over and underestimation but at higher loads and deflections, shows convergence towards the fictious dashed line of matched predicted and experimental deflections. The Rational method had an initial scatter of data that continued and did not have a generalized trend. Initially the Trilinear method shows greater level of scatter initially; test groups that predicted higher deflections were estimated with both conservative and unconservative results. The lack of convergence for any method in this sample signals a need for more testing with full scale members to failure.

Filtering the data to exclude Kulzer specimens highlights different trends in the prediction methods. As mentioned in 4.2, the measured deflections did not behave as predicted and are not representative of the other specimens in this study. Figure 4.33 through Figure 4.37 show the data excluding the Kulzer specimens and plotting them with respect to their prestressed reinforcement ratio.

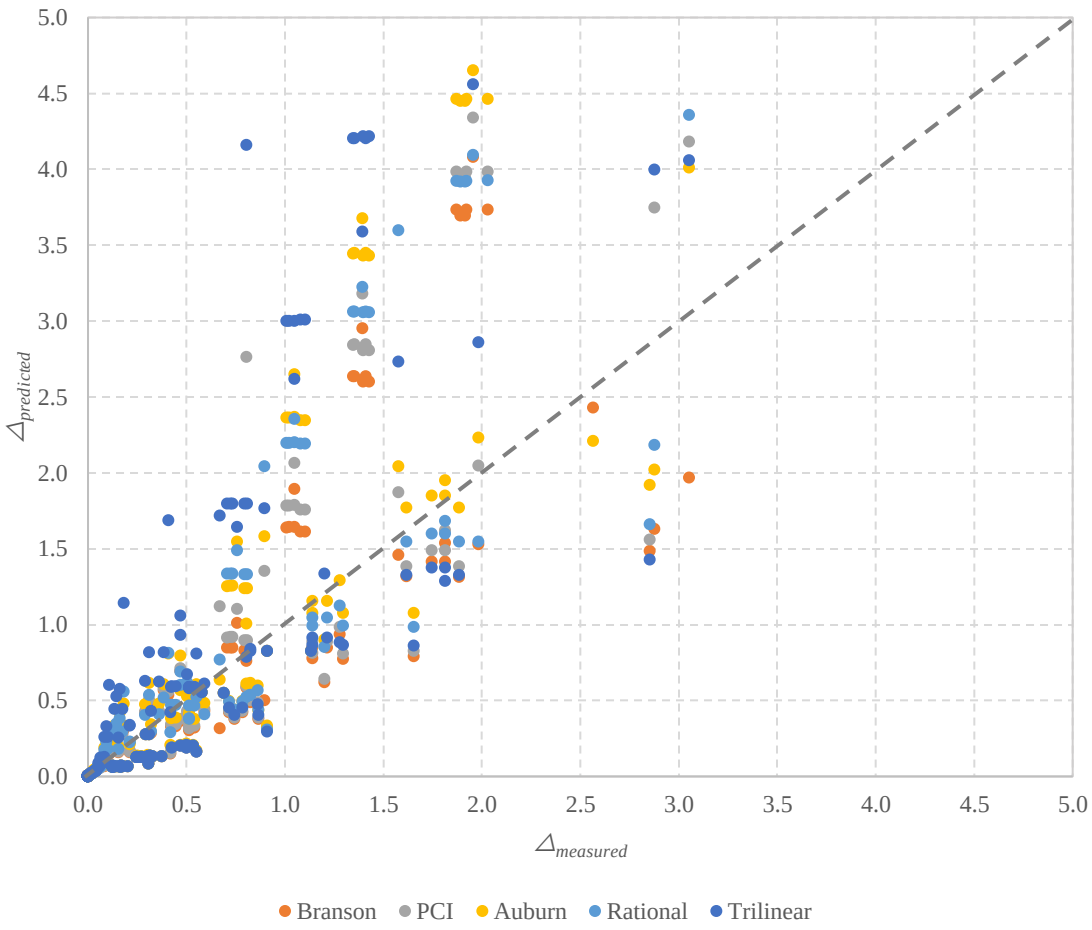

Figure 4.27 Predicted deflection plotted against measured deflection with all specimens and methods used to calculate deflections

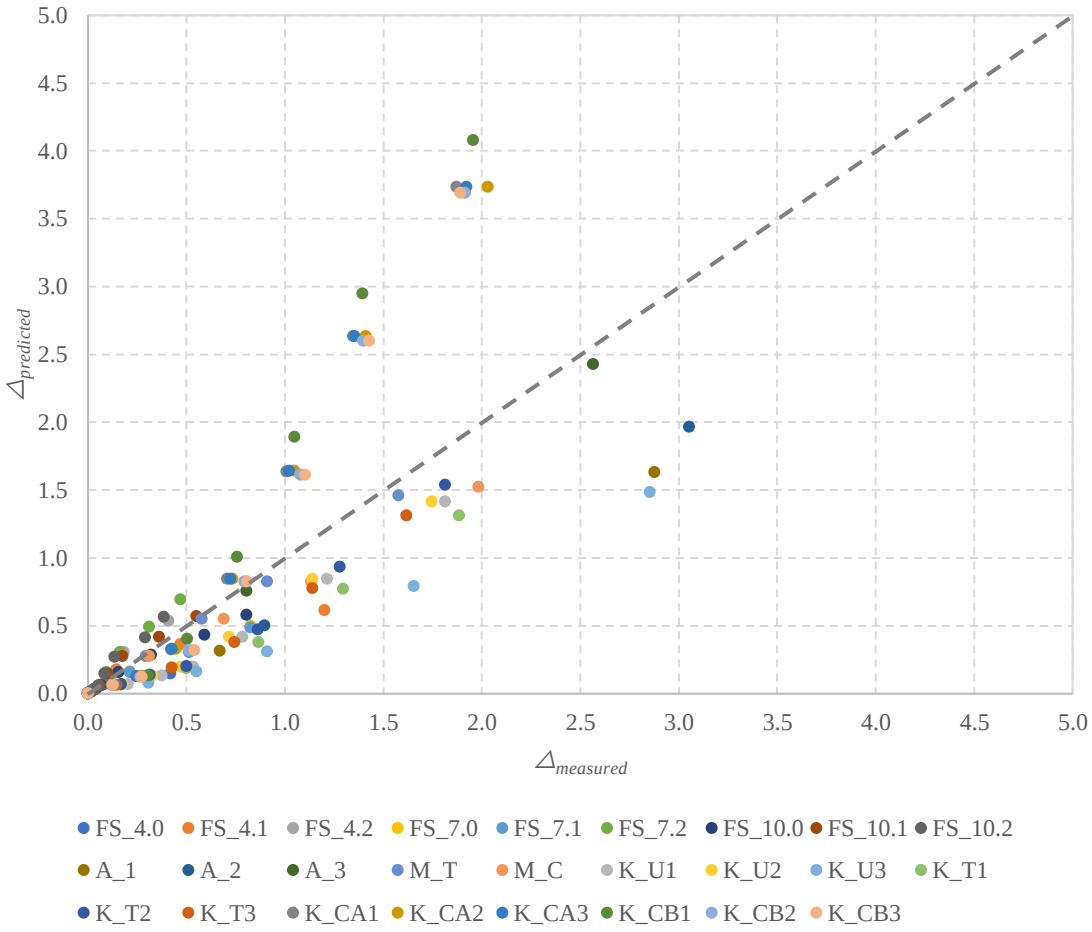

Figure 4.28 Predicted deflection plotted against measured deflection with all specimens using the Branson method

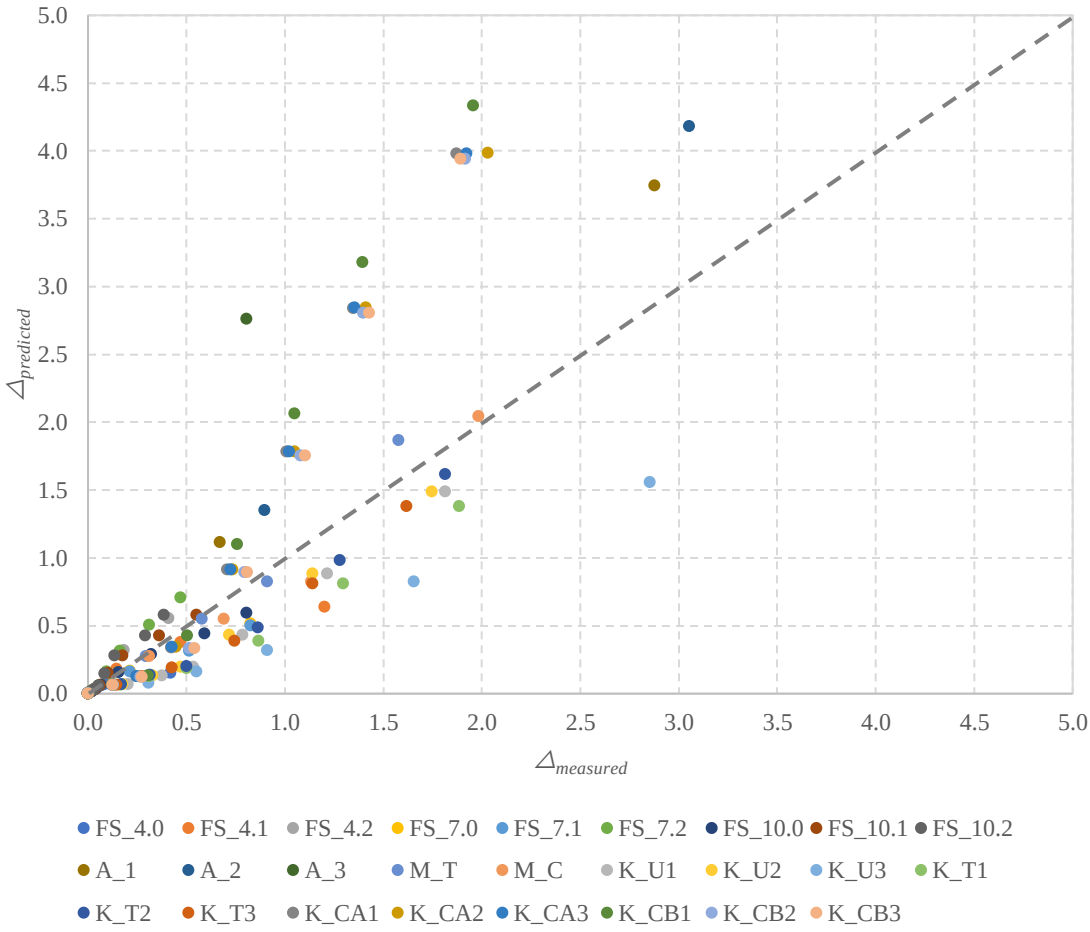

Figure 4.29 Predicted deflection plotted against measured deflection with all specimens using the PCI method

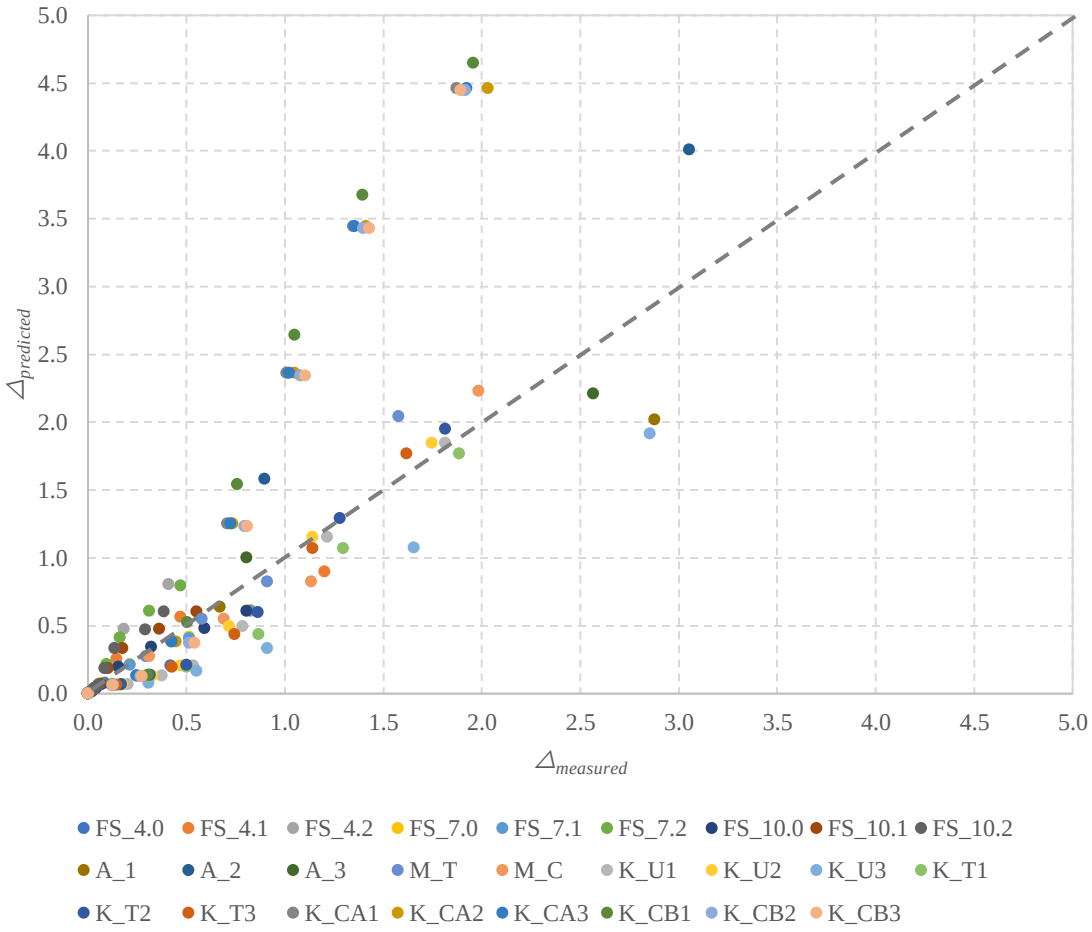

Figure 4.30 Predicted deflection plotted against measured deflection with all specimens using the Auburn method

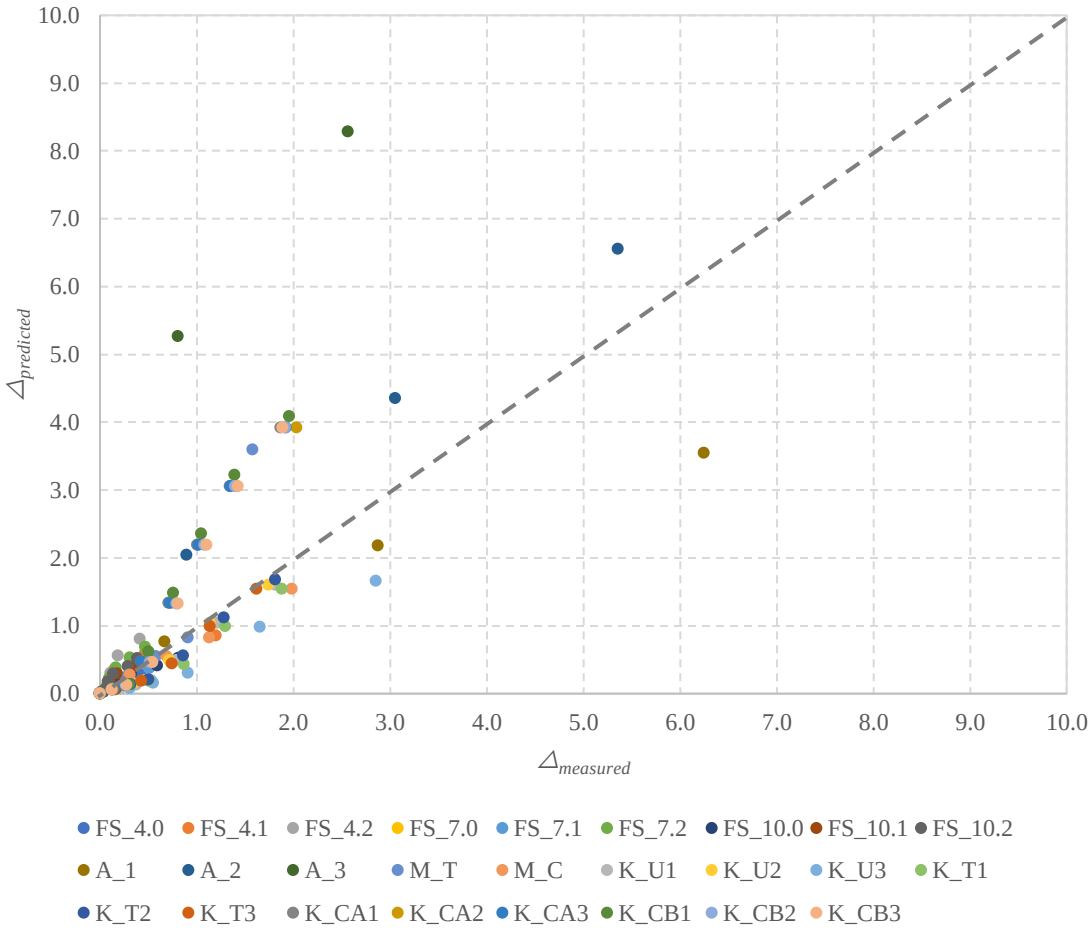

Figure 4.31 Predicted deflection plotted against measured deflection with all specimens using the Rational method

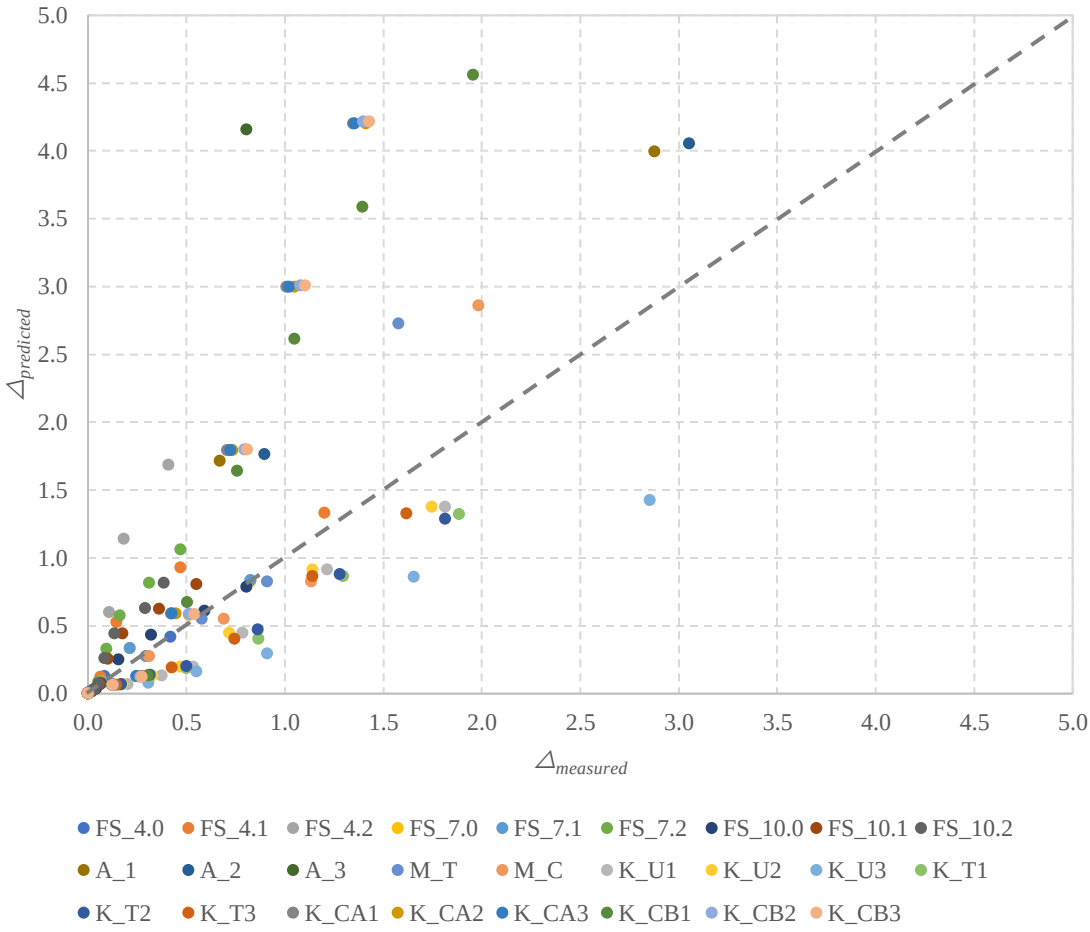

Figure 4.32 Predicted deflection plotted against measured deflection with all specimens using the Trilinear method

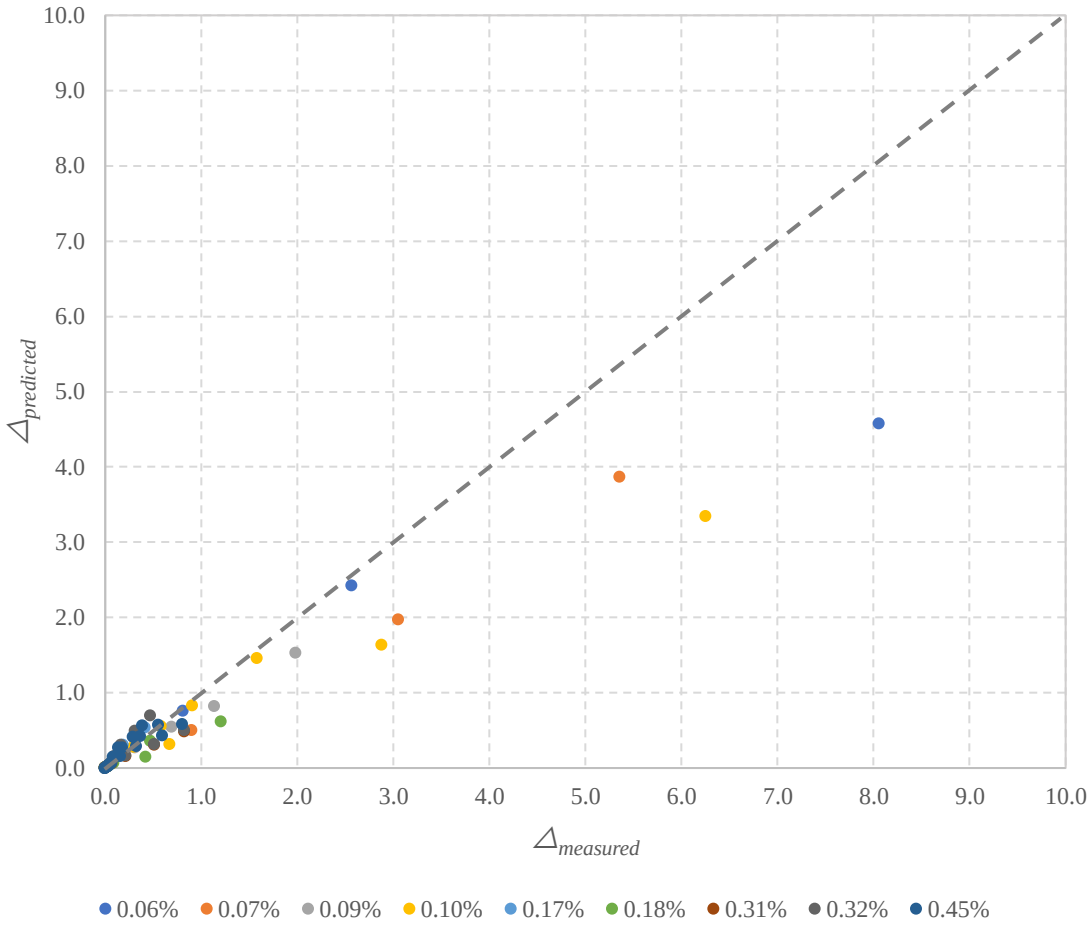

Figure 4.33 Predicted deflection plotted against measured deflection without Kulzer specimens using the Branson method, specimens are labeled by their prestressed reinforcement ratio

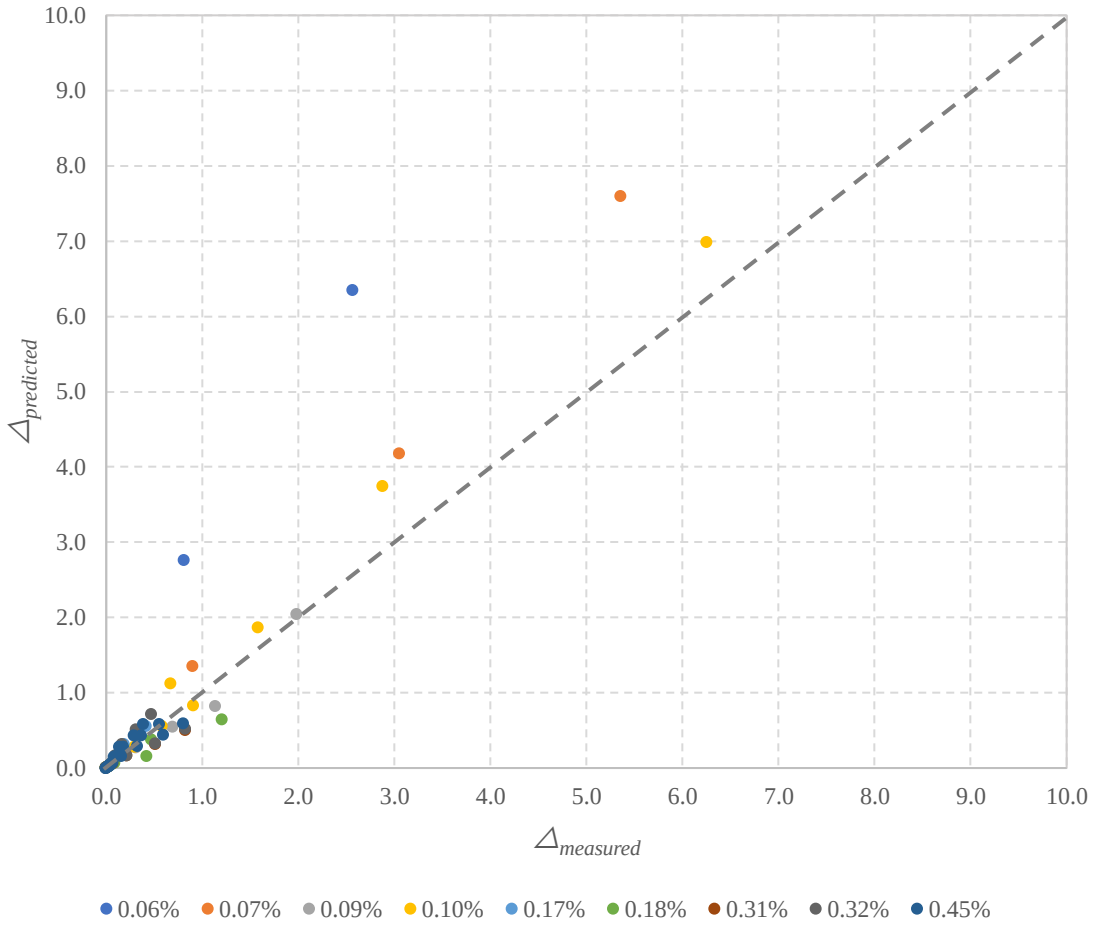

Figure 4.34 Predicted deflection plotted against measured deflection without Kulzer specimens using the PCI method, specimens are labeled by their prestressed reinforcement ratio

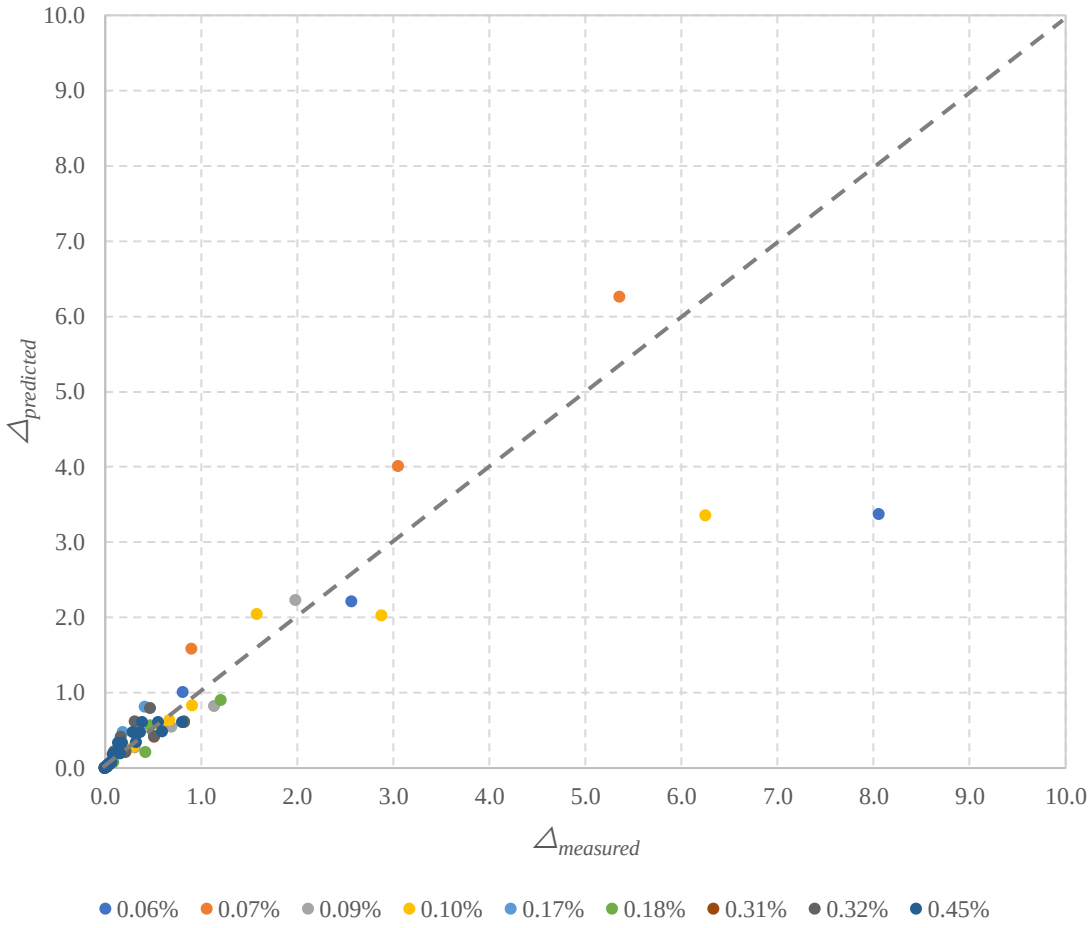

Figure 4.35 Predicted deflection plotted against measured deflection without Kulzer specimens using the Auburn method, specimens are labeled by their prestressed reinforcement ratio

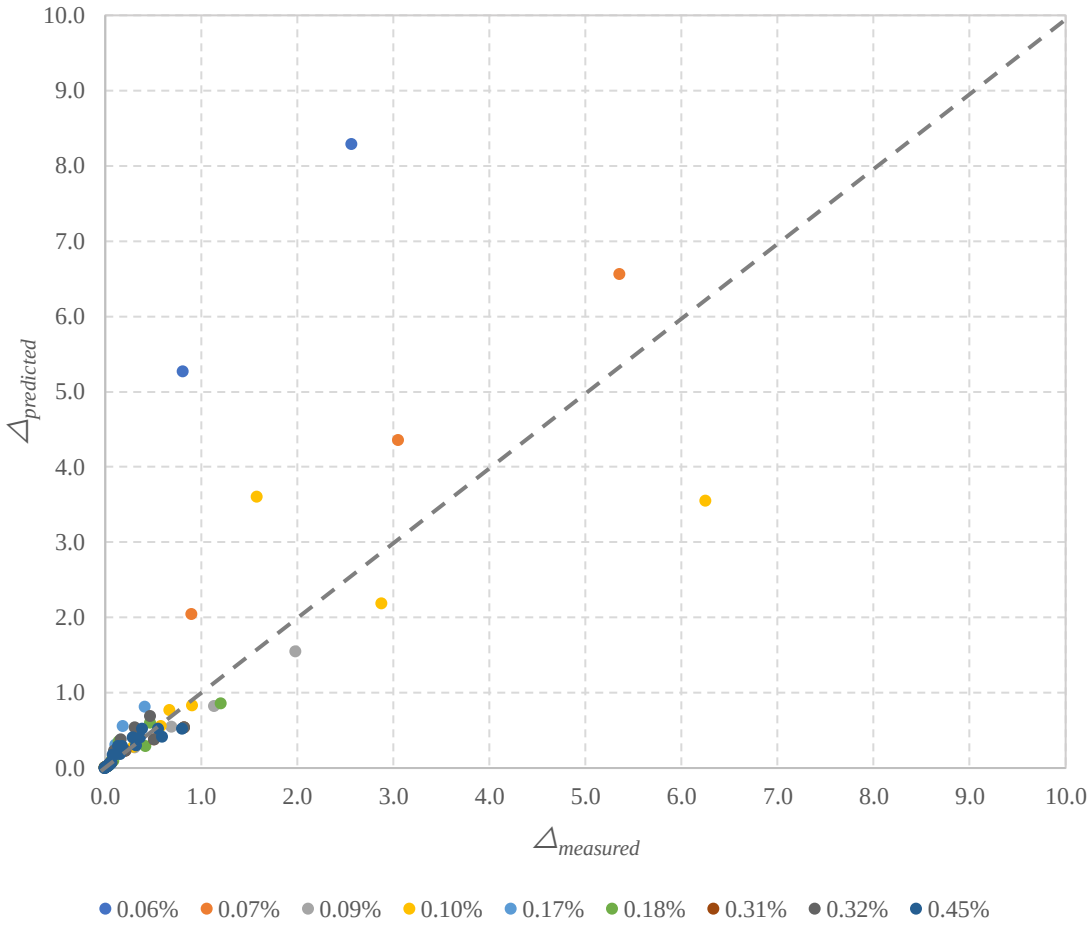

Figure 4.36 Predicted deflection plotted against measured deflection without Kulzer specimens using the Rational method, specimens are labeled by their prestressed reinforcement ratio

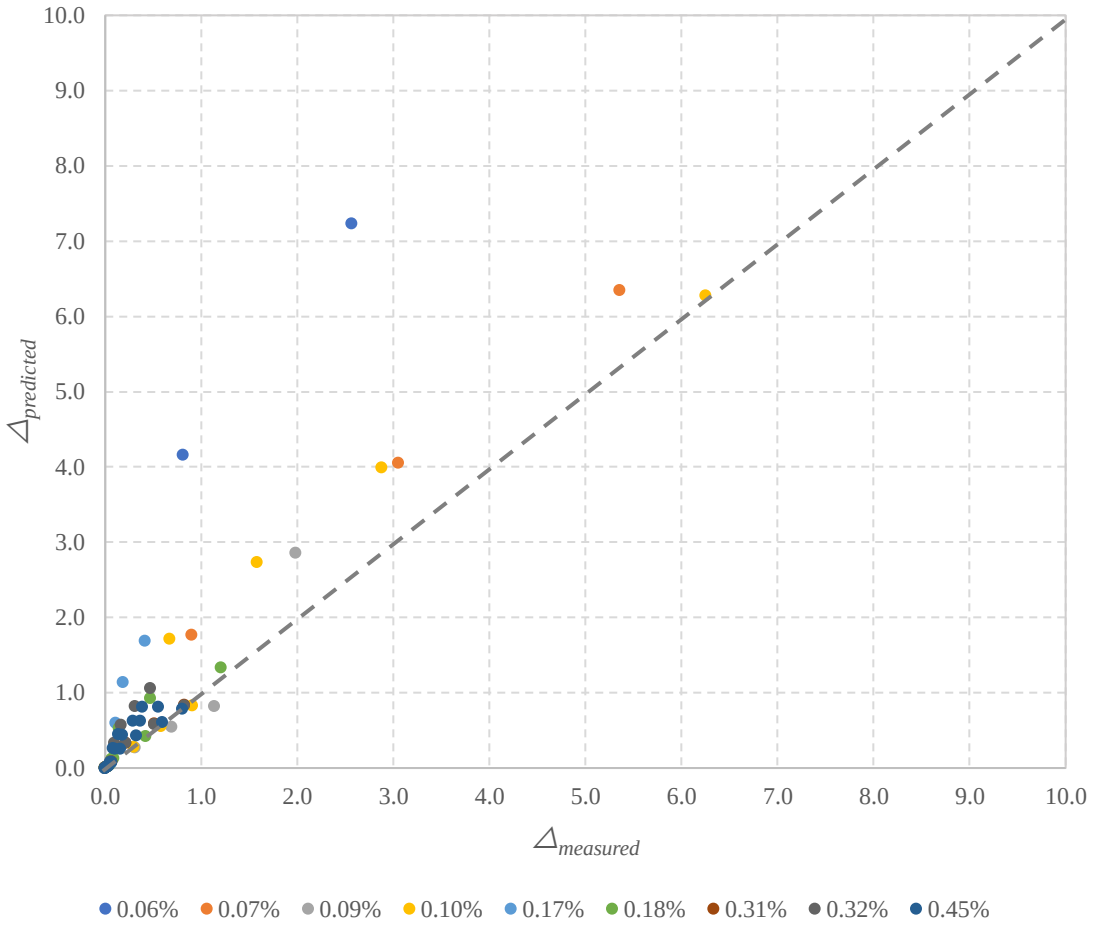

Figure 4.37 Predicted deflection plotted against measured deflection without Kulzer specimens using the Trilinear method, specimens are labeled by their prestressed reinforcement ratio

4.4 Double Tee Behavior in Deflection Tests

Filtering the data to the double tee specimens reinforces the lack of data for the study of full-scale transition and cracked deflections. With the data in this sample, the performance of the PCI and Auburn methods was superior to the other methods. PCI generated results that consistently were conservative but showed signs of diverging with the lowest reinforcement ratio specimen, see **Error! Reference source not found.**. The A uburn method showed signs of convergence, but this was not displayed at all reinforcement ratios. Further testing and implementation of these prediction methods would identify the correct direction in deflection modeling for transition and cracked prestressed sections.

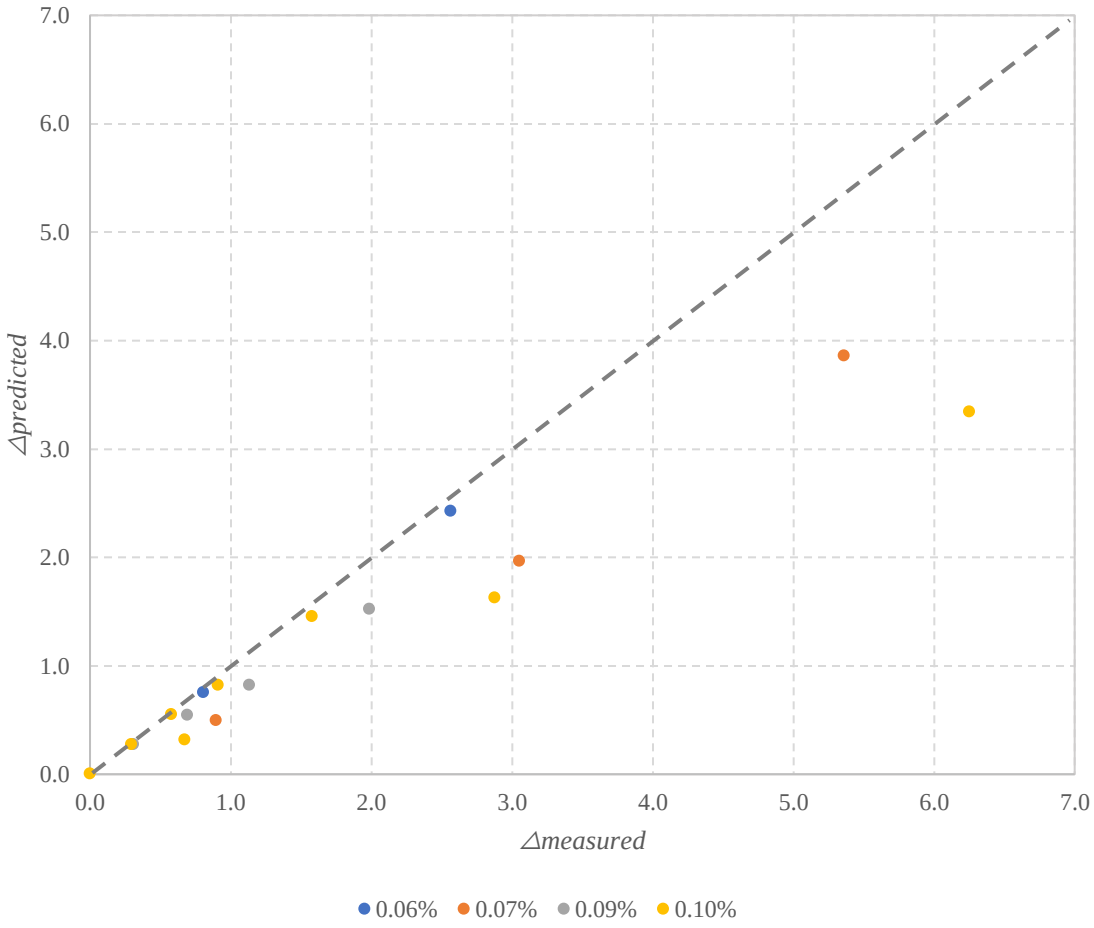

Figure 4.38 Predicted deflection plotted against measured deflection with double tee specimens using the Branson method

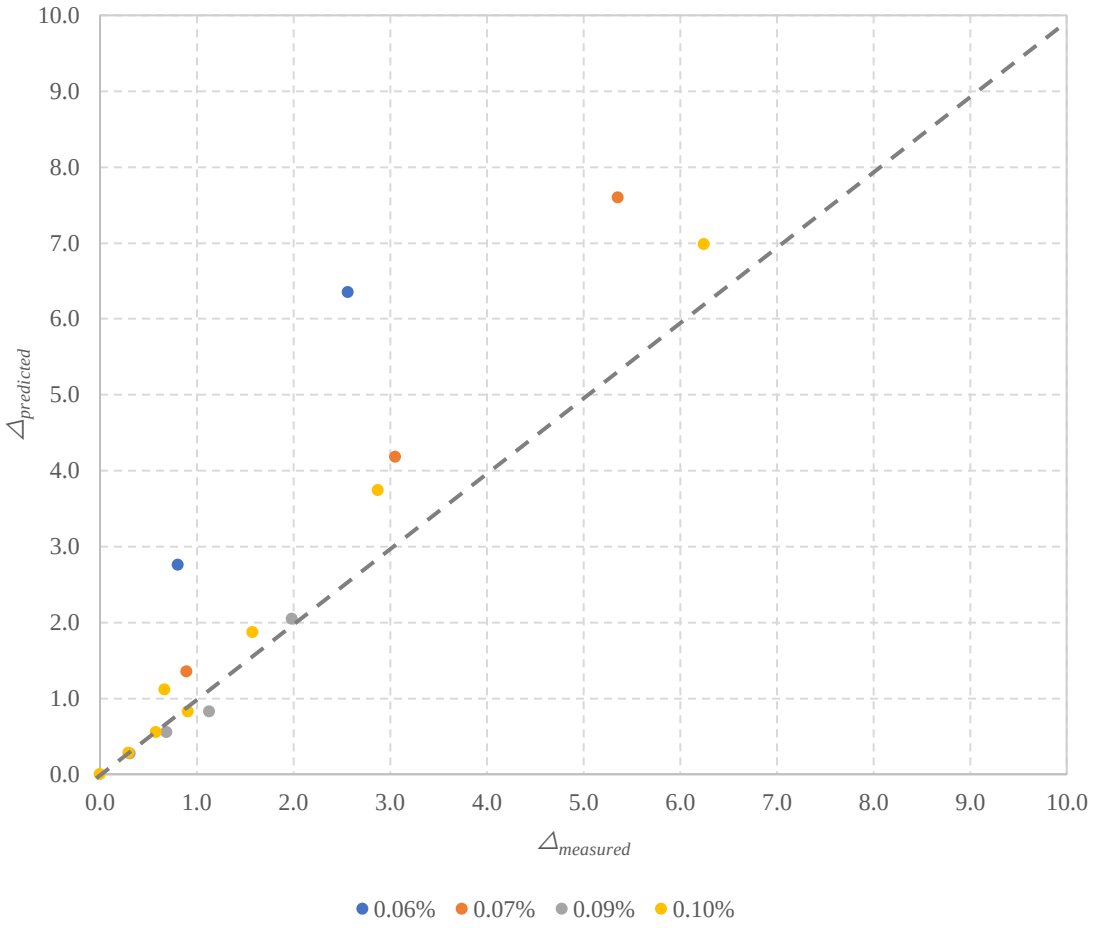

Figure 4.39 Predicted deflection plotted against measured deflection with double tee specimens using the PCI method

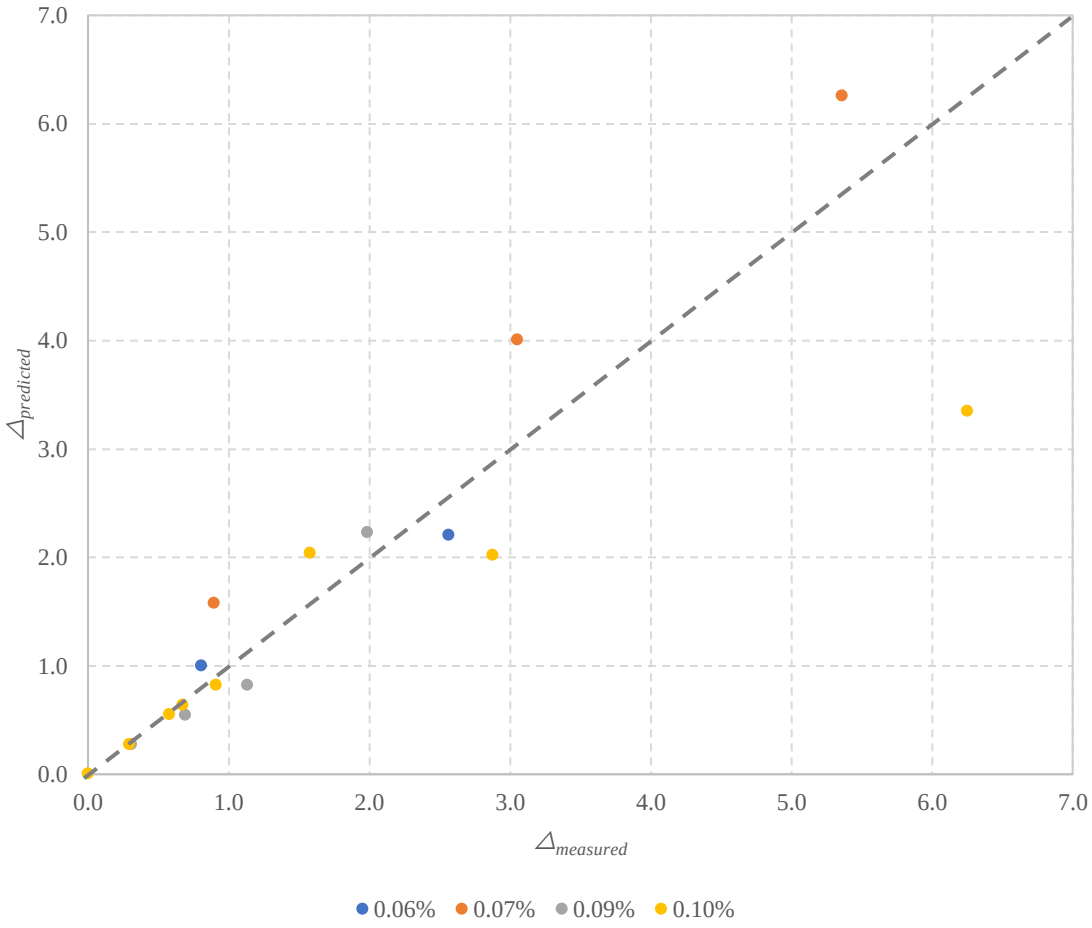

Figure 4.40 Predicted deflection plotted against measured deflection with double tee specimens using the Auburn method

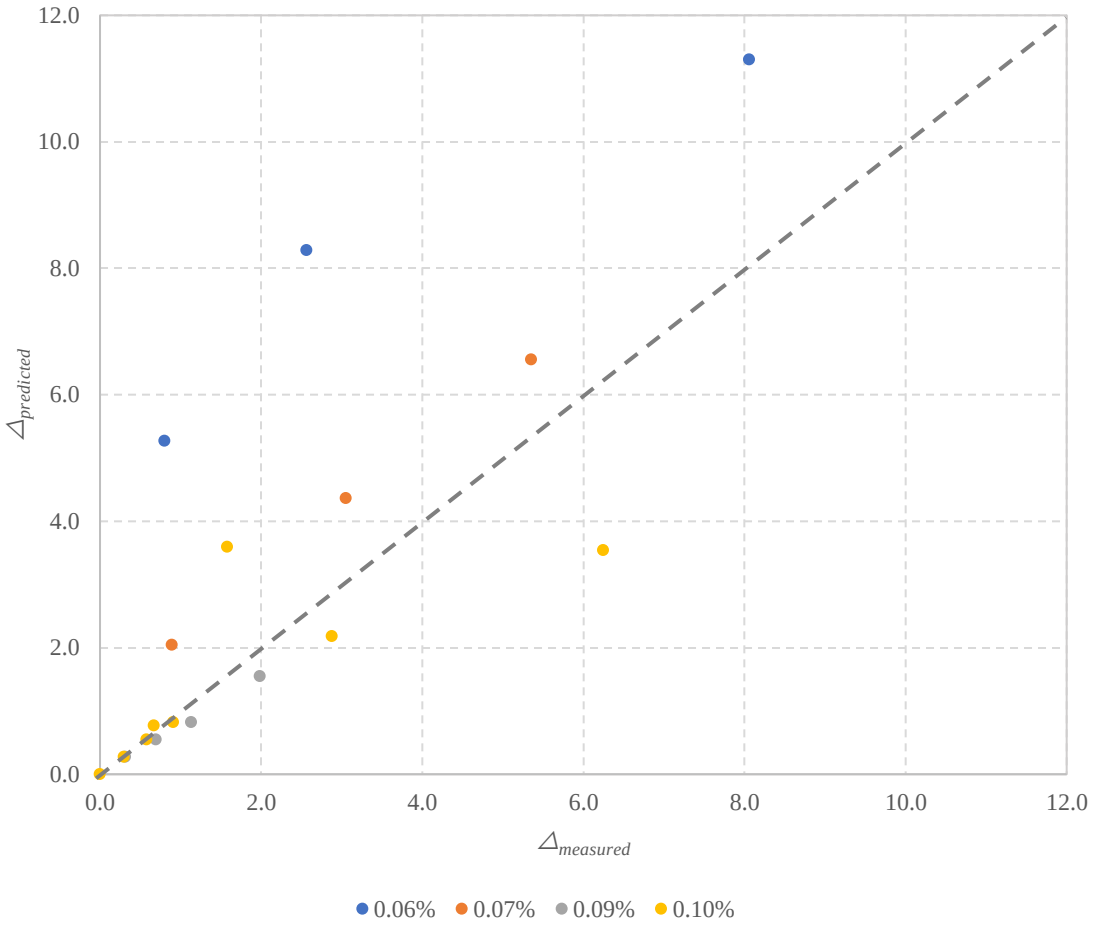

Figure 4.41 Predicted deflection plotted against measured deflection with double tee specimens using the Rational method

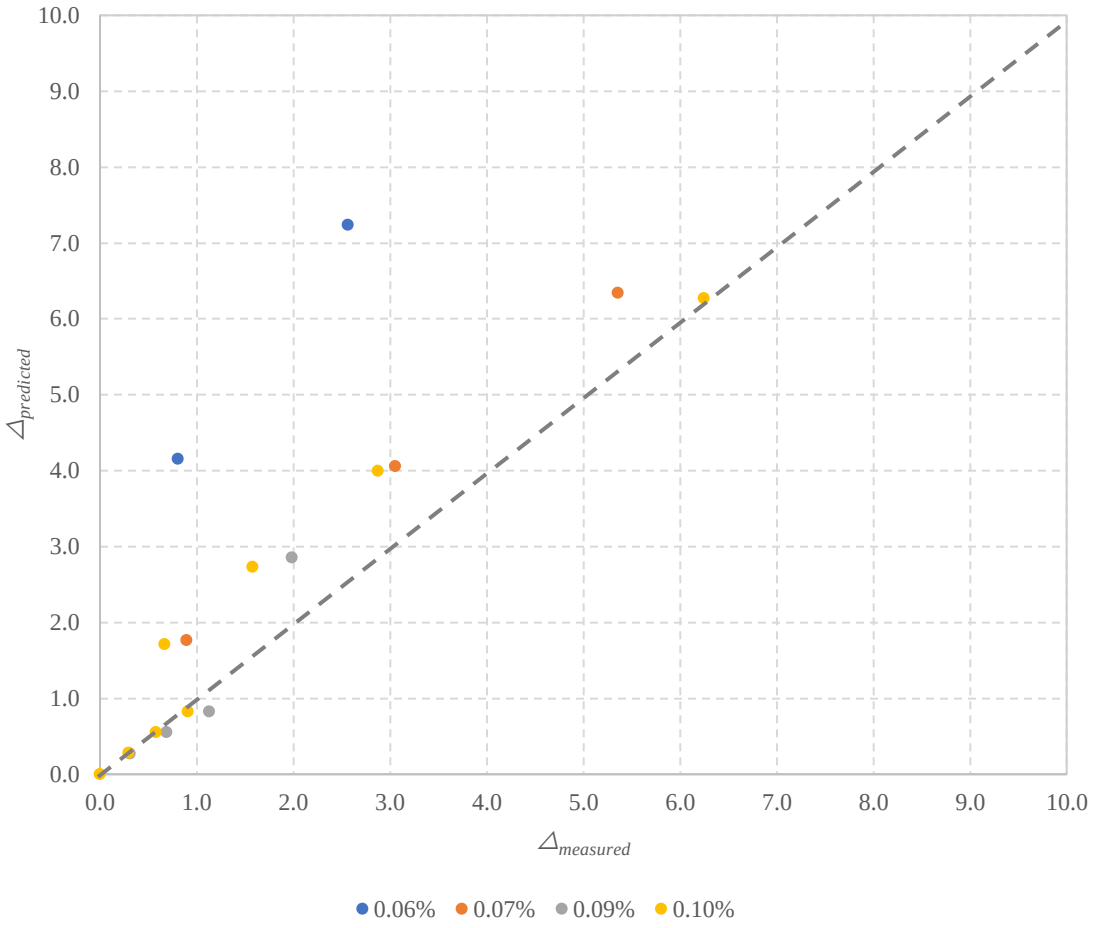

Figure 4.42 Predicted deflection plotted against measured deflection with double tee specimens using the Trilinear method

5 Conclusions and Recommendations

5.1 Conclusions

Deflection modeling in prestressed members is limited due to the complex relationship between the prestressed reinforcement and concrete. Multiple methods introduced ways to estimate the progressive decline in stiffness associated with cracking due to loads. In the sample studied, the extra effort required by the alternative methods did not measurably improve the accuracy or consistency of deflection predictions than the current PCI method. Focusing on the double tee specimens which are the only full-scale specimen data available, showed better performance in predicting the deflections with both the PCI and Auburn methods.

5.2 Recommendations

For further investigation into transition and cracked prestressed concrete members, more data points will be required to validate current and future methods. As of this study, the number specimens of full-scale double tee deflection tests are very small. Furthermore, the lack of testing these specimens to failure is also limited and this data would provide useful information to determine an effective deflection prediction method. At this time, no change is recommended to the present practice of use of the PCI Method despite the introduction of many other, often more complex, methods. The Auburn Method shows promise and should be further considered with additional full-scale specimen data when it becomes available.

Bibliography

ACI Committee 318. (2014). Building Code Requirement for Structural Concrete (ACI 318-14) and Commentary (ACI 318R-14), Farmington Hills, MI.

ACI Committee 318. (2019). Building Code Requirement for Structural Concrete (ACI 318-19) and Commentary (ACI 318R-19), Farmington Hills, MI.

Aswad, A., Burnley, G., Cleland, N. M., Orndorff, D., & Wynings, C. (2004). "Load Testing of Prestressed Concrete Double Tees Without Web Reinforcement." *PCI Journal*, *49*(2), 66–77.

Bachmann, H. (1984). "Design of Partially Prestressed Concrete Structures Based on Swiss Experiences." *PCI Journal*, *29*(4), 84–105.

Bischoff, P. H. (2005). "Reevaluation of Deflection Prediction for Concrete Beams Reinforced with Steel and Fiber Reinforced Polymer Bars." *Journal of Structural Engineering*, *131*(5), 752–767.

Bischoff, P. H., & Scanlon, A. (2007). "Effective Moment of Inertia for Calculating Deflections of Concrete Members Containing Steel Reinforcement and Fiber-Reinforced Polymer Reinforcement." *ACI Structural Journal*, *104*(1), 68–75.

Bischoff, P. H., Naito, C. J., & Ingaglio, J. P. (2018). "Immediate Deflection of Partially Prestressed Concrete Flexural Members." *ACI Structural Journal*, *115*(6), 1683–1693.

Bischoff, P. H. (2020). "Comparison of Existing Approaches for Computing Deflection of Reinforced Concrete." *Structural Journal*, *117*(1), 231–240.

Bischoff, P. H. (2022). "Deformation Model for Reinforced and Cracked Prestressed Concrete." *ACI Structural Journal*, *119*(1), 243–252.

Branson, D. E. & Alabama Highway Department. (1963). *Instantaneous and Time-Dependent Deflections of Simple and Continuous Reinforced Concrete Beams* (HPR Report No. 7).

Branson, D. E., & Trost, H. (1982). "Application of the I-Effective Method in Calculating Deflections of Partially Prestressed Members." *PCI Journal*, *27*(5), 62–77.

Branson, D. E., & Shaikh, A. F. (1985). "Deflection of Partially Prestressed Members." *Special Publication*, *86*, 323–364.

Burns, N. H. (1964). “Moment Curvature Relationships For Partially Prestressed Concrete Beams.” *PCI Journal*, *9*(1), 52–63.

Hernandez, G. (1958). “Strength of Prestressed Concrete Beams with Web Reinforcement.” Ph.D. Thesis, University of Illinois. Issued as a part of the Seventh Progress Report of the Investigation of Prestressed Concrete for Highway Bridges, Civil Engineering Studies, Structural Research Series No. 153.

Janney, J. R., Hognestad, E., & McHenry, D. (1956). “Ultimate Flexural Strength of Prestressed and Conventionally Reinforced Concrete Beams.” *Journal of the American Concrete Institute*, *52*(2), 601–620.

Kerekes, F., Reid, H. B., & Jr. (1954). “Fifty Years of Development in Building Code Requirements for Reinforced Concrete.” *Journal Proceedings*, *50*(6), 441–471.

Kulzer, A. D. (2022). “Experimental Evaluation of Post-Cracking Deflection Behavior in Prestressed Concrete Beams.” Master’s Thesis, University of Minnesota, Duluth, MN.

Mast, R. F. (1998). “Analysis of Cracked Prestressed Concrete Sections: A Practical Approach.” *PCI Journal*, *43*(4), 80–91.

Naaman, A. E. (1985). “Partially Prestressed Concrete: Review and Recommendations.” *Prestressed Concrete Institute*, *30*(6), 30–71.

Nilson, A. H. (1976). “Flexural stresses after cracking in partially prestressed beams.” *PCI Journal*, *21*(4), 72–61.

Precast/Prestressed Concrete Institute (PCI). (2017). *PCI Design Handbook: Precast and Prestressed Concrete* (8th ed.).

Saqan, E. I., & Frosch, R. J. (2009). “Influence of Flexural Reinforcement on Shear Strength of Prestressed Concrete Beams.” *ACI Structural Journal*, *106*(1), 60–68.

Tadros, M. K. (1982). “Expedient Service Load Analysis of Cracked Prestressed Concrete Sections.” *PCI Journal*, *27*(6), 86–111.

Yendle Hughes, H. (2023) “Immediate Deflections of Simply Supported, Bonded, Class T and C Prestressed Concrete Beams.” Master’s Thesis, Auburn University, Auburn, AL.

Appendix A: Moment Deflection Curves

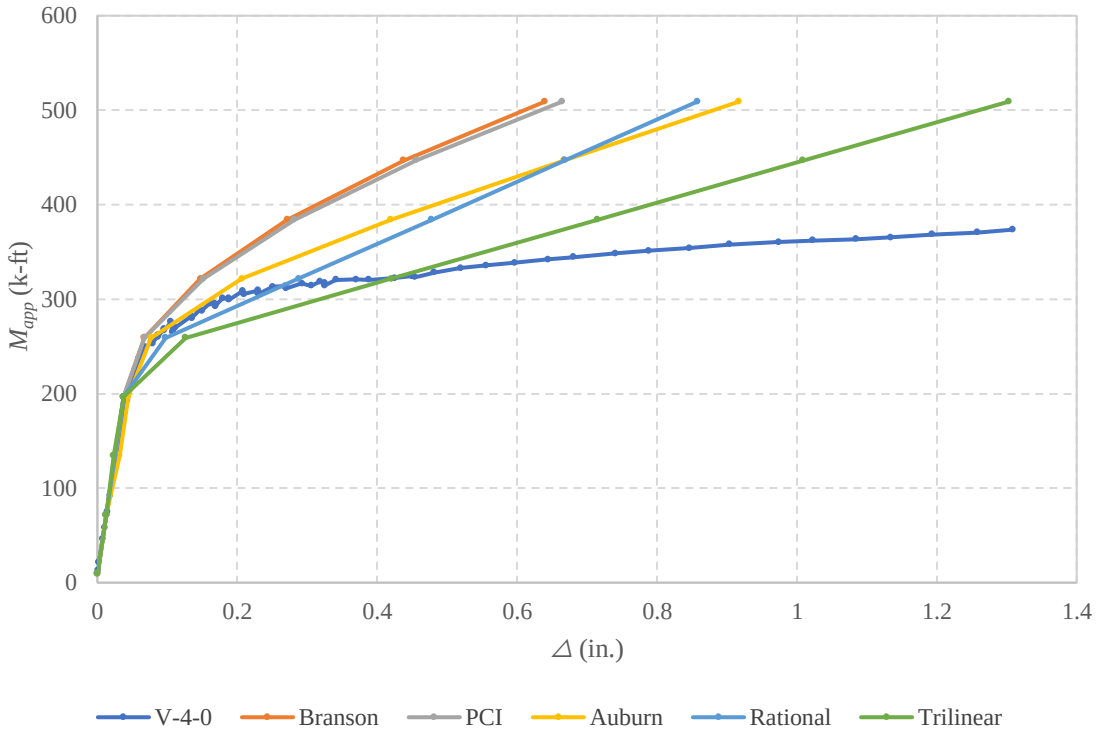

Figure A.1 Moment deflection curve for FS_4.0

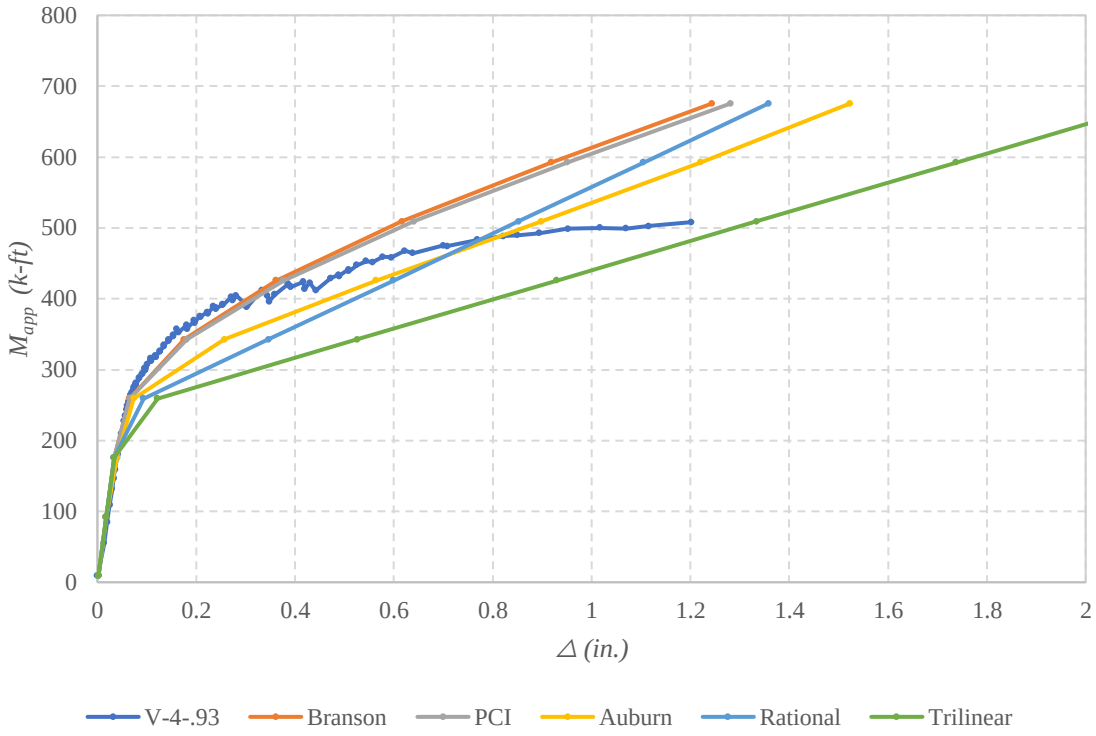

Figure A.2 Moment deflection for FS_4.1

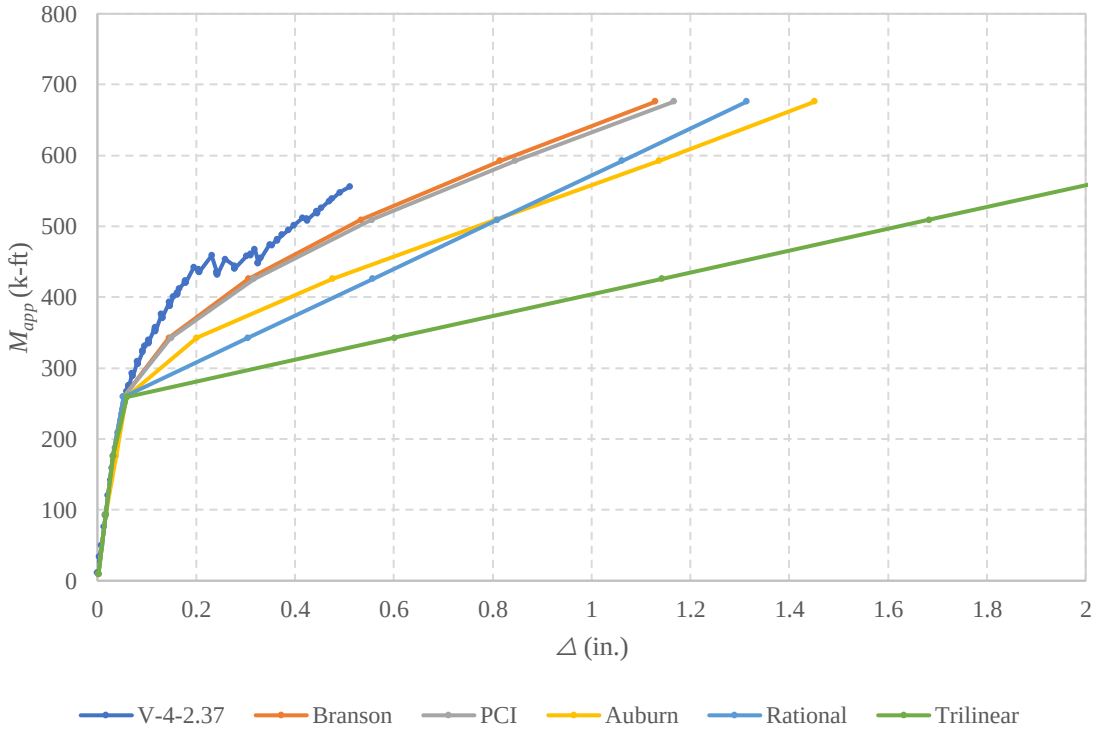

Figure A.3 Moment deflection curve for FS_4.2

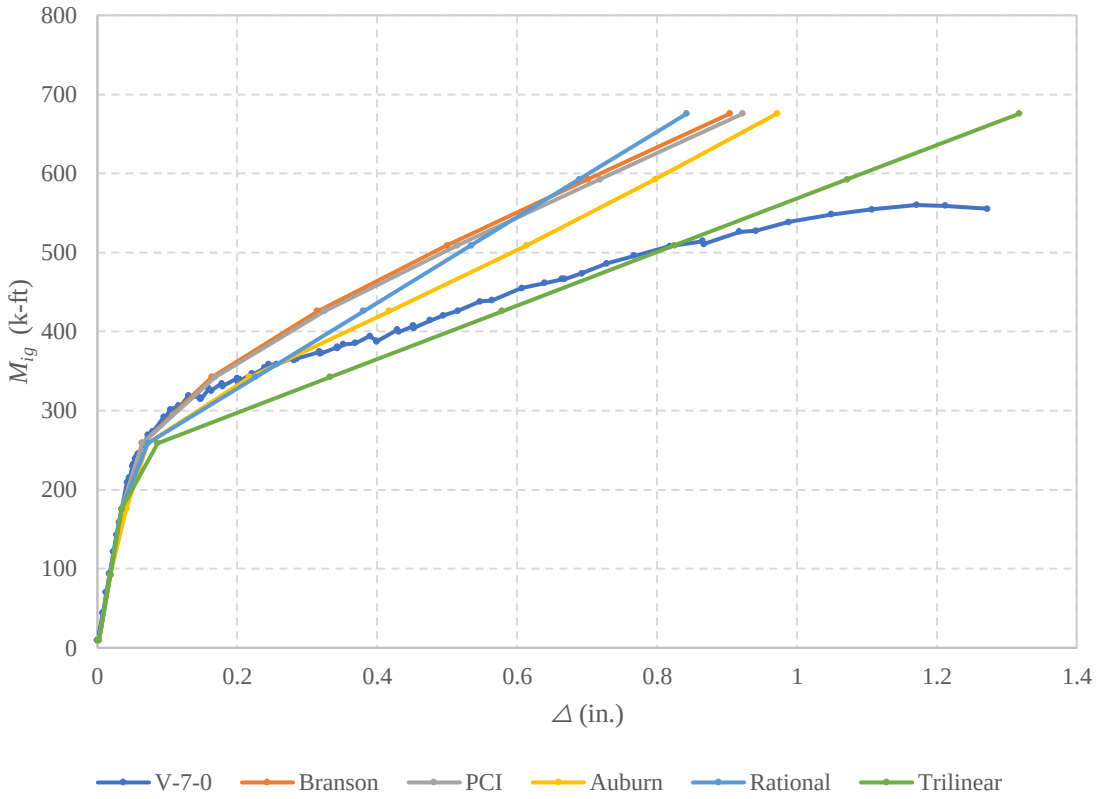

Figure A.4 Moment deflection curve for FS_7.0

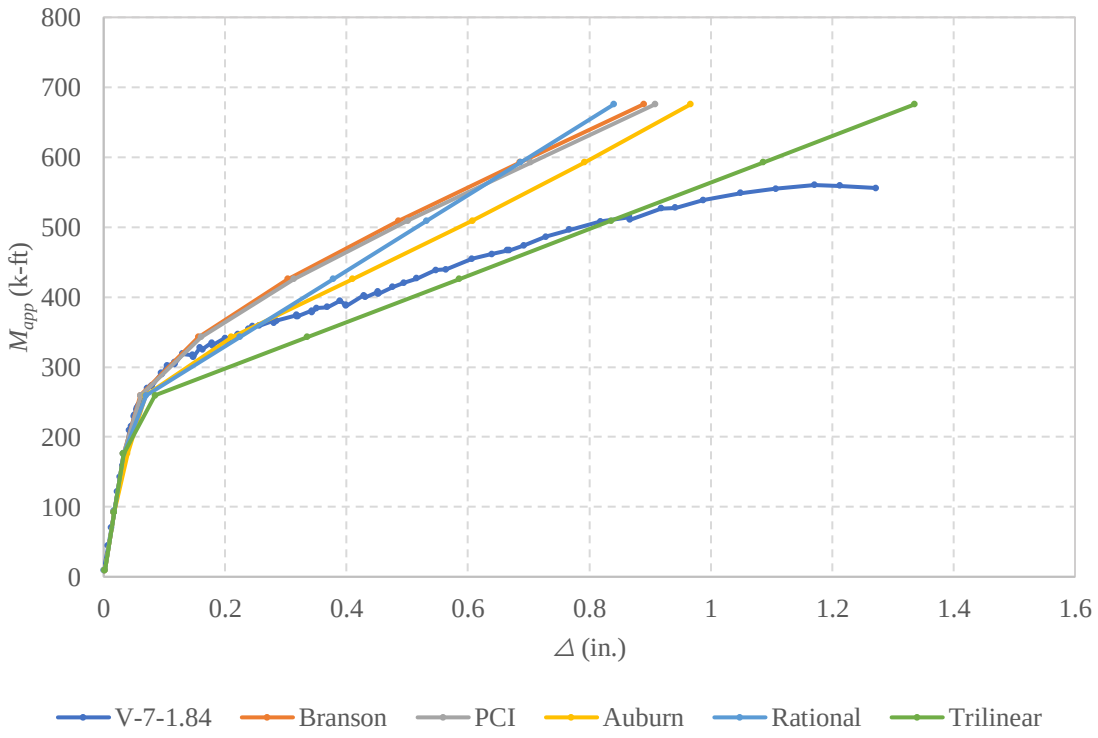

Figure A.5 Moment deflection curve for FS_7.1

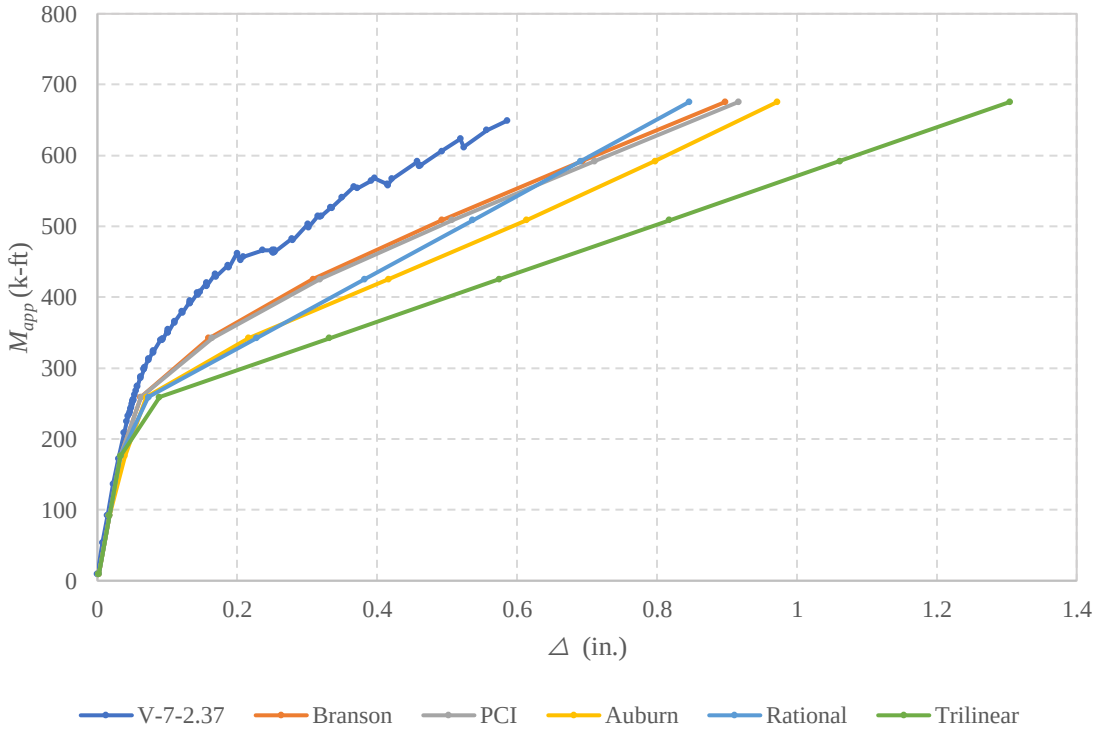

Figure A.6 Moment deflection curve for FS_7.2

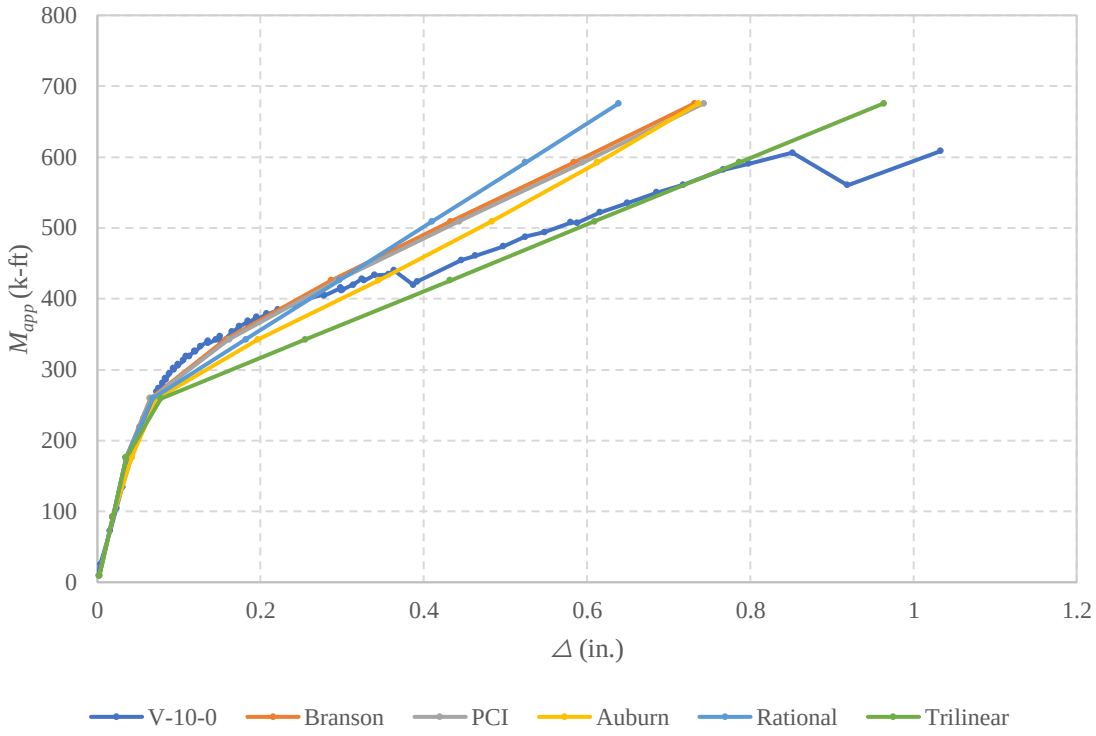

Figure A.7 Moment deflection curve for FS_10.0

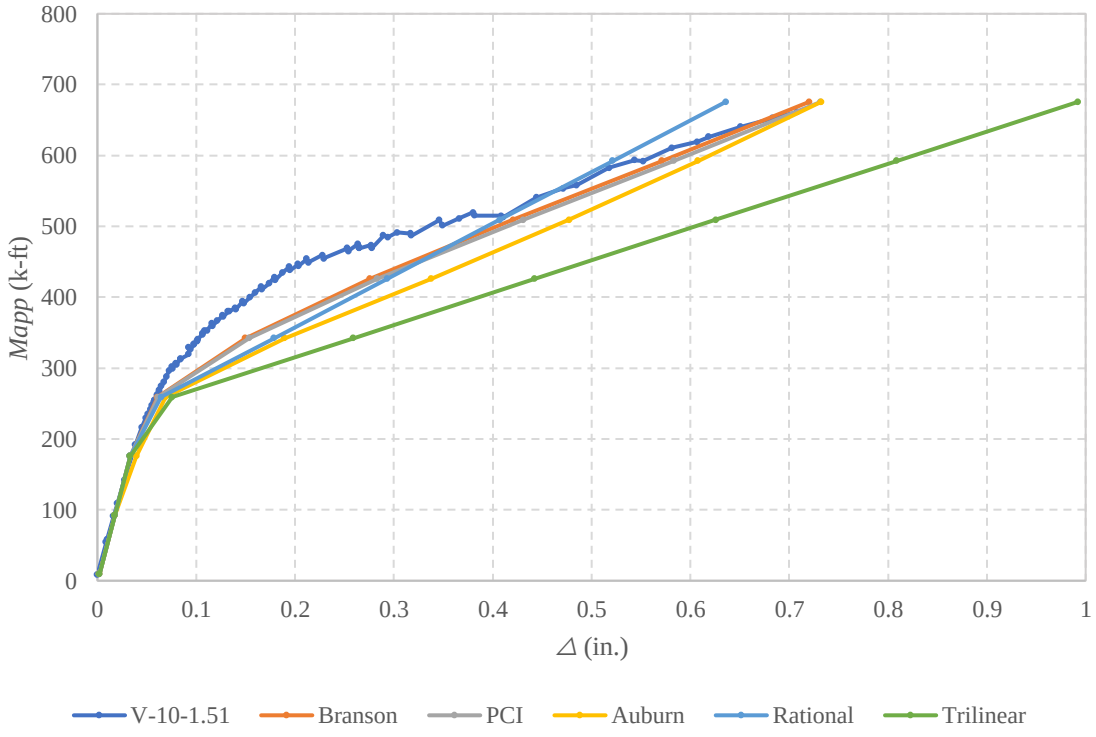

Figure A.8 Moment deflection curve for FS_10.1

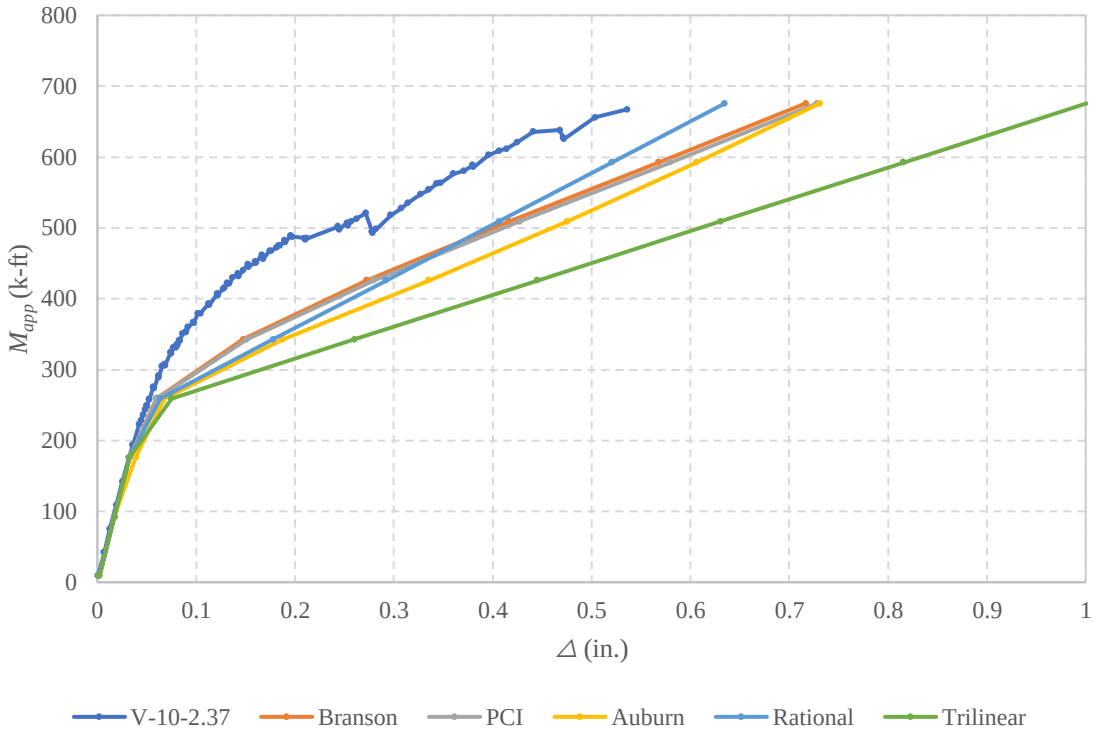

Figure A.9 Moment deflection curve for FS_10.2

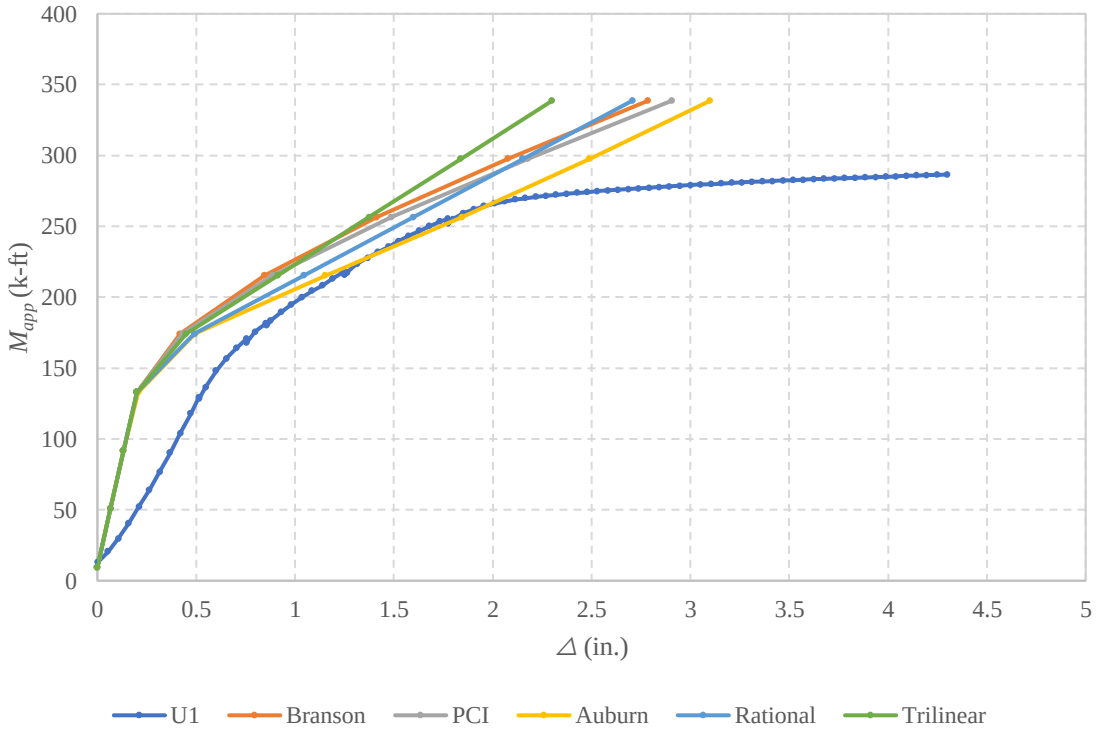

Figure A.10 Moment deflection curve for K_U1

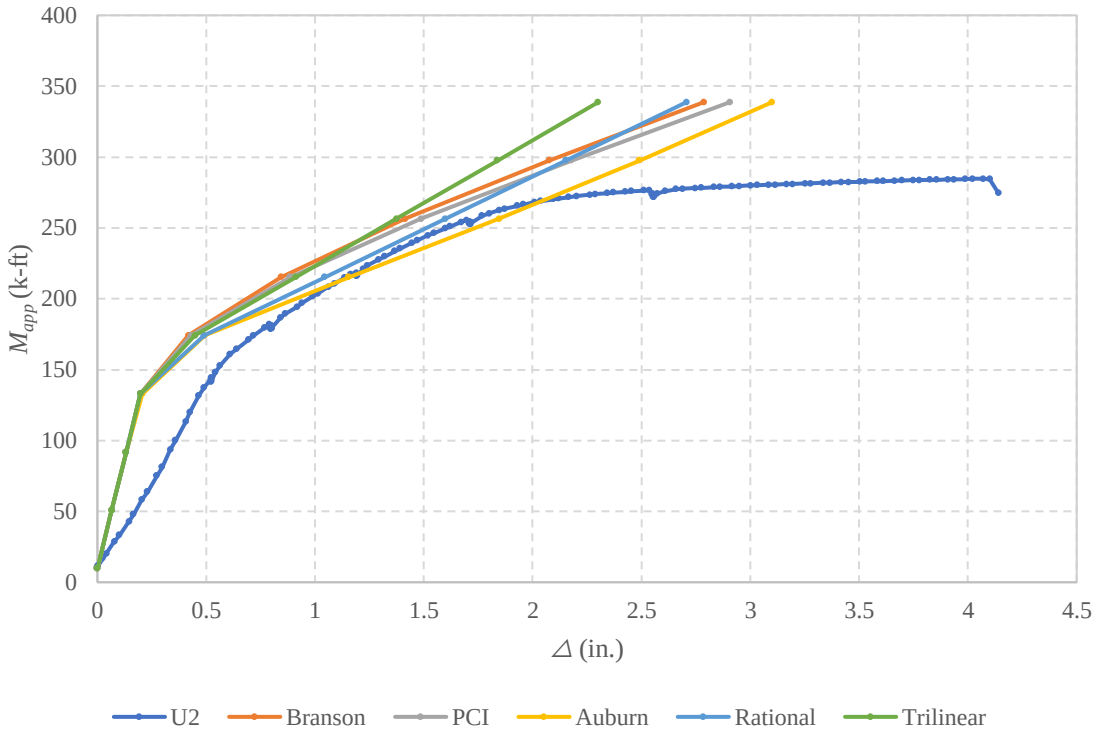

Figure A.11 Moment deflection curve for K_U2

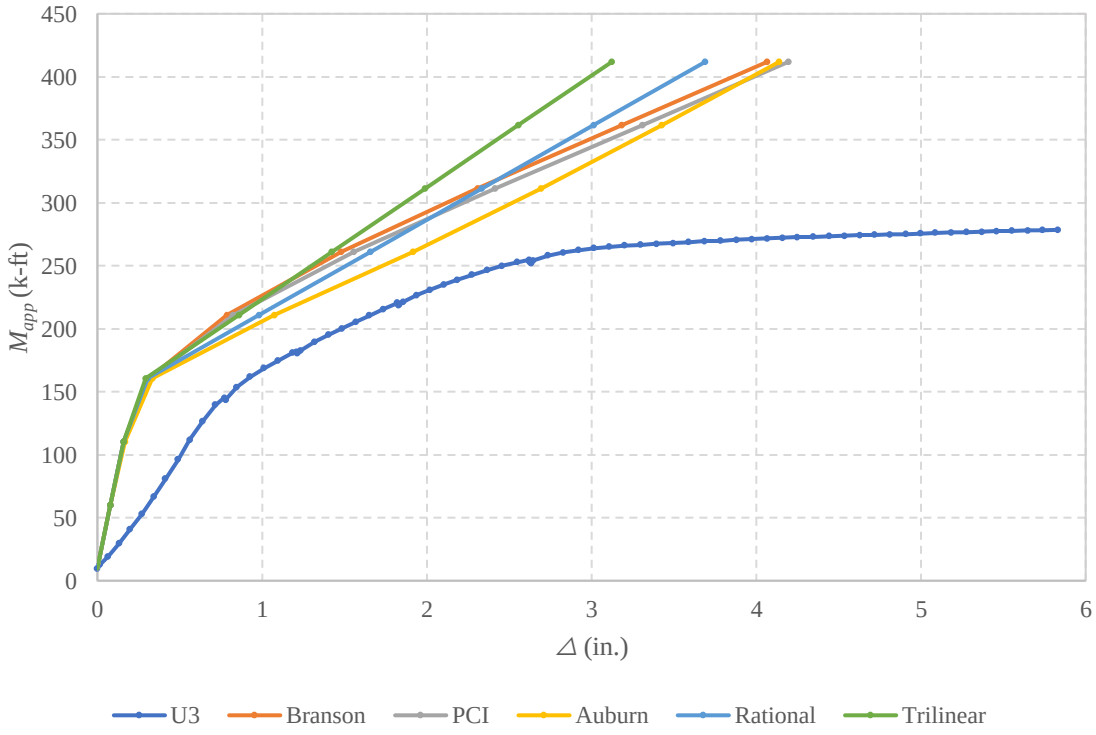

Figure A.12 Moment deflection curve for K_U3

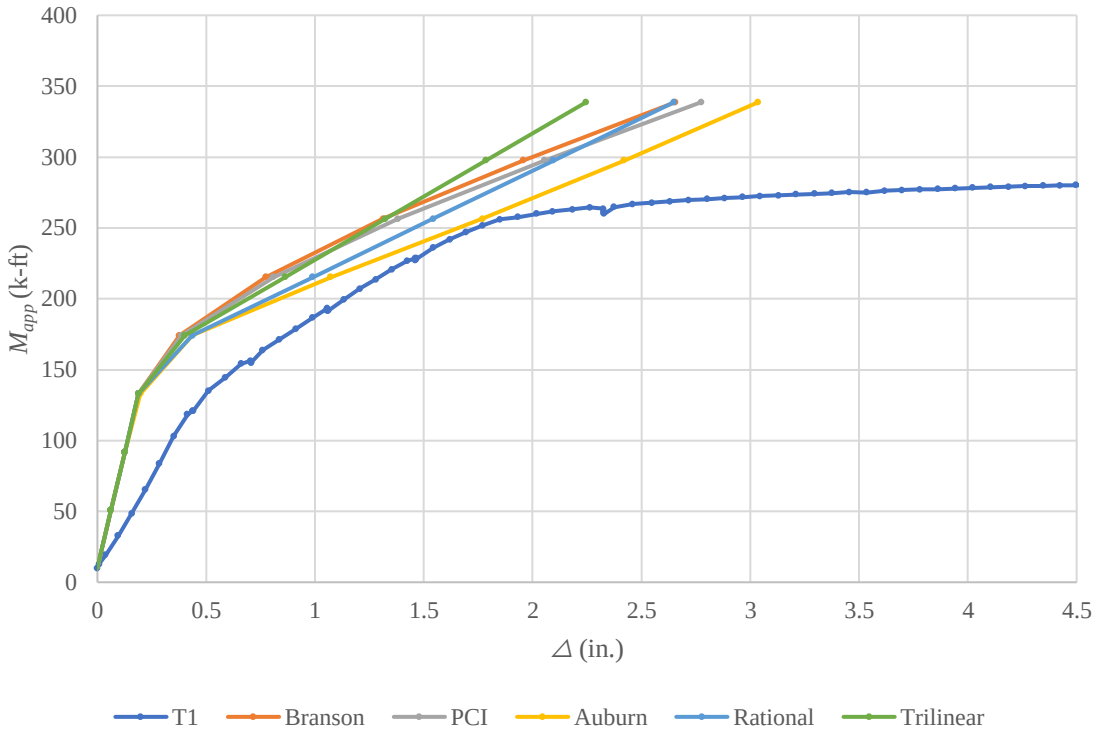

Figure A.13 Moment deflection curve for K_T1

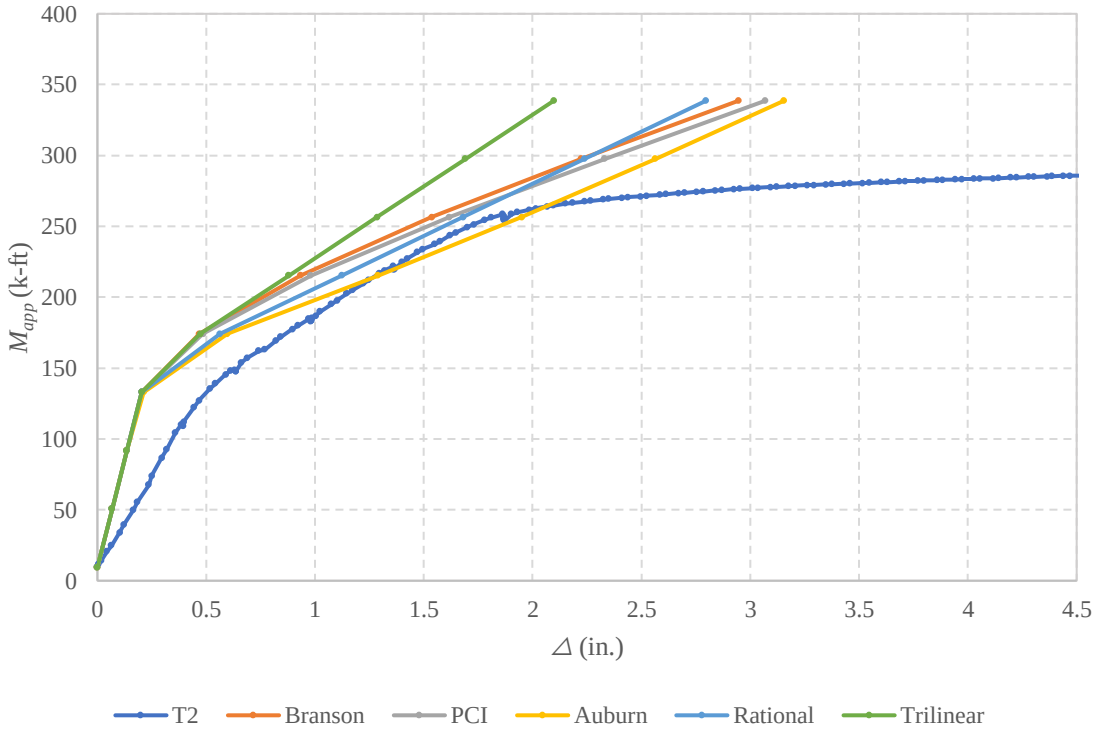

Figure A.14 Moment deflection curve for K_T2

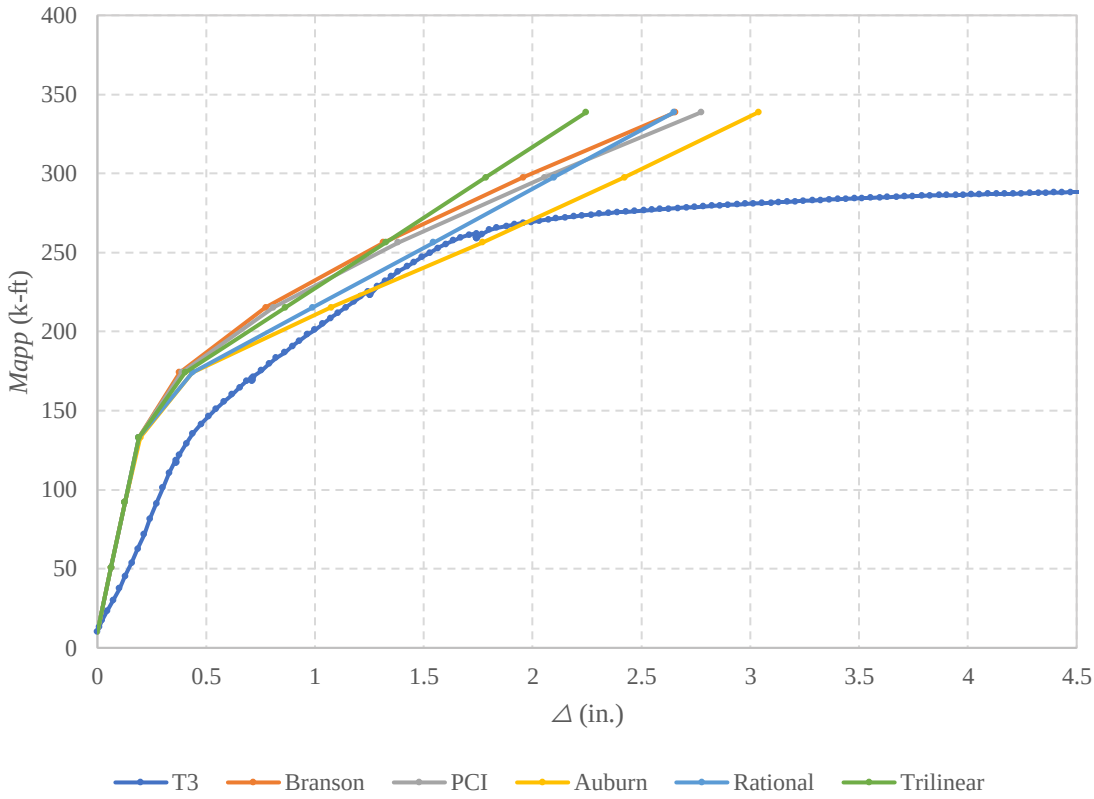

Figure A.15 Moment deflection curve for K_T3

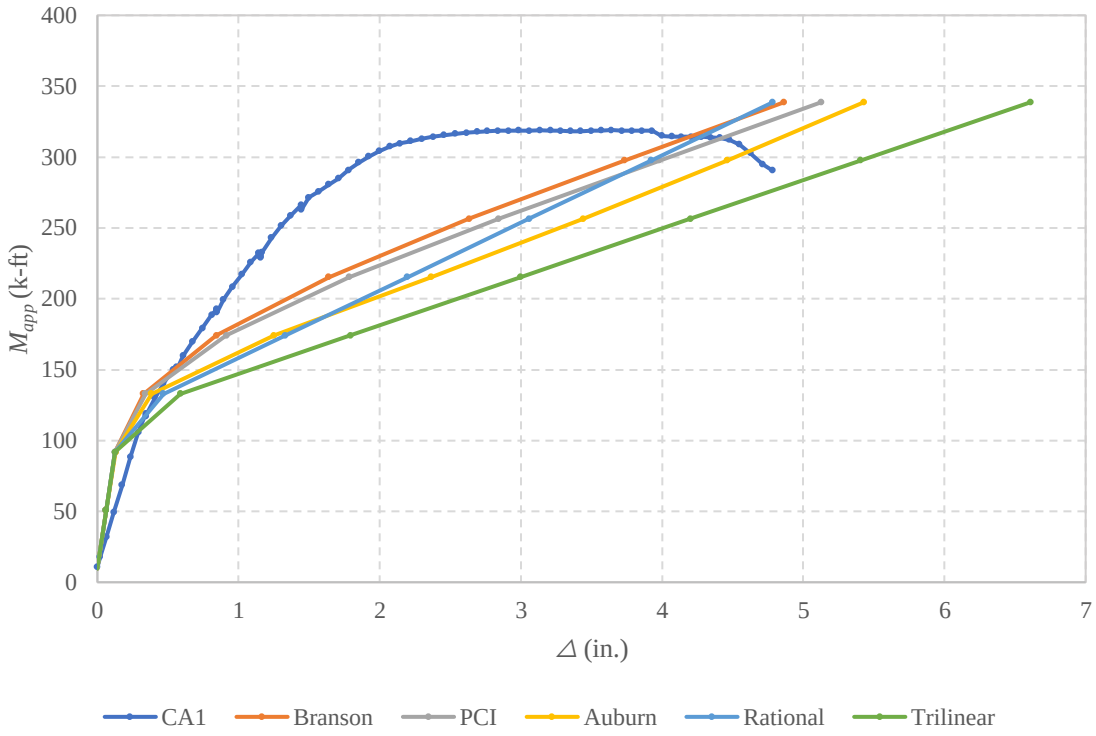

Figure A.16 Moment deflection curve for K_CA1

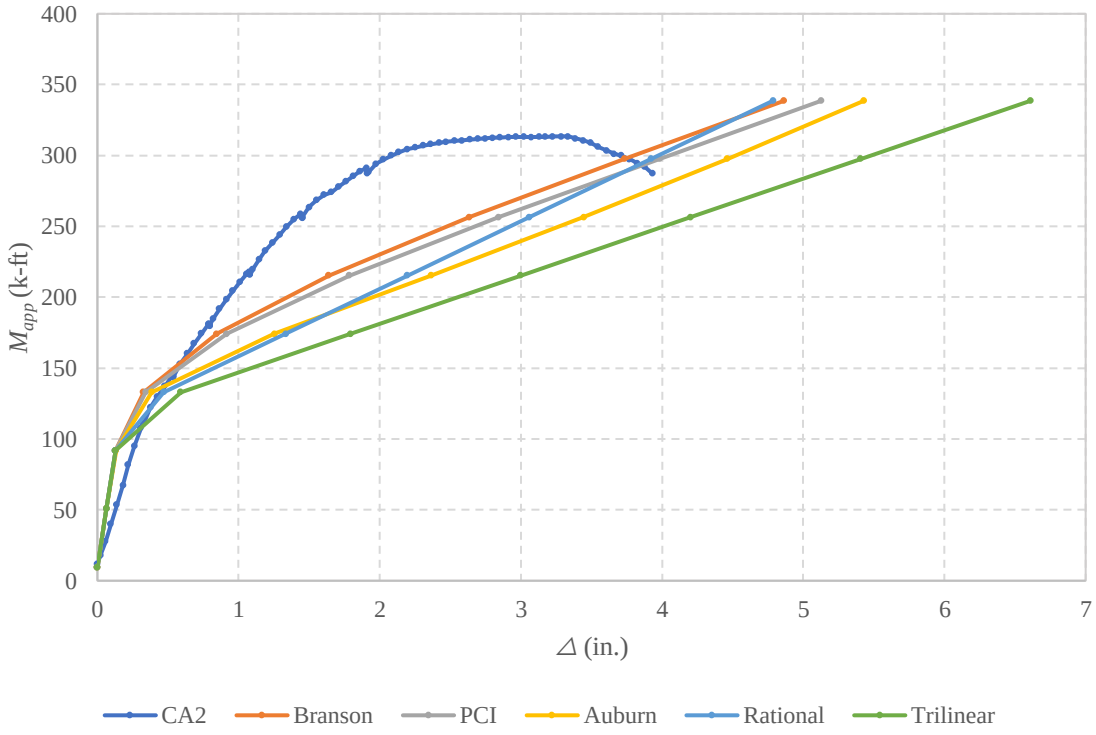

Figure A.17 Moment deflection curve for K_CA2

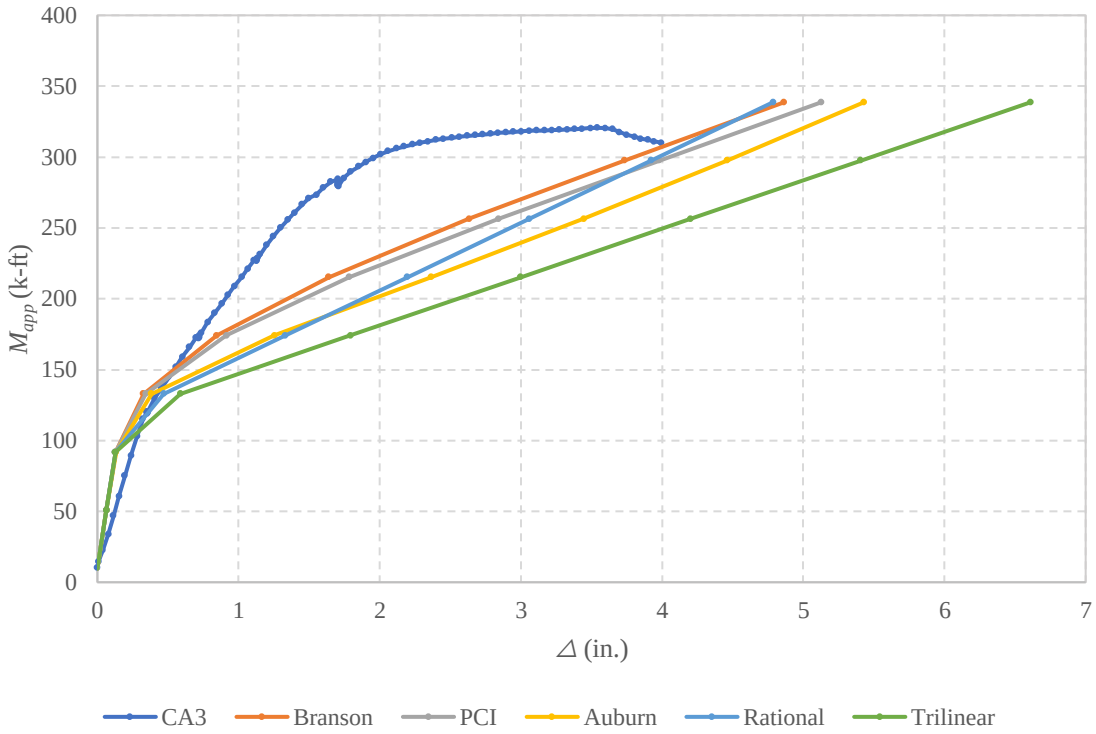

Figure A.18 Moment deflection curve for K_CA3

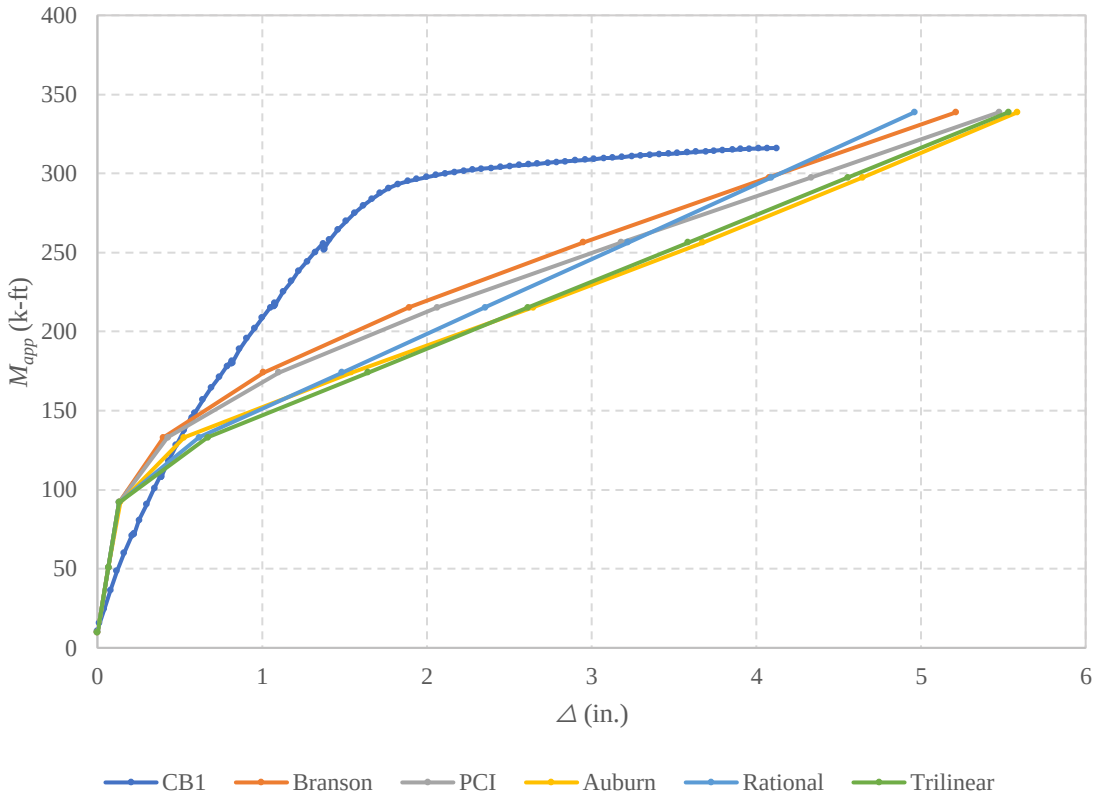

Figure A.19 Moment deflection curve for K_CB1

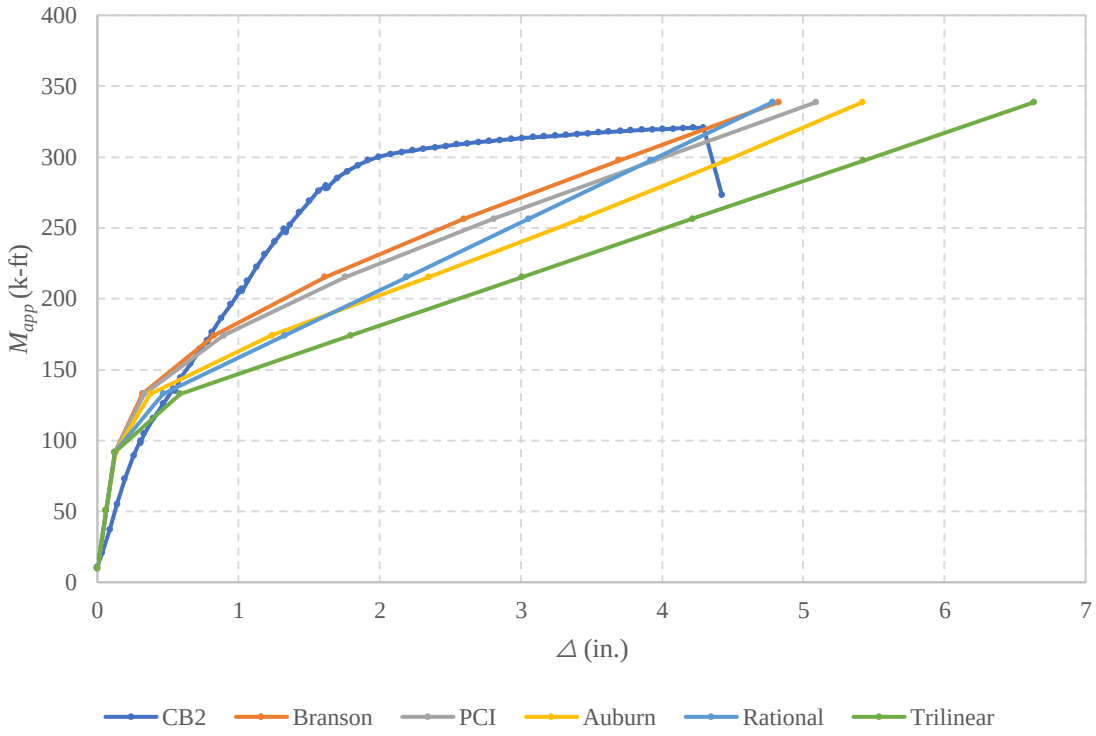

Figure A.20 Moment deflection curve for K_CB2

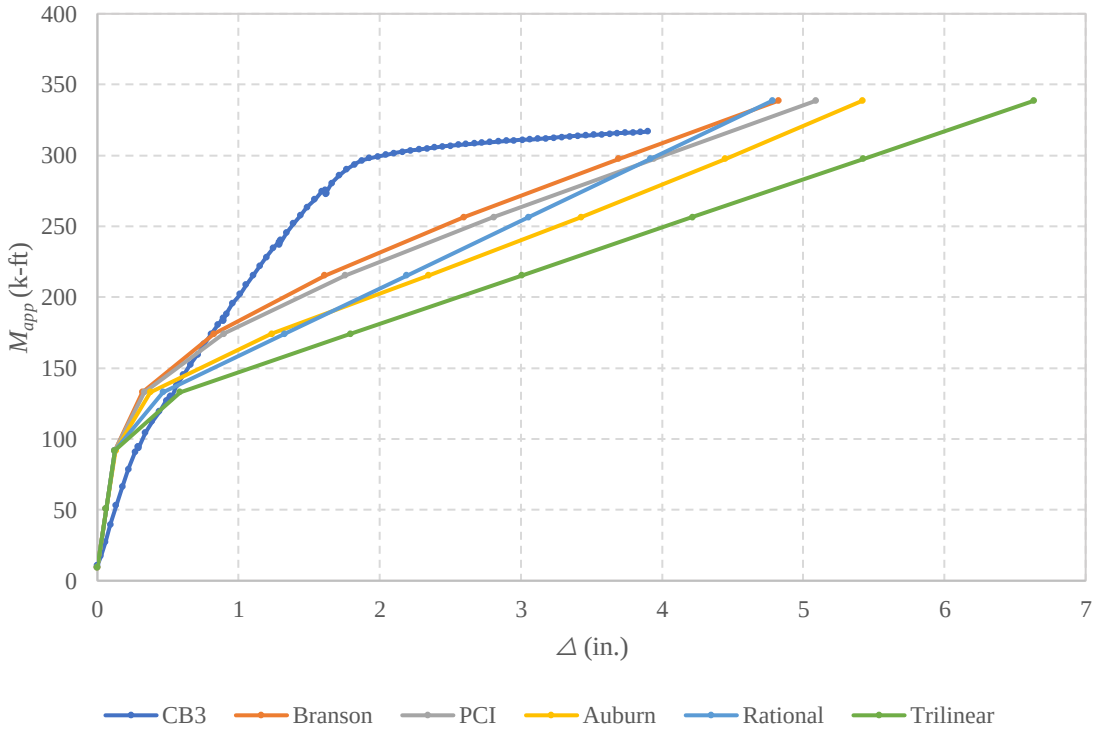

Figure A.21 Moment deflection curve for K_CB3

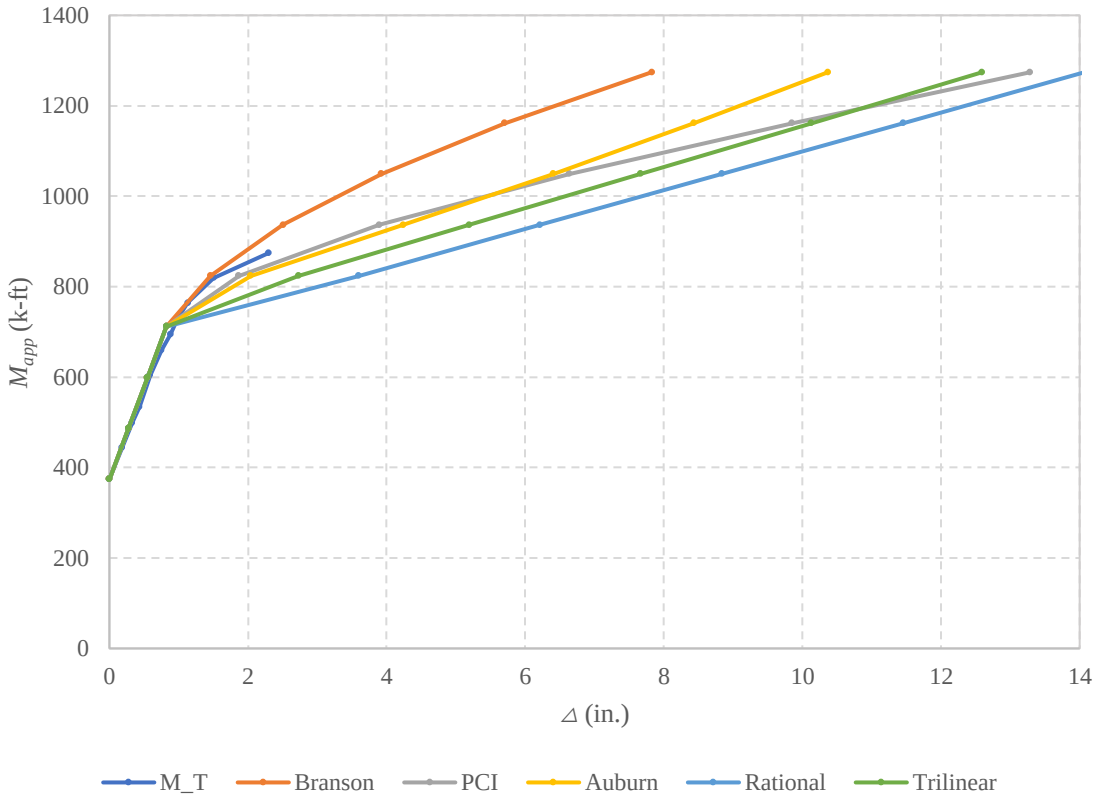

Figure A.22 Moment deflection curve for M_T

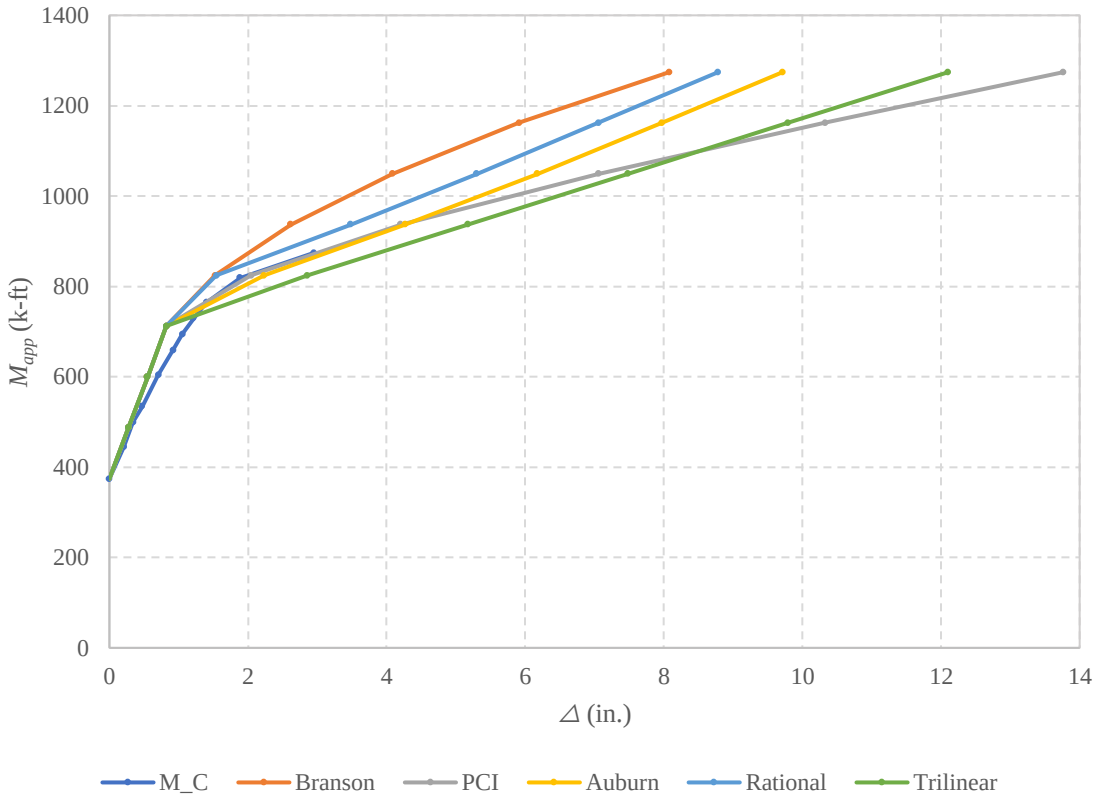

Figure A.23 Moment deflection curve for M_C

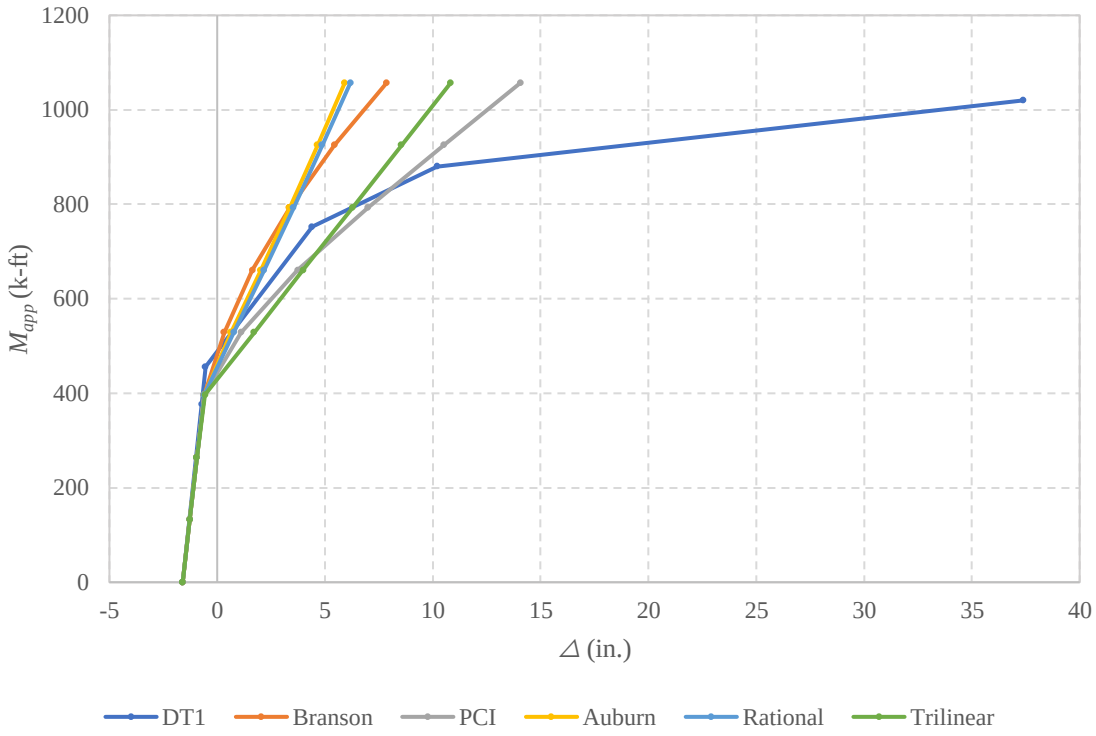

Figure A.24 Moment deflection curve for A_1

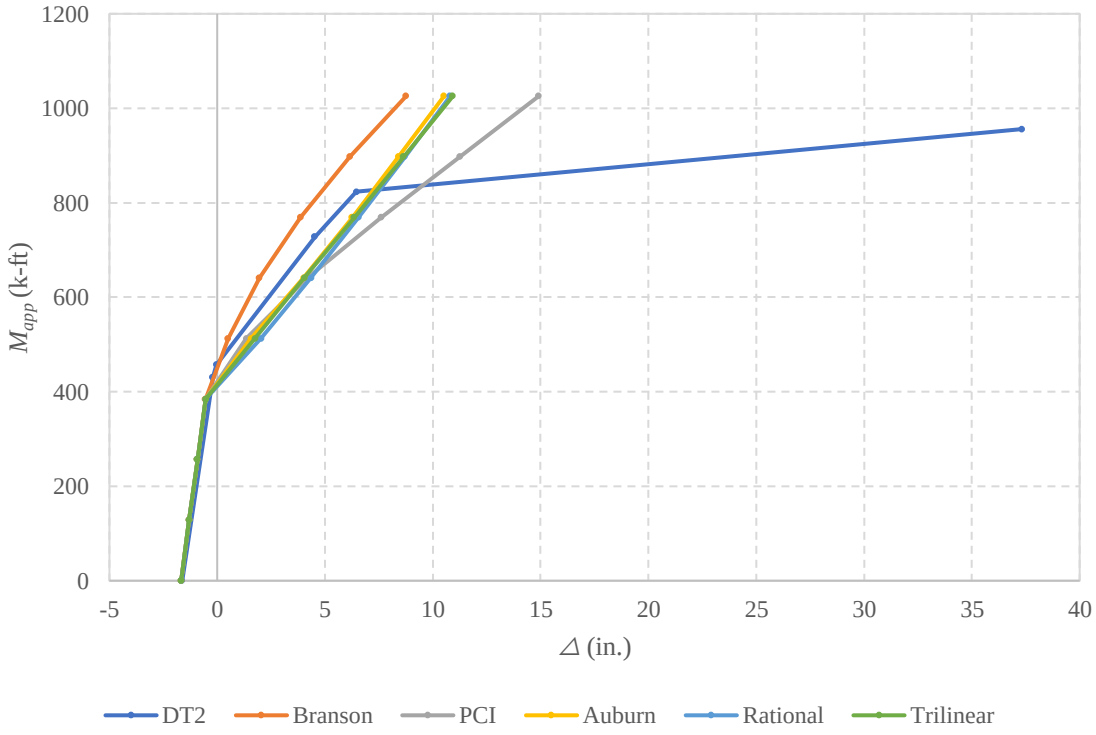

Figure A.25 Moment deflection curve for A_2

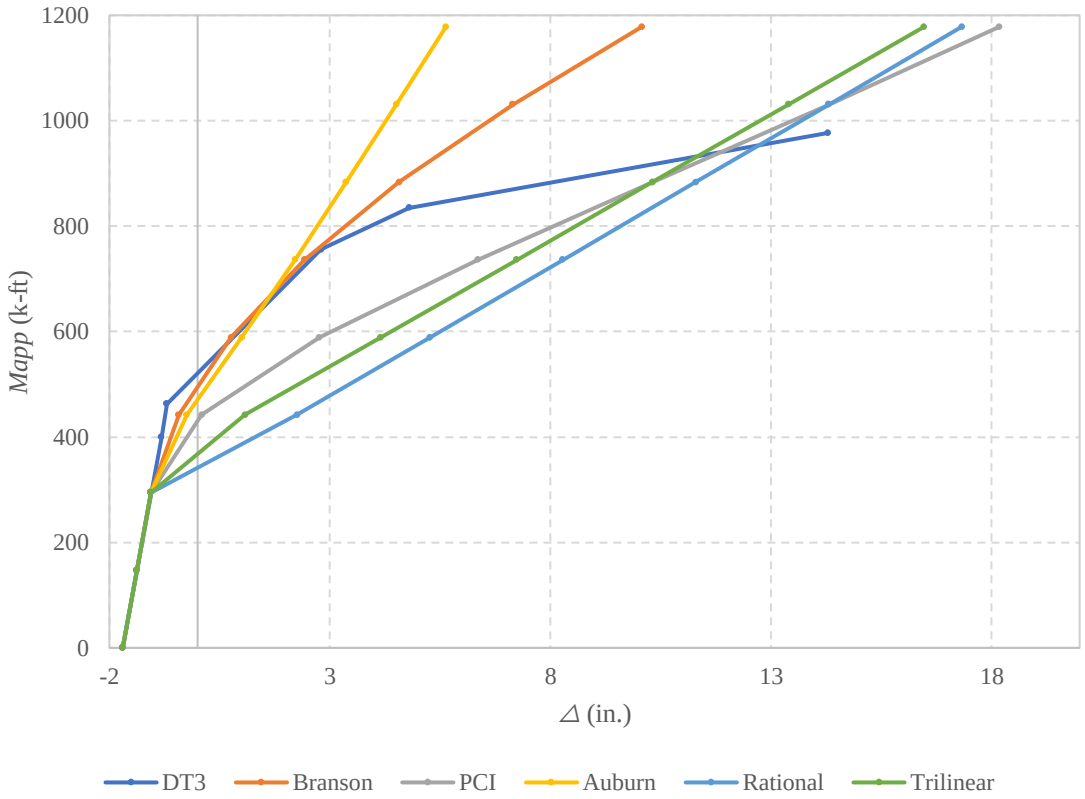

Figure A.26 Moment deflection curve for A_3